



U.S. DEPARTMENT OF
ENERGY

PNNL-20551

Prepared for the U.S. Department of Energy
Under Contract DE-AC05-76RL01830

Secondary Waste Form Screening Test Results—THOR[®] Fluidized Bed Steam Reforming Product in a Geopolymer Matrix

RP Pires
JH Westsik, Jr.
RJ Serne
SV Mattigod

EC Golovich
MM Valenta
KE Parker

July 2011



Pacific Northwest
NATIONAL LABORATORY

*Proudly Operated by **Battelle** Since 1965*

DISCLAIMER

This report was prepared as an account of work sponsored by an agency of the United States Government. Neither the United States Government nor any agency thereof, nor Battelle Memorial Institute, nor any of their employees, makes **any warranty, express or implied, or assumes any legal liability or responsibility for the accuracy, completeness, or usefulness of any information, apparatus, product, or process disclosed, or represents that its use would not infringe privately owned rights.** Reference herein to any specific commercial product, process, or service by trade name, trademark, manufacturer, or otherwise does not necessarily constitute or imply its endorsement, recommendation, or favoring by the United States Government or any agency thereof, or Battelle Memorial Institute. The views and opinions of authors expressed herein do not necessarily state or reflect those of the United States Government or any agency thereof.

PACIFIC NORTHWEST NATIONAL LABORATORY

operated by

BATTELLE

for the

UNITED STATES DEPARTMENT OF ENERGY

under Contract DE-AC05-76RL01830

Printed in the United States of America

Available to DOE and DOE contractors from the
Office of Scientific and Technical Information,
P.O. Box 62, Oak Ridge, TN 37831-0062;

ph: (865) 576-8401

fax: (865) 576 5728

email: reports@adonis.osti.gov

Available to the public from the National Technical Information Service,
U.S. Department of Commerce, 5285 Port Royal Rd., Springfield, VA 22161

ph: (800) 553-6847

fax: (703) 605-6900

email: orders@nits.fedworld.gov

online ordering: <http://www.ntis.gov/ordering.htm>

Secondary Waste Form Screening Test Results—THOR[®] Fluidized Bed Steam Reforming Product in a Geopolymer Matrix

RP Pires
JH Westsik, Jr.
RJ Serne
SV Mattigod

EC Golovich
MM Valenta
KE Parker

July 2011

Prepared for
the U.S. Department of Energy
Under Contract DE-AC05-76RL01830

Pacific Northwest National Laboratory
Richland, Washington 99352

Executive Summary

Screening tests are being conducted to evaluate waste forms for immobilizing secondary liquid wastes from the Hanford Tank Waste Treatment and Immobilization Plant (WTP). Plans are underway to add a stabilization treatment unit to the Effluent Treatment Facility to provide the needed capacity for treating these wastes from WTP. The current baseline is to use a Cast Stone cementitious waste form to solidify the wastes. Through a literature survey, DuraLith alkali-aluminosilicate geopolymer, fluidized-bed steam reformation (FBSR) granular product encapsulated in a geopolymer matrix, and a Ceramicrete phosphate-bonded ceramic were identified both as candidate waste forms and alternatives to the baseline. These waste forms have been shown to meet waste disposal acceptance criteria, including compressive strength and universal treatment standards for Resource Conservation and Recovery Act (RCRA) metals (as measured by the toxicity characteristic leaching procedure [TCLP]). Thus, these non-cementitious waste forms should also be acceptable for land disposal. Information is needed on all four waste forms with respect to their capability to minimize the release of technetium. Technetium is a radionuclide predicted to be in the secondary liquid wastes in small quantities, but the Integrated Disposal Facility (IDF) risk assessment analyses show that technetium, even at low mass, produces the largest contribution to the estimated IDF disposal impacts to groundwater.

To support a final waste form down-selection, Pacific Northwest National Laboratory (PNNL) is conducting screening tests on the candidate waste forms to provide a basis for comparison. This report documents the screening test results on the FBSR granular product encapsulated in a geopolymer (GEO-7) matrix. Ultimately, either one or a few waste forms will be chosen in a down-selection process. The down-selected waste form(s) will be compliant with regulations and performance criteria and will lead to cost-effective disposal of the WTP secondary wastes. Later, more comprehensive and longer term performance testing will be conducted, following the guidance provided by the secondary waste form selection, development, and performance evaluation roadmap.

Three draft test protocols (e.g., 1313, 1315, and 1316) being developed for the U.S. Environmental Protection Agency (EPA) were used to screen the encapsulated FBSR stabilization technologies.

- EPA draft Method 1313—Leaching Test (Liquid-Solid Partitioning as a Function of Extract pH) of Constituents in Solid Materials Using a Parallel Batch Extraction Test (EPA 2009a)
- EPA draft Method 1315—Mass Transfer Rates of Constituents in Monolith or Compacted Granular Materials Using a Semi-Dynamic Tank Leaching Test (EPA 2009b)
- EPA draft Method 1316—Leaching Test (Liquid-Solid Partitioning as a Function of Liquid-to-Solid Ratio) of Constituents in Solid Materials Using a Parallel Batch Extraction Test (EPA 2009c).

These EPA draft methods are a combination of static and semi-dynamic leach experiments that can be used to provide more detailed mechanistic information on material performance in comparison to the current standard leach methods, such as ANSI/ANS 16.1 and TCLP. The EPA draft Method 1313 is a static-leach test method where extraction experiments are conducted in dilute acid or base with deionized water (DIW) over a range of pHs at a fixed liquid-to-solid ratio. Instead of a dilute acid or base at a fixed liquid-to-solid ratio, draft Method 1316 uses DIW as the leachant for a range of liquid-to-solid ratios. The EPA draft Method 1315 is a 63-day, semi-dynamic, leach experiment that consists of submerging a monolithic sample (with a fixed geometry) in water at a fixed liquid-to-solid ratio for a fixed period of time. At each of the nine pre-determined leaching intervals, the sample mass is recorded, and the leachant is changed. This method is similar to American National Standards Institute/American Nuclear Society (ANSI/ANS) 16.1, but the leaching intervals are different.

As part of the Advanced Remediation Technologies (ART) Project, a simulated WTP secondary waste stream (WTP-SW) was processed through the THOR[®] FBSR Engineering Scale Technology Demonstration (ESTD) located at the Hazen Research facility in Golden, Colorado. Savannah River National Laboratory evaluated a number of binder technologies for the FBSR low-activity waste (LAW) granular product and selected a geopolymer material designated GEO-7 as providing the best overall performance for making monoliths for the simulated LAW stream. The GEO-7 geopolymer was also used as the binder for the WTP-SW secondary waste stream. The FBSR/geopolymer cylinders were provided to PNNL by Savannah River National Laboratory.

For the screening tests, 4-in. by 2-in.-diameter cylinders of FBSR product encapsulated in geopolymer (GEO-7) were used as the source material for the EPA leach test methods. The supplied FBSR monoliths were prepared by encapsulating the FBSR granular product collected from the high temperature filter and product receiver into an alkali-aluminosilicate geopolymer. The waste simulant fed into the steam reformer was spiked with rhenium at 10× the expected ⁹⁹Tc concentration in the secondary waste stream. It was formulated to resemble an SW simulant based on an early LAW operating scenario in which the secondary wastes would include condensates from the LAW melter submerged bed scrubber and wet electrostatic precipitator. Therefore, this WTP-SW simulant contained different concentrations of target constituents compared to the baseline secondary waste simulant based on just the LAW off-gas caustic scrubber used to test other secondary waste forms. The waste loading of the supplied FBSR monolithed waste forms contains 65.2^(a) wt% FBSR granular product encapsulated in the geopolymer binding material composed primarily of fly ash and NaOH.

The FBSR monolithed waste form was characterized with respect to chemical and crystalline composition. Solids characterization (X-ray diffraction [XRD] analysis) of the supplied waste forms confirmed the presence of target alkali aluminosilicate (NAS) minerals (e.g., nepheline, sodalite, nosean) plus low-carnegeite previously observed in the FBSR granular product. Other phases identified in the geopolymer waste form included quartz, zeolite rho, Na-faujasite, and a sodium carbonate phase. Scanning electron microscopy (SEM) with energy dispersive spectrometry (EDS) analysis confirmed the presence and even distribution of NAS-like minerals, quartz, and iron oxide compounds.

The EPA draft methods 1313 and 1316 were conducted on the FBSR waste form to get an indication of the impact of pH and the solution-to-solids ratio on the release of contaminant. The natural solution pH after soaking the FBSR granular product/geopolymer in DIW is approximately 12. This is probably due to residual sodium hydroxide from the geopolymer formulation.

The diffusivity of Re (⁹⁹Tc surrogate) in FBSR encapsulated in Geopolymer (GEO-7) was determined by EPA draft Method 1315 and ANSI/ANS 16.1. The diffusivity for the release of rhenium in the FBSR monolith was $\sim 5.5 \times 10^{-9}$ cm²/s after 7 days and $\sim 2.7 \times 10^{-10}$ cm²/s after 63 days by EPA draft Method 1315 and $\sim 5 \times 10^{-9}$ cm²/s after 3 days and $\sim 1.8 \times 10^{-10}$ cm²/s after 90 days per ANSI/ANS 16.1. The associated leachability index (LI) for rhenium bettered the target LI for Tc (>9) after approximately 42 days of leaching. Supplied FBSR monoliths demonstrated comparable leaching trends between EPA draft Method 1315 and ANSI/ANS 16.1 methods.

Following a final waste form selection, the secondary waste form testing will be directed toward 1) testing to support a detailed design of the Solidification Treatment Unit for IDF; 2) data collection to support risk assessments and long-term performance assessments; and, as appropriate, 3) further optimization of the waste form to reduce costs and improve performance (Pierce et al. 2010).

(a) Waste loading published at 68.8% in “Report for Treating Hanford LAW and WTP SW Simulants: Pilot Plant Mineralizing Flowsheet,” RT-21-002 rev. 1, April 2009, THOR Treatment Technologies, LLC. Test Plan (57925-P2-T3-Rev. 1) review comments indicated that this value was corrected in a later revision.

Acknowledgements

The authors wish to acknowledge Kris Colosi, Kim Smith, Tom May, and Max Melvin at Washington River Protection Solutions, LLC (Richland, Washington) for providing project funding and technical guidance. The authors would also like to thank Jesse Lang, Brian Riley, Jerrod Crum, Steve Baum, Christian Iovin, Keith Geiszler, Dennese Smith, Bruce Arey, and Mark Bowden (all from Pacific Northwest National Laboratory), for helping carry out various aspects of the work described in this report. We are particularly grateful to Eric Pierce for his technical guidance related to the testing plan and the reporting of the results to aid in client and down-select activities. We are thankful to Wayne Cosby and Virginia Sliman for completing the editorial review of this technical report.

Acronyms and Abbreviations

ANS	American Nuclear Society
ANSI	American National Standards Institute
ART	Advanced Remediation Technologies
ASTM	American Society for Testing and Materials
BET	Brunauer-Emmett-Teller
BSE	backscatter electron
COC	contaminants of concern
CRR	Carbon Reduction Reformer
DIW	deionized water
DOE	U.S. Department of Energy
DMR	Denitration and Mineralization Reformer
EC	electrical conductivity
Ecology	Washington State Department of Ecology
EDS	energy dispersive spectrometry
Eh	oxidation-reduction potential
EM	U.S. Department of Energy Office of Environmental Management
EPA	U.S. Environmental Protection Agency
ESTD	Engineering Scale Technology Demonstration
ETF	Effluent Treatment Facility
FBSR	fluidized-bed steam reformation
FEP	Waste Feed Evaporation System
HEPA	high-efficiency particulate air
HF	hydrogen fluoride
HLW	high-level waste
HTF	high temperature filter
IC	ion chromatography
ICDD	International Committee for Diffraction Data
ICP-MS	inductively coupled plasma mass spectroscopy
ICP-OES	inductively coupled plasma optical emission spectroscopy
IDF	Integrated Disposal Facility
ILAW	immobilized low-activity waste
KOH	potassium hydroxide
LAW	low-activity waste
LI	Leachability Index

LLRW	low-level radioactive waste
LOI	loss on ignition
MS	mass spectroscopy
NAS	sodium aluminosilicate ($\text{Na}_2\text{O}-\text{Al}_2\text{O}_3-\text{SiO}_2$)
NBS	National Bureau of Standards
ND	not detected
NDIR	non-dispersive infrared
NIST	National Institute of Standards and Technology
OE&T	Office of Engineering and Technology (DOE)
OGF	off-gas filter
ORP	U.S. Department of Energy Office of River Protection
PCT	product consistency test
pH	measure of the acidity of a solution, where pH is the negative of the logarithm of the activity of H^+ in solution
PNNL	Pacific Northwest National Laboratory
POHC	Principal Organic Hazardous Constituent
PR	Product Receiver
RCRA	Resource Conservation and Recovery Act
SBS	Submerged Bed Scrubber
SDD	silicon drift detector
SE	secondary electron
SEM	scanning electron microscopy
SRNL	Savannah River National Laboratory
SSA	specific surface area
STU	Solidification Treatment Unit
SW	secondary waste
TC	total carbon
TCLP	Toxicity Characteristics Leaching Procedure
TLP	Treated LAW Evaporation Process
TSCA	Toxic Substances Control Act
TTT	THOR Treatment Technologies, LLC
USGS	U.S. Geological Survey
WESP	Wet Electrostatic Precipitator
WRPS	Washington River Protection Solutions, LLC
WTP	Hanford Tank Waste Treatment and Immobilization Plant
XRD	X-ray diffraction

Units of Measure

θ	angle of incidence (Bragg angle)
Å	angstrom (10^{-10} m or 10^{-1} nm)
°C	temperature in degrees Celsius [$T(^{\circ}\text{C}) = T(\text{K}) - 273.15$]
cm	centimeter
g	gram
μ	micro (prefix, 10^{-6})
μm	micrometer
mS/cm	millisiemens per centimeter (electrical conductance)
M	molarity, mol/L
mL	milliliter
rpm	revolutions per minute
λ	wavelength
wt%	weight percent

Contents

Executive Summary	iii
Acknowledgements.....	vii
Acronyms and Abbreviations	ix
Units of Measure.....	xi
1.0 Introduction.....	1.1
1.1 Overview—Disposal of Hanford Tank Wastes	1.1
1.2 Purpose and Scope.....	1.2
1.3 Report Contents and Organization.....	1.2
2.0 FBSR Overview	2.1
2.1 FBSR Process Description.....	2.1
2.2 FBSR Product Description	2.1
3.0 FBSR Simulant Feed	3.1
3.1 FBSR Processing Parameters	3.5
4.0 FBSR Secondary Waste Forms.....	4.1
4.1 FBSR Granular Product Preparation.....	4.1
4.2 FBSR WTP SW Granular Product Encapsulated in Geopolymer	4.5
5.0 FBSR Waste Form Characterization Methods.....	5.1
5.1 Material Preparation Techniques.....	5.1
5.2 Leachate Solution Characterization	5.1
5.3 Solid Characterization	5.2
5.3.1 Chemical Composition.....	5.2
5.3.2 X-Ray Diffraction	5.3
5.4 FBSR Waste Form Leaching Tests.....	5.4
5.4.1 EPA Draft Method 1313—pH Effects	5.4
5.4.2 EPA Draft Method 1316—Liquid-to-Solid Ratio Effects.....	5.5
5.4.3 EPA Draft Method 1315 – Mass Transfer Rates.....	5.5
5.4.4 ANSI/ANS 16.1	5.7
5.4.5 Diffusivity Calculation.....	5.9
6.0 Results.....	6.1
6.1 FBSR Waste Form Solids Characterization.....	6.1
6.1.1 Chemical Composition.....	6.1
6.1.2 SEM with EDS.....	6.2
6.1.3 X-Ray Diffraction	6.8
6.2 Effect of Leachant pH—EPA Draft Method 1313	6.15

6.3	Effect of Liquid-to-Solid Ratio—EPA Draft Method 1316	6.20
6.4	Leachability—EPA Draft Method 1315	6.22
6.5	Leachability—ANSI/ANS 16.1	6.27
7.0	Discussion.....	7.1
8.0	Conclusions and Recommendations	8.1
9.0	References.....	9.1
Appendix A: Scanning Electron Microscopy and Energy Dispersive Spectroscopy on FBSR Waste Form Specimen		A.1
Appendix B: Dimensions of Supplied FBSR Test Monoliths Used in EPA Draft Method 1315 and ANSI/ANS 16.1 Leach Tests.....		B.1

Figures

2.1.	ESTD Flow Diagram for the Hanford WTP-SW and LAW FBSR Process Demonstration	2.3
4.1.	Typical DMR Bed Material Sample. The large dark particles are the unreacted carbon.....	4.2
4.2.	Typical PR Material Sample	4.2
4.3.	Microprobe Photographs of Product Fines Collected from the HTF	4.3
5.1.	An Example of the Type of Static Container Used to Conduct the EPA 1313 and 1316 Draft Test Methods	5.5
5.2.	A Schematic of the 1315 Test Method.....	5.6
5.3.	Monoliths Submerged into DIW in the Leaching Vessels.....	5.6
5.4.	A Schematic of the ANSI/ANS 16.1 Test Method	5.8
6.1.	SEM Collage Showing Different Regions Analyzed by EDS	6.4
6.2.	Low Magnification SEM BSE Image of the Dry-Cut Surface of a FBSR Monolith.....	6.5
6.3.	SEM BSE Images and Corresponding EDS: a and b: Long Prismatic Mineral Phase; b–f: the Monolith Matrix; g and h: Zr and Si Rich Phase; i–l: Fe-Rich Spherical Particles	6.6
6.4.	XRD Pattern for FBSR Product Sample	6.11
6.5.	XRD Patterns for FBSR Intact and Ground Monolith Samples.....	6.12
6.6.	Patterns for FBSR Leached and Unleached Intact Monolith Samples.....	6.13
6.7.	Micro-XRD Pattern of Surface Coating of FBSR Intact Monolith.....	6.14
6.8.	FBSR Monolith Cross Sectioned for XRD Sample Collection.....	6.15
6.9.	Partial FBSR Monolith Cross Section.....	6.15
6.10.	Titration Curves with Leaching Data for FBSR Encapsulating Waste Form	6.16
6.11.	Leached Re (Tc surrogate) of the FBSR Encapsulated Waste Form in EPA Draft Method 1313	6.17
6.12.	Leached Re (Tc surrogate) of the FBSR Encapsulated Waste Form in EPA Draft Method 1316.....	6.20
6.13.	Diffusivity of Re in FBSR Monolith Waste Form for EPA Draft Method 1315	6.24
6.14.	Diffusivity of Re in FBSR Monolith Waste Form for EPA Draft Method 1315 and ANSI/ANS 16.1	6.29

Tables

3.1. Selection Basis for Constituents WTP SW Simulant Solution	3.2
3.2. Compositions of Simulants Used in Secondary Waste Form Testing	3.3
3.3. Composition of Mineralizing Clay Used for WTP SW Simulant.....	3.4
3.4. Composition of WTP SW Simulant Solution with Clay Added	3.5
3.5. Operating Conditions for the WTP SW Production Test.....	3.6
3.6. Summary of DMR Production Test Operating Parameters.....	3.6
3.7. Summary of CRR and Off-gas Production Test Operating Parameters.....	3.7
4.1. Product Summary for WTP SW Tests	4.1
4.2. Average Composition (wt%) of FBSR Product From Hazen Research Facility 2008 WTP-SW Tests	4.4
4.3. Data Measured for the Large-Scale Cylinders	4.6
6.1. Chemical Composition of FBSR Granular Material Encapsulated in GEO-7 Binder	6.2
6.2. Phases Identified in FBSR Product and Monolith Samples.....	6.10
6.3. The Values of pH, EC, and Alkalinity of FBSR Waste Form Measured from EPA Draft Method 1313	6.16
6.4. The Concentrations of Major Cations in Eluate for the FBSR Waste Form from EPA Draft Method 1313.....	6.18
6.5. The Concentrations of Select RCRA Metals, Iodine and Rhenium in Eluate for the FBSR Waste Form from EPA Draft Method 1313	6.19
6.6. The Concentrations of Major Anions in Eluate for the FBSR Waste Form from EPA Draft Method 1313.....	6.19
6.7. The Values of pH, EC, and Alkalinity of FBSR Waste Form Measured from EPA Draft Method 1316.....	6.20
6.8. The Concentrations of Major Elements in Eluate for the FBSR Waste Form from EPA Draft Method 1316.....	6.21
6.9. The Concentrations of Select RCRA Metals, Iodine and Rhenium in Eluate for the FBSR Waste Form from EPA Draft Method 1316.....	6.22
6.10. The Concentrations of Major Anions in Eluate for the FBSR Waste Form from EPA Draft Method 1316.....	6.22
6.11. The Values of pH, EC, and Alkalinity of FBSR Waste Form Measured from EPA Draft Method 1315	6.24
6.12. The Concentrations of Major Cations in Eluate for the FBSR Waste Form from EPA Draft Method 1315	6.25
6.13. The Concentrations of Select Elements in Eluate for the FBSR Waste Form from Draft Method 1315	6.26
6.14. The Concentrations of Major Anions in Eluate for the FBSR Waste Form from Draft Method 1315	6.27
6.15. The Values of pH, EC, and Alkalinity of FBSR Waste Form Leachates from ANSI/ANS 16.1	6.28

6.16. The Concentrations of Major Cations in Eluate for the FBSR Waste Form from ANSI/ANS 16.1	6.30
6.17. Concentrations of Select RCRA Metals, Iodine and Rhenium in Leachate for the FBSR Waste Form from ANSI/ANS 16.1	6.31
6.18. The Concentrations of Major Anions in Leachate for the FBSR Waste Form from ANSI/ANS -16.1	6.32
7.1. The Diffusivity and Leachability Index for Cd and Pb in Eluate for FBSR Waste Form from EPA Method 1315	7.2
7.2. The Diffusivity and Leachability Index for Al, Ti and Fe in Eluate for FBSR Waste Form from EPA Method 1315	7.3
7.3. The Diffusivity and Leachability Index for Re and Na in Eluate for FBSR Waste Form from EPA Draft Method 1315	7.4
7.4. The Diffusivity and Leachability Index for Cd and Pb in Eluate for FBSR Waste Form from ANSI/ANS 16.1	7.5
7.5. The Diffusivity and Leachability Index for Al, Ti and Fe in Eluate for FBSR Waste Form from ANSI/ANS 16.1	7.6
7.6. The Diffusivity and Leachability Index for Re and Na in Eluate for FBSR Waste Form from ANSI/ANS 16.1	7.7

1.0 Introduction

The federal facilities located on the Hanford Site in southeastern Washington State were used by the U.S. government to produce nuclear materials for the U.S. strategic defense arsenal. Currently, the Hanford Site is under the stewardship of the U.S. Department of Energy (DOE) Office of Environmental Management (EM). A large inventory of radioactive and mixed waste, resulting from the production of nuclear materials, has accumulated, mainly in 177 underground single- and double-shell tanks located in the central plateau of the Hanford Site (Mann 2002). The DOE EM Office of River Protection (ORP) is proceeding with plans to permanently dispose of the liquid and solid wastes contained in the tanks. Pacific Northwest National Laboratory (PNNL) was contracted to initiate a waste form testing program to support evaluation of the long-term durability of a waste form for solidifying secondary wastes generated from treating and immobilizing Hanford radioactive tank wastes.

1.1 Overview—Disposal of Hanford Tank Wastes

Under the ORP Hanford tank waste disposal plans, liquid and solid wastes will be retrieved from the tanks and transferred to processing facilities at the Hanford Tank Waste Treatment and Immobilization Plant (WTP). In the pretreatment facility, the sludges (insoluble material) will be washed and the liquids processed to generate a high-level waste (HLW) fraction and a low-activity waste (LAW) fraction. The HLW fraction will contain the bulk of the radionuclides, particularly the actinides, cesium, and strontium. The low-activity fraction will contain predominately inactive sodium and aluminum from LAW processing with a much lower inventory of the radionuclides. Both waste streams will be converted to glass at vitrification facilities in the WTP. The LAW fraction will be disposed of on the Hanford Site in the Integrated Disposal Facility (IDF) (Ecology et al. 1989), and the HLW fraction will be transferred to a HLW repository to be identified. In addition to the vitrified HLW and immobilized LAW (ILAW) glass, the waste processing steps being implemented at the WTP will generate secondary wastes that must be processed, stabilized, and disposed of in the IDF.

The secondary wastes that will be generated from processing tank wastes include routine solid wastes and liquid process effluents. Because ^{99}Tc and iodine-129 (^{129}I) will volatilize when exposed to the high processing temperatures used to produce glass, the solid and liquid secondary waste streams are expected to contain a portion of the total ^{99}Tc and ^{129}I inventory. Solid wastes from the waste-treatment facilities may include failed equipment, decontamination wastes, high-efficiency particulate air (HEPA) filters, carbon absorption beds, silver mordenite iodine sorbent beds, and spent ion-exchange resin. Liquid wastes may include process condensates and scrubber and/or off-gas treatment liquids from the thermal waste treatment processes. After packaging, the solid secondary wastes will be sent to the IDF for disposal. The liquid-effluent secondary wastes will be sent to the Effluent Treatment Facility (ETF) for further treatment and disposal, either as treated liquid effluents under the ETF State Wastewater Discharge Permit or as solidified liquid effluents under the Dangerous Waste Permit for disposal at the IDF. This report focuses on the testing of Fluidized Bed Steam Reforming (FBSR) granular product encapsulated in a geopolymer binder, candidate secondary waste form.

The ETF is a Resource Conservation and Recovery Act (RCRA)-permitted multi-waste treatment and storage unit that can accept dangerous, low-level, and mixed wastewaters for treatment. The ETF receives liquid effluents from cleanup projects on the Hanford Site, which are disposed of after being treated. Currently, ETF supports the 242-A Evaporator, Mixed Waste Burial Trench, and Environmental Restoration Disposal Facility leachates; groundwater treatment projects; and other decontamination and decommissioning projects. The liquid effluents are treated to remove toxic metals, radionuclides, and

ammonia and to destroy organic compounds. Plans are to increase the capacity of the ETF to process the increased volume of secondary wastes when the WTP begins waste treatment and immobilization operations (Koci 2005). A Solidification Treatment Unit (STU) will be added to the ETF to provide the necessary additional capacity. The current baseline calls for solidifying the ETF evaporator concentrate in a cement-based waste form.

Washington River Protection Solutions, LLC (WRPS) is evaluating alternatives for disposition of the secondary wastes, including the design and construction of the STU for the ETF. To receive secondary liquid wastes from the WTP, the STU needs to be operational by 2018. There will be a formal decision on the waste form for the secondary liquid wastes, including agreement with the Washington State Department of Ecology (Ecology) by 2012. Screening tests of candidate waste forms are being conducted to support the DOE Critical Decision process and the selection of the waste form for the secondary wastes.

Significant uncertainties are associated with the processing of these secondary wastes, and in 2008, the DOE Office of Engineering and Technology (OE&T) sponsored a meeting to develop a roadmap to outline the steps necessary to design the secondary waste forms. At the highest level, the secondary waste roadmap (PNNL 2009) includes elements addressing regulatory and performance requirements, waste composition, preliminary waste form screening, waste form development, process design and support, and validation. The regulatory and performance requirements activity will provide the secondary waste form performance requirements. The waste-composition activity will provide workable ranges of secondary waste compositions and formulations for simulants and surrogates. Preliminary waste form screening will identify candidate waste forms for immobilizing the secondary wastes. The waste form development activity will mature the waste forms, leading to a selected waste form(s) with a defensible understanding of the long-term release rate and input into the Critical Decision process for a secondary waste treatment process and/or facility. The process and design support activity will provide a reliable process flowsheet and input to support a robust facility design. The validation effort will confirm that the selected waste form meets regulatory requirements. The final outcome of implementing the secondary waste roadmap is the compliant, effective, timely, and cost-effective disposal of the secondary wastes.

1.2 Purpose and Scope

The work documented in this report is part of PNNL's effort to conduct an initial evaluation (i.e., screening) of candidate stabilization technologies that have the potential to successfully treat liquid effluent produced by the WTP as part of the secondary waste stream. Four candidate stabilization technologies were identified as viable and were selected for further evaluation as part of a Phase I secondary waste form testing program. The candidate stabilization technologies selected include Cast Stone, DuraLith alkali-aluminosilicate geopolymer, FBSR encapsulated in a geopolymer matrix, and a Ceramicrete phosphate bonded ceramic. This report documents results of screening tests on the encapsulated FBSR product waste form. Separate reports are being prepared on the development and optimization of the other three waste forms.

1.3 Report Contents and Organization

Section 2 of this report provides background information on the FBSR process. The ensuing sections of this report document the materials and steps used to prepare the simulant (Section 3.0), as well as the batches of encapsulated FBSR product (Section 4.0). Section 5.0 describes the methods used to characterize and evaluate the processes that affect contaminant release from the encapsulated FBSR product. The results collected to date from these methods are presented, discussed, and summarized in Sections 6.0, 7.0, and 8.0.

2.0 FBSR Overview

This section provides background information on the FBSR product and the FBSR process.

2.1 FBSR Process Description

The FBSR process was designed by THOR Treatment Technologies, LLC (TTT) to treat radioactive wastes (U.S. Patents 6,280,694; 7,001,800; 7,125,531). The THOR FBSR process is being used commercially to process both liquid and solid low-level radioactive waste (LLRW) waste streams, including ion exchange resins, charcoal, graphite, sludge, oil, and solvents that contain up to 400 R/hr radioactivity (Mason et al. 2003). The FBSR granular product used in the current testing was simulated waste prepared at the FBSR Engineering Scale Technology Demonstration (ESTD) facility in Golden, Colorado. Figure 2.1 shows the flowsheet for the ESTD.

In the proposed application of FBSR to Hanford wastes, a clay mineralizing agent is added to the wastes in the feed tank. The resulting slurry is injected into the fluidized bed. The bed is fluidized with superheated steam at 670° to 800°C and near-ambient pressure. A carbon source, such as coal, wood product, or sucrose, is injected into the bed as a fuel source and reducing agent. Within the fluidized bed, the waste-feed droplets coat the bed particles and rapidly dry. Nitrates, nitrites, and organics are destroyed (TTT 2009, Vora et al. 2009). Organic nitrogen is converted to N₂, and organic carbon is converted to CO or CO₂ (Olson et al. 2004). In the presence of a reducing agent such as organic carbon, nitrates and nitrites are converted to nitrogen gas (Vora et al. 2009). In addition, the steam reforming process reacts with organics to form carbon monoxide, hydrogen, and some hydrocarbon gases. With the addition of oxygen, these gases oxidize to form carbon dioxide and water vapor. The FBSR process can destroy organic constituents of the initial waste fluids, including RCRA and Toxic Substances Control Act (TSCA) organics (Mason et al. 2003).

In the steam environment at 700° to 750°C, the clay mineralizing agent injected with the wastes becomes unstable as hydroxyl groups are driven out of the clay structure (Jantzen 2008). The clays become amorphous, and the silicon and aluminum atoms become very reactive. Alkali elements, including sodium, potassium, and cesium in the wastes, “alkali activate” the unstable Al³⁺ to form the new mineral phases. The other waste component cations and anions are captured in the cage structures as the sodium aluminosilicate minerals form.

The granular product is removed from the FBSR either as product from the bottom of the bed or as particulates removed from the fluidizing gases by the high temperature filter (HTF). These two materials are then combined and encapsulated in a binder for final disposal. A binder has not been selected for the FBSR waste form. The FBSR waste form tested here was prepared by encapsulating the FBSR granular product in a geopolymer matrix prepared by mixing fly ash and a sodium hydroxide solution.

2.2 FBSR Product Description

The FBSR waste form is composed of two main components. The wastes are processed in the FBSR to form a granular product. This is the primary waste form. The granular product is then encapsulated in a binder material to produce a monolithic form to limit dispersability and provide some structural integrity for subsidence prevention in the disposal facility. The primary product from the FBSR process is a granular product composed of sodium aluminosilicate minerals. The sodium aluminosilicate FBSR granular product is a multiphase mineral assemblage of sodium aluminosilicate (NAS) feldspathoid minerals (sodalite, nosean, and nepheline) with cage and ring structures that sequester anions and cations

(Jantzen et al. 2007). Nepheline is the basic sodium aluminosilicate mineral with the formula $\text{Na}_2\text{O} \cdot \text{Al}_2\text{O}_3 \cdot 2\text{SiO}_2$. When sulfates are captured within the cage structure, nosean forms with the formula $3\text{Na}_2\text{O} \cdot 3\text{Al}_2\text{O}_3 \cdot 6\text{SiO}_2 \cdot \text{Na}_2\text{SO}_4$. When chlorides are captured within the cage structure, sodalite forms with the formula $3\text{Na}_2\text{O} \cdot 3\text{Al}_2\text{O}_3 \cdot 6\text{SiO}_2 \cdot 2\text{NaCl}$. Depending on the waste compositions, process additives such as magnetite are included to form iron-bearing spinel minerals to sequester Cr and Ni in the waste. (Jantzen et al. 2007). Minor waste components then substitute inside the cage structures or attach to the cage or ring structures through ionic bonds with oxygen in the mineral structure. (Jantzen 2008).

The FBSR granular product is composed of two fractions from the FBSR process. Solids collected from the bottom of the fluidized bed are captured in the product receiver (PR). Figure 2.1 shows a photograph of the PR material from the 2008 Hazen pilot-scale test with the Hanford LAW simulant. The PR material includes residual carbon from coal or wood products used in the FBSR as an energy source and as a reductant. The PR material may also include residual alumina used as an initial seed material when the FBSR is first started up. Solids leaving the FBSR entrained in the fluidizing gases are captured in the high-temperature filter.

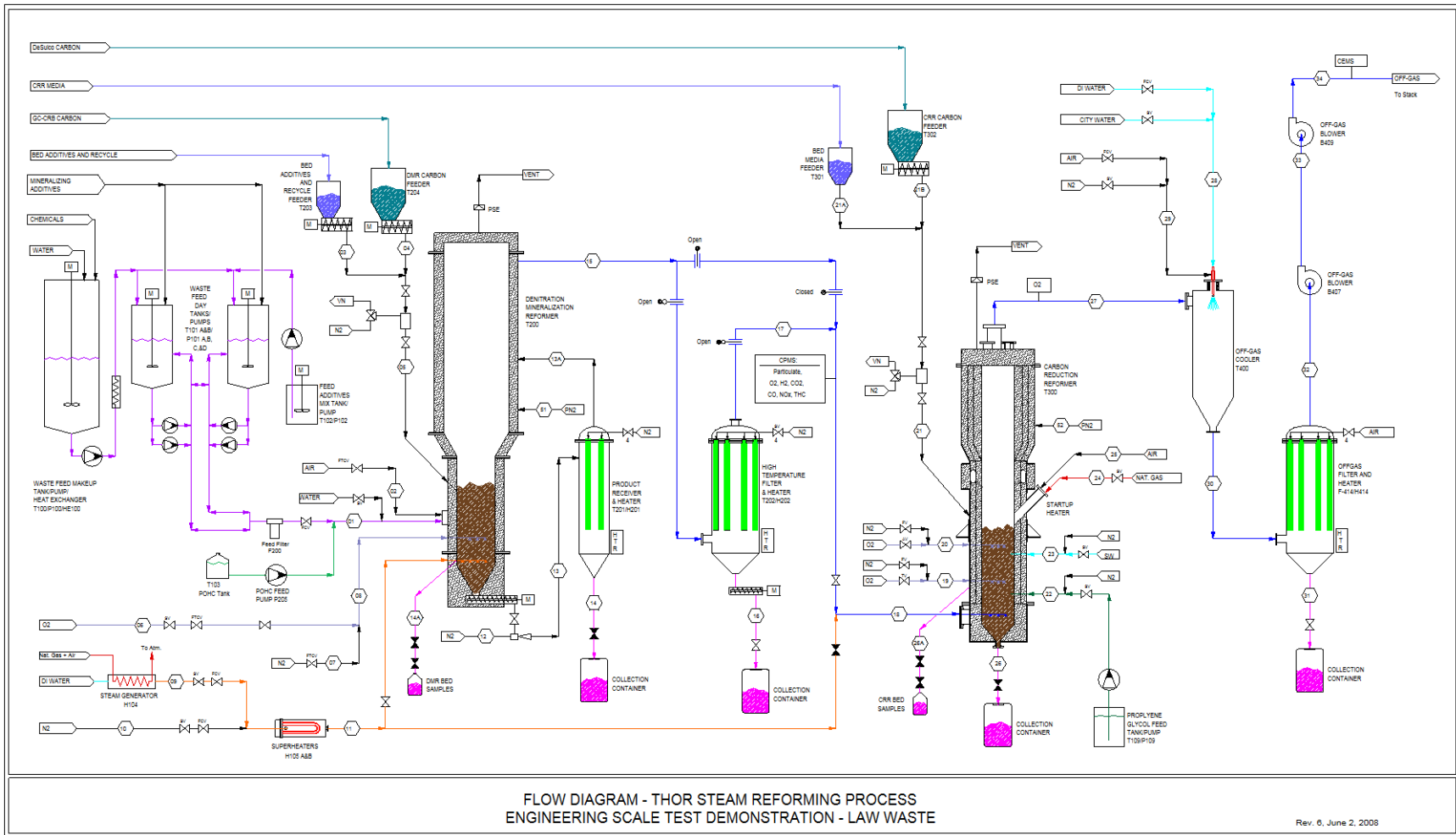


Figure 2.1. ESTD Flow Diagram for the Hanford WTP-SW and LAW FBSR Process Demonstration (from TTT 2009)

3.0 FBSR Simulant Feed

The integrated THOR[®] FBSR process was demonstrated at the ESTD unit built and operated at the Hazen Research facility in Golden, Colorado. This engineering scale process with full fluidized bed capability was used to process simulated WTP secondary waste (WTP SW). The discussion below is intended to summarize the FBSR simulant feed composition.

It has previously been shown that the THOR[®] FBSR process is effective at converting certain LAW liquid wastes into insoluble, mineralized solid products capable of immobilizing radioactive and hazardous metal constituents. DOE, as part of the Advanced Remediation Technologies (ART) Project, chose to demonstrate this process on Hanford LAW and WTP SW simulants as a potential waste stabilization process. For the THOR[®] FBSR ESTD pilot plant test, a secondary waste stream was formulated based on the combined liquid effluent from the Submerged Bed Scrubber (SBS) condensate, the Wet Electrostatic Precipitator (WESP) drainage, and the Caustic Scrubber effluent. This simulant was for a flowsheet option in which the planned phased startup of WTP would result in the operation of the LAW and HLW facilities before the Pretreatment Plant becomes available. The effluent streams designed to purge the LAW process loop (and not able to terminate at the Pretreatment Plant as designed) would require a secondary waste form alternative.

Currently, the WTP secondary waste refers to the combination of the LAW off-gas Caustic Scrubber^(a) effluent, Treated LAW Evaporation Process System (TLP) evaporator condensate, and Waste Feed Evaporation Process System (FEP) evaporators condensate to be transferred to the ETF for treatment and solidification. The other WTP SW immobilization waste form candidates (Cast Stone, DuraLith geopolymer, and Ceramicrete) selected for the secondary waste form screening effort are to be formulated to the current secondary waste feed stream, based on mass-balance-derived estimates. The THOR[®] FBSR supplied samples contain the ESTD process product resulting from the LAW off-gas effluent loop estimates and thus contain surrogate radionuclide and hazardous constituent concentrations at differing levels.

Aqueous simulant solutions of metal salts were prepared for use as WTP SW waste feed streams in the ESTD pilot plant FBSR. The liquid WTP SW simulant feed stream composition for the ESTD demonstration was developed based on the combined LAW SBS, WESP, and caustic scrubber effluent prediction as calculated by the G2 model run (TTT 2009). Organics were not included in the WTP SW test (Vora et al. 2009).

Components selected for inclusion in the WTP SW simulant are presented in Table 3.1 with their target test concentrations and the basis for their selections. The first column lists the components, the next five columns identify the rationale used to select the particular component, and the last column indicates the target molar concentration. Table 3.2 shows a comparison of the various simulants used for secondary waste form testing. Included are the simulants used in the 2006 low temperature immobilization study of DuraLith, Ceramicrete, and a hydroceramic cement (Russell et al. 2006), the Phase 1 and Phase 2 simulants used in the Secondary Waste Form Testing project evaluation of Cast Stone, Ceramicrete, and DuraLith (Sundaram et al. 2011) and the FBSR WTP-SW simulant (TTT 2009). All simulants have been normalized to 2 M sodium.

(a) The LAW off-gas Caustic Scrubber is the final unit operation before exhausting to the atmosphere and removes iodine and provides final NO_x and SO_x destruction.

Table 3.1. Selection Basis for Constituents WTP SW Simulant Solution (from TTT 2009)^(a)

Components	Selection Basis ^(a)					mol/L
	1	2	3	4	5	
Ag ⁺			X			5.75E-08
Al/Al ³⁺		X				4.34E-04
As ⁺⁵			X			7.01E-06
B ⁺³	X					8.91E-03
Cl ⁻	X					7.13E-03
CO ₃ ⁻²	X					1.35E-02
Cr/Cr ⁺³		X	X			4.07E-04
Total Cs ⁺ (bounds ¹³⁷ Cs)				X		9.88E-10
F	X					1.47E-02
Hg ⁺²			X			8.65E-07
K ⁺		X				7.04E-04
Na ⁺	X				X	6.17E-02
NH ₃ /NH ₄	X				X	1.97E-02
Ni ⁺²			X			3.08E-02
NO ₂ ⁻	X				X	2.45E-03
NO ₃ ⁻	X				X	3.99E-03
OH ⁻					X	5.40E-05
Pb ⁺²			X			8.84E-07
PO ₄ ⁻³		X				4.95E-04
Si ⁺⁴		X				1.21E-03
SO ₄ ⁻²		X				3.68E-04
Zn ⁺²		X				4.91E-04
Sb			X			2.26E-06
Ba			X			3.58E-08
Cd			X			4.51E-08
Se			X			1.03E-05
Tl			X			2.25E-06
Re(⁹⁹ Tc)				X		7.63E-06
I (¹²⁹ I)				X		5.30E-07

(a) Following are the specifics of the selection basis:

1= Component included 90% of solute mass/moles

2= Component included 99% of solute mass/moles

3= Component in list for Constituents of Concern

4= Radionuclide of Interest

5= Added as characteristic of solution

Target constituent concentrations in the simulant were increased to enhance the detectability of the minor constituents in the FBSR off-gas and products in an effort to provide information for mass balance calculations and to measure the immobilization performance of the FBSR waste product and encapsulated product monolith. The concentration of Re (surrogate for ⁹⁹Tc) was increased by a factor of 10, Ni and Pb by a factor of 100, Ag by 1,000, and Cs by 1,000,000. Target concentrations of Ba, Cd, Sb, Se, and Tl were increased to levels 1000× the analytical detection limit in the feed solution. This was done to have reasonably high concentrations to facilitate Toxicity Characteristics Leaching Procedure (TCLP) measurements and mass balance calculations.

(a) Table 4-5, “Report for Treating Hanford LAW and WTP SW Simulants: Pilot Plant Mineralizing Flowsheet.” April 2009, THOR Treatment Technologies, LLC.

Table 3.2. Compositions of Simulants Used in Secondary Waste Form Testing

	Phase 1 ^(a)	Phase 2 Simulants ^(b)				FBSR	LTI ^(d)
	Mole/Liter	Baseline Mole/Liter	Cluster 1 Mole/Liter	Cluster 2 Mole/Liter	Mixed Mole/Liter	WTP-SW Mole/L	Mole/Liter
Na	2.00E+00	2.00E+00	2.00E+00	2.00E+00	2.00E+00	2.00E+00	2.00E+00
Al(OH) ₃	2.30E-01	1.88E-01	2.28E-01	1.84E-01	8.48E-02	4.11E-01	1.10E-02
Si	---	3.76E-03	4.08E-03	1.55E-03	2.78E-02	1.35E-02	---
K	---	1.16E-03	1.30E-03	4.36E-03	5.74E-02	7.50E-03	---
NH ₄ ⁺	---	---	---	---	8.82E-01	2.19E-01	---
OH ⁻	1.20E+00	7.96E-01	8.70E-01	4.90E-01	2.04E-08	1.17E+00	9.40E-02
NO ₃ ⁻	6.90E-01	6.56E-01	3.80E-01	7.94E-01	2.26E+00	1.49E+00	1.80E-02
CO ₃ ⁻²	1.50E-06	4.56E-02	9.32E-02	7.88E-02	2.08E-02	1.50E-01	9.60E-01
Cl ⁻	---	4.50E-02	4.34E-02	5.82E-02	2.08E-02	7.95E-02	---
NO ₂ ⁻	---	2.40E-02	2.10E-02	7.66E-02	8.62E-02	2.70E-02	---
PO ₄ ⁻³	1.70E-02	1.37E-02	9.70E-03	1.21E-02	1.02E-02	5.25E-03	---
SO ₄ ⁻²	9.70E-03	8.82E-03	1.16E-02	1.03E-02	8.72E-02	3.75E-03	---
F ⁻	---	1.11E-03	7.50E-04	8.84E-04	2.04E-08	1.64E-01	---
Cr	3.70E-04	4.06E-04	4.06E-04	4.06E-04	2.18E-03	4.54E-03	2.80E-04
Ni	---	---	---	---	---	3.43E-3	---
Zn	---	---	---	---	---	5.46E-03	---
B	---	---	---	---	---	9.90E-02	---
Cs	---	---	---	---	---	1.10E-02	---
Ag	2.50E-04	1.25E-05	1.25E-05	1.25E-05	4.70E-05	6.45E-04	2.20E-04
As	---	6.96E-05	6.96E-05	6.96E-05	3.22E-05	7.50E-05	---
Cd	5.00E-05	3.14E-06	3.14E-06	3.14E-06	4.32E-05	6.52E-04	1.40E-05
Hg	3.30E-05	2.26E-05	2.26E-05	2.26E-05	1.06E-05	---	2.40E-06
Pb	7.90E-04	1.80E-05	1.80E-05	1.80E-05	1.66E-05	9.82E-04	1.50E-04
Sb	---	---	---	---	---	1.20E-03	---
Ba	---	---	---	---	---	1.50E-05	---
Se	---	---	---	---	---	1.85E-03	---
Tl	---	---	---	---	---	7.20E-04	---
Re	---	3.62E-05	3.62E-05	3.62E-05	1.12E-03	8.47E-04	6.00E-07
⁹⁹ Tc ^(d)	1.30E-05	6.10E-05	6.10E-05	6.10E-05	1.88E-03	---	---
I	2.90E-06	9.24E-06	9.24E-06	9.24E-06	1.26E-04	7.50E-04	2.90E-06
¹²⁹ I ^(d)	---	1.91E-07	1.91E-07	1.91E-07	2.60E-06	---	---
TOC	2.30E-01	1.88E-01	2.28E-01	1.84E-01	8.48E-02	---	1.80E-01

(a) Pierce et al. 2010. *Secondary Waste Form Screening Test Results - Cast Stone and Alkali Alumino-Silicate Geopolymer*. PNNL-19505, Richland, Washington.

(b) Sundaram SK, J Chun, W Um, KE Parker, C-W Chung, JH Westsik Jr, ME Valenta, ML Kimura, SG Pitman, and CA Burns. 2011. *Secondary Waste Form Development and Optimization—Cast Stone*. PNNL-20159, Pacific Northwest National Laboratory, Richland, Washington.

(c) Russell et al. 2006. *Low Temperature Waste Immobilization Testing*. PNNL-16052, Rev 1.

(d) Ci/Liter.

The WTP SW simulant feed stream was prepared by combining a “lite” solution containing the simulant constituents other than the heavy metals with a second feed stream consisting of the heavy metals in solution and a third feed stream consisting of the kaolinite clay additive. The clay additive (mineralizing additive) consisted of a 55% OptiKasT and 45% Sagger XX mixture. The clay mixture composition is provided in Table 3.3.

The WTP SW simulant FBSR feed slurry containing the target constituents was added to the mineralizing clay at 307 g of clay per liter of waste simulant. Table 3.4 illustrates the target simulant

concentrations for the constituents of interest added to the clay solution and thus in the final target FBSR feed concentration(s).

Table 3.3. Composition of Mineralizing Clay Used for WTP SW Simulant^(a)

Oxide	Clay Type		
	OptiKasT %	Sagger XX %	55% OptiKasT/45% Sagger XX Mixture %
Al ₂ O ₃	37.76	31.48	34.94
SiO ₂	44.67	55.09	49.35
Fe ₂ O ₃	0.55	0.84	0.68
TiO ₂	1.67	0.63	1.20
CaO	0.04	0.13	0.08
MgO	0.03	0.15	0.08
Na ₂ O	0.02	0.09	0.06
K ₂ O	0.11	0.65	0.36
P ₂ O ₅	0.07	0.00	0.04
H ₂ O	15.08	10.94	13.22
Sum	100.0	100.0	100.0

(a) Table 4-3, "Report for Treating Hanford LAW and WTP SW Simulants: Pilot Plant Mineralizing Flowsheet," April 2009, THOR Treatment Technologies, LLC.

Table 3.4. Composition of WTP SW Simulant Solution with Clay Added^(a)

Component	Component	Target Component Concentration with 307 g clay/L [g/L]
Hydroxide	OH ⁻	23.850
Carbonate	CO ₃ ²⁻	10.773
Sulfate	SO ₄ ²⁻	0.471
Chloride	Cl ⁻	3.370
Fluoride	F ⁻	3.727
Iodide	I ⁻	0.090
Nitrate	NO ₂ ⁻	1.502
Phosphate	PO ₄ ³⁻	0.764
Aluminum	Al	64.171
Potassium	K	1.180
Sodium	Na	50.489
Nitrate	NO ₃	110.716
Silver	Ag	0.083
Arsenic	As	0.007
Barium	Ba	0.003
Cadmium	Cd	0.088
Chromium	Cr	0.282
Cesium	Cs	1.751
Nickel	Ni	0.241
Lead	Pb	0.244
Rhenium	Re	0.189
Antimony	Sb	0.175
Selenium	Se	0.175
Thallium	Tl	0.175
Ammonium	NH ₄ ⁺	4.728
Boron	B	1.284
Silicon	Si	63.971
Zinc	Zn	0.428
Iron	Fe	1.311
Titanium	Ti	1.983
Calcium	Ca	0.151
Magnesium	Mg	0.138

(a) Table 4-6, "Report for Treating Hanford LAW and WTP SW Simulants: Pilot Plant Mineralizing Flowsheet." April 2009, THOR Treatment Technologies, LLC.

3.1 FBSR Processing Parameters

Two WTP SW simulant tests were run, the first with a Denitration and Mineralization Reformer (DMR) temperature of about 680°C and the second with a DMR temperature of about 700°C. The Carbon Reduction Reformer (CRR) was operated at the optimal temperature of about 950°C. Table 3.5 through Table 3.7 summarizes the operational conditions of the two WTP SW simulant tests (TTT 2009).

The WTP SW simulant tests were performed without adding Principal Organic Hazardous Constituents (POHCs), benzene, as the WTP SW waste steam is not expected to contain organics.

Table 3.5. Operating Conditions for the WTP SW Production Test^(a)

Test Number	Start/Stop	Test Duration (hours)	Feed Rate (gpm)	DMR Temp (°C)	CRR Temp (°C)	Approximate Clay Conc. (g/L)	POHC	Off-gas Testing Methods
ART-P-2A	02May 02:00/ 05May 07:30	75	0.2	680	950	307	No	29, 5/26A
ART-P-2B	05May 07:30/ 06May 10:29	27	0.2	700	950	307	No	None
ART-P-2 Total		102						

(a) Table 5-2, "Report for Treating Hanford LAW and WTP SW Simulants: Pilot Plant Mineralizing Flowsheet", April 2009, THOR Treatment Technologies, LLC.

Table 3.6. Summary of DMR Production Test Operating Parameters^(a)

Condition		WTP SW		
		ART-P-2A	ART-P-2B	Entire P-2
Start		5/2/2008 02:00	5/5/2008 07:30	
Finish		5/5/2008 07:30	5/6/2008 10:29	
Duration	Hours	75	27	102
Simulant	gpm	0.19	0.20	0.20
N ₂ purge	scfm	53.4	52.5	53.2
DMR coal	lb/hr	35.6	44.0	37.8
DMR Gas Additions	scfm	48.5	49.0	48.5
HTF	Δp (inches water)	25.6	27.1	26.2
DMR freeboard pressure	psig	4.2	4.3	4.2
DMR bed height	inches	44.5	45.5	44.8
DMR bed fluidized specific gravity	---	0.85	0.69	0.81
DMR- bed temp. (6" NNW)	°C	680	702	686
DMR- bed temperature (24" E)	°C	679	700	685
DMR- freeboard temperature (92" S)	°C	677	694	682
DMR- outlet gas temperature	°C	589	602	592
HTF outlet gas temperature	°C	448	454	449

(a) Table 7-4, "Report for Treating Hanford LAW and WTP SW Simulants: Pilot Plant Mineralizing Flowsheet," April 2009, THOR Treatment Technologies, LLC.

Table 3.7. Summary of CRR and Off-gas Production Test Operating Parameters^(a)

Condition		WTP SW		
		ART-P-2A	ART-P-2B	Entire P-2
CRR Gas Additions	scfm	66.0	67.1	66.3
CRR outlet O ₂ (%)	%	3.1	3.0	3.1
CRR carbon	lb/hr	6.59	4.94	6.29
CRR propylene glycol	lb/hr	37.9	38.0	37.9
OGC atomizing air	scfm	5.4	2.8	4.7
OGC cooling water	gpm	.48	.51	.49
Mass flow rate to stack	lb/min	18.32	18.84	18.41
CRR bed height	inches	47.6	46.4	47.3
CRR bed specific gravity (fluidized)	----	2.11	2.13	2.11
CRR freeboard pressure	Pressure (psia)	11.6	11.6	11.6
OGF	Δp (inches water)	1.1	0.8	1.1
CRR- bed (8" W)	°C	945	948	946
CRR- free-board T (54" SE)	°C	950	952	951
CRR- freeboard T (150" NE)	°C	916	926	919
CRR- outlet gas T	°C	826	840	829
OGC outlet gas T	°C	206	200	203
OCF outlet gas T	°C	171	172	172
Stack T	°C	171	171	171

(a) Table 7-5, "Report for Treating Hanford LAW and WTP SW Simulants: Pilot Plant Mineralizing Flowsheet," April 2009, THOR Treatment Technologies, LLC.

4.0 FBSR Secondary Waste Forms

The granular product produced by processing WTP SW simulated waste in the engineering scale FBSR built and operated at the Hazen Research facility was sent to Savannah River National Laboratory (SRNL) for final encapsulation. The encapsulation formulation summary is presented below.

4.1 FBSR Granular Product Preparation

The mineralized solid products for WTP SW tests ART-P-2A and ART-P-2B were collected at the DMR discharge via the PR and at the HTF downstream of the DMR off-gas port (TTT 2009). Test ART-P-2A with a duration of about 75 hours processed 899.56 gallons of simulant feed into 1001.1 lb of DMR product and 2766 lb of HTF product, also referred to as fines. Test ART-P-2B processed 323.49 gallons of feed in 27 hours, resulting in 334.34 lb of DMR product and 1025.6 lb of fines. Test ART-P-2B was run from 5/5/2008 07:30 until 5/6/2008 10:29 and generated the FBSR product used in the FBSR secondary waste form monoliths supplied for PNNL screening activities. Table 4.1 summarizes the products collected for the two WTP SW tests.

Table 4.1. Product Summary for WTP SW Tests^(a)

Test	Start	End	Operating Hours	Simulant Processed (gal)	Product:				
					DMR + PR		Fines: HTF		
					(lb)	(lb/hr)	(lb)	(lb/hr)	
ART-P-2A	5/2/2008 02:00	5/5/2008 07:30	75	899.56	1001.1	13.35	2766	36.88	
ART-P-2B	5/5/2008 07:30	5/6/2008 10:29	27	323.49	334.34	12.38	1025.6	37.99	
Totals			102	1223.05	1335.44	13.09	3791.6	37.17	
								Product:Fines Ratio	0.35

(a) Table 7-3, "Report for Treating Hanford LAW and WTP SW Simulants: Pilot Plant Mineralizing Flowsheet", April 2009, THOR Treatment Technologies, LLC.

The larger mineralized product particles were collected from the DMR product discharge and from the Product Receiver. A sample of the DMR bed material is illustrated in Figure 4.1 (TTT 2009). A 5-mm scale is visible in the lower right corner of the photograph. Product particles appear to be mostly spherical in shape with a nodular appearance. The large dark particles are unreacted carbon remnants from the carbon addition used as an energy source and reductant in the DMR. Figure 4.2 is a photograph of the DMR granular product recovered from the PR vessel, which retains the material drained off the bottom of the DMR (TTT 2009).

The DMR and PR material was screened to remove particles larger than ~1.0 mm as these were primarily large carbon particles. These particles would be removed in the full-scale process and returned to the DMR feed, and thus, the removal of large carbon particles was representative of the material from a full-scale process.

Fine solids elutriated from the top of the DMR by the off-gas stream were collected in the HTF vessel, and the vessel was periodically emptied. Individual particles tended to clump together, but were relatively easy to collect. Figure 4.3 shows two micrographs of the HTF product magnified at 100× and 400×. A 300-μm scale is shown on the bottom left corner of the 100× micrograph, and a 90-μm scale is shown on the 400× image.

The particle size distribution of the HTF fines presents a generally bi-modal size distribution, with modes at ~0.25 microns and ~30 microns. The first mode is thought to be due to a spray drying effect in the DMR, and the second is likely due to attrition in the DMR. The majority of the mineralizing clay additives are ~8 microns, which is between the two size distribution modes.

Table 4.2 gives the chemical composition of the granular product captured in the PR, the HTF, and the off-gas filter (OGF) as reported by Vora et al. (2009).



Figure 4.1. Typical DMR Bed Material Sample. The large dark particles are the unreacted carbon.^(a)

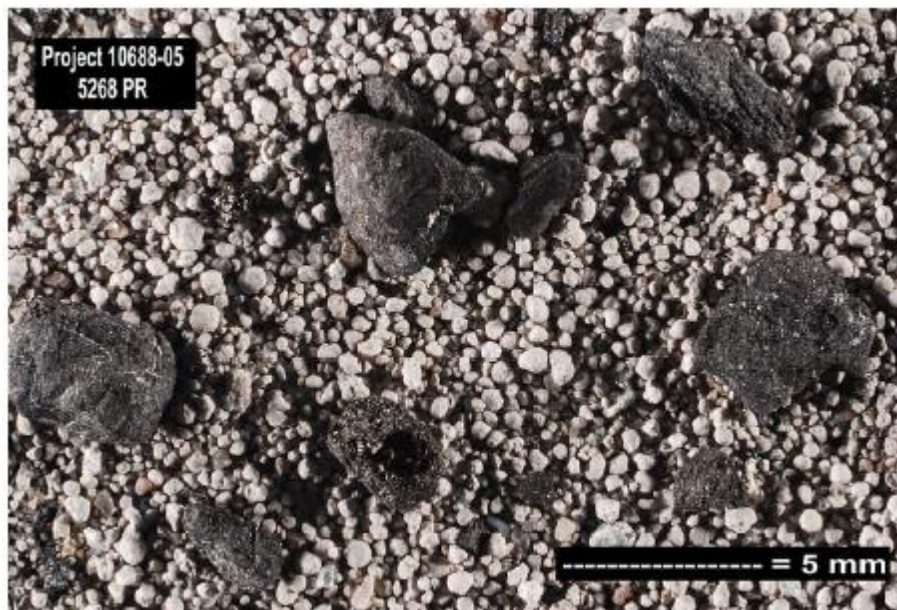


Figure 4.2. Typical PR Material Sample^(a)

(a) Figure 10-1, “Report for Treating Hanford LAW and WTP SW Simulants: Pilot Plant Mineralizing Flowsheet,” April 2009, THOR Treatment Technologies, LLC.

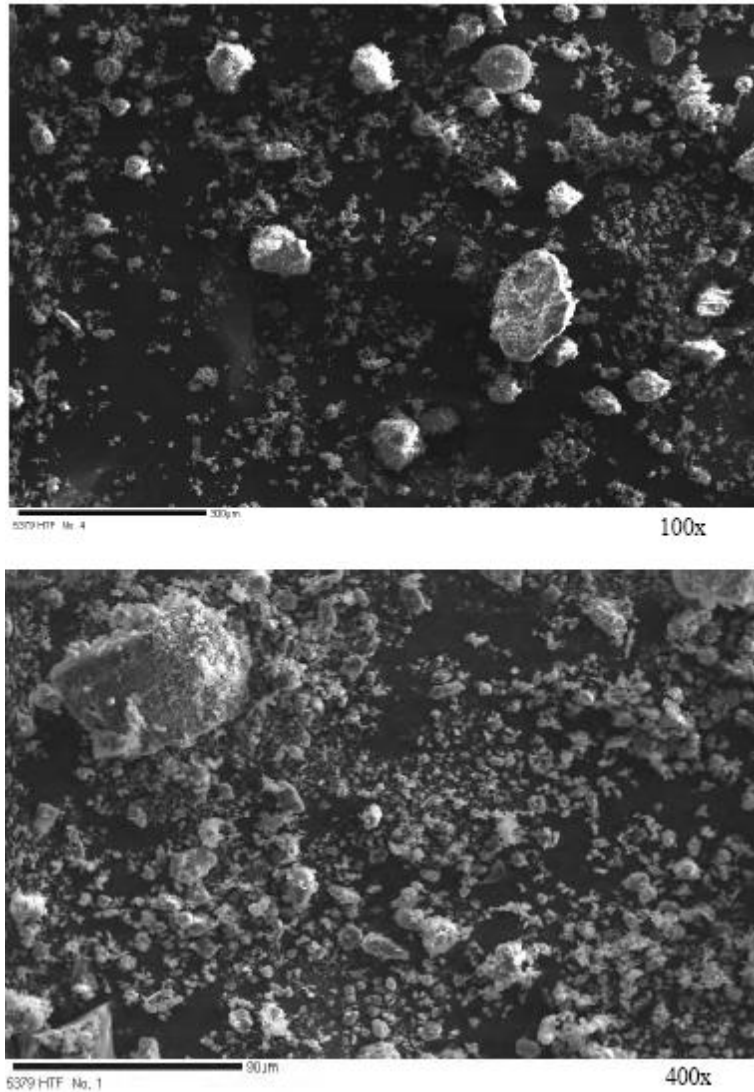


Figure 4.3. Microprobe Photographs of Product Fines Collected from the HTF^(b)

-
- (a) Figure 10-2, “Report for Treating Hanford LAW and WTP SW Simulants: Pilot Plant Mineralizing Flowsheet,” April 2009, THOR Treatment Technologies, LLC.
- (b) Figure 10-3, “Report for Treating Hanford LAW and WTP SW Simulants: Pilot Plant Mineralizing Flowsheet,” April 2009, THOR Treatment Technologies, LLC.

Table 4.2. Average Composition (wt%) of FBSR Product From Hazen Research Facility 2008 WTP-SW Tests (from Vora et al. 2009)

Constituent	OGF	HTF	PR
Al	27	18	28
Ag	0.01	0.02	0.02
As	0.01	0.004	0.001
B	0.02	0.13	0.25
Ba	0.00	0.02	0.01
Ca	0.13	0.14	0.05
Cd	0.05	0.03	0.03
Fe	0.4	0.6	4.5
Mg	0.02	0.03	0.03
I	0.05	0.03	0.02
Na	8	10	7
K	0.08	0.2	0.2
Si	9	15	10
Sb	0.03	0.04	0.02
Se	0.03	0.02	0.004
Ti	0.4	0.6	0.4
Tl	0.03	0.09	-
Cs	0.14	0.36	0.12
Cr	0.02	0.04	0.03
Pb	0.10	0.05	0.06
Ni	0.06	0.06	0.04
Zn	0.003	0.04	0.08
Re	0.01	0.02	0.04
Cl	0.18	0.15	0.04
F	0.15	0.47	0.08
NO ₃	-	-	-
NO ₂	-	-	-
PO ₄	0.4	0.4	0.2
SO ₄	0.8	0.4	0.3
CO ₃	-	-	-
Total Carbon	2.2	14.8	7.6
O (calculated)	37	38	40

4.2 FBSR Granular Product Encapsulated in Geopolymer

The final waste form testing was performed at SRNL to determine the best binder material candidates for producing solid waste forms containing the FBSR WTP SW granular products. SRNL evaluated a number of binder technologies for the FBSR LAW granular product and selected a geopolymer material designated GEO-7 as providing the best overall performance for making monoliths for the simulated LAW stream. The GEO-7 geopolymer was also used as the binder for the WTP-SW secondary waste stream. No independent down-selection of binder formulations was done for the WTP-SW FBSR granular product. The mineralized FBSR product will have to be encapsulated into a final monolithic waste form before disposal at the IDF to eliminate dispersability and to provide a waste form with a compressible strength greater than 500 psi.

The selected FBSR products collected from the DMR and PR were screened to remove particles greater than about 1 mm in size (TTT 2009). These particles were assumed to be unreacted carbon used as an additive in the DMR to add energy and reductant to the THOR® process. These carbon particles would be removed and returned to the DMR inlet in the full-scale process, and therefore, their removal provided material representative of that expected in the full-scale process. The DMR materials were combined with a representative amount of product fines from the HTF to meet the product to fines ratio of 0.33. Since this material was intended to be representative of that produced in a production facility and then incorporated into a final waste form, the carbon particles smaller than the 1-mm particles initially removed were not roasted out of the FBSR mineral product. A small quantity of carbon less than 900 µm in size, perhaps 2 to 5 wt%, was not removed from the granular product and was therefore incorporated into the monolithic waste forms.

Table 4.3 summarizes the data measured for some of the WTP SW large-scale monolith cylinders used for formulating the final waste forms. The final test monoliths were prepared by mixing the FBSR solids with a geopolymer binder. The GEO-7 geopolymer (amorphous to semi-crystalline, three-dimensional, silico-aluminate material) was prepared by mixing fly ash with sodium hydroxide solution. This binder formulation used fly ash in place of the heat-treated meta-kaolin clay, and test monoliths were prepared with a waste loading of 65.2%^(a).

PNNL was supplied six previously prepared 2-in.-diameter by 4-in.-long cylindrical monolithic waste forms containing WTP SW simulant FBSR product encapsulated in geopolymer (GEO-7). The FBSR product loading of the supplied waste forms was reported to be 65.2%^(a). The FBSR product used in the supplied monoliths was collected from WTP SW simulant test P-2B, and the reformer product was screened and blended in a PR/HTF ratio of 0.33.

(a) Waste loading published at 68.8% in “Report for Treating Hanford LAW and WTP SW Simulants: Pilot Plant Mineralizing Flowsheet,” RT-21-002 rev. 1, April 2009, THOR Treatment Technologies, LLC. Test Plan (57925-P2-T3-Rev. 1) review comments indicated that this value was corrected in a later revision.

Table 4.3. Data Measured for the Large-Scale Cylinders^(a)

Binder & Size	Compressive Strength (psi)	Cure Time (days)	Density (g/cc)	BET ^(b) Surface Area (m ² /g)
FON-2				
74.16 % waste loading				
3-in.-dia × 6-in.-dia cylinder	570	18	1.68	30.83
6-in.-dia × 12-in.-dia cylinder	420	28	1.67	30.83
S71-2				
74.16 % waste loading				
3-in.-dia × 6-in.-dia cylinder	820	17	1.67	8.99
6-in.-dia × 12-in.-dia cylinder	660	19	1.66	8.99
GEO-1				
67 % waste loading				
3-in.-dia × 6-in.-dia cylinder	890	14	1.83	12.55
6-in.-dia × 12-in.-dia cylinder	1710	19	1.83	12.55
GEO-7				
68.8 % waste loading				
2-in.-dia × 4-in.-dia cylinder ^(c)	2313	28	1.78	--
3-in.-dia × 6-in.-dia cylinder	1980	14	1.83	26.86
6-in.-dia × 12-in.-dia cylinder	520	28	NM	26.86

Table 10-9 "Report for Treating Hanford LAW and WTP SW Simulants: Pilot Plant Mineralizing Flowsheet," April 2009, THOR Treatment Technologies, LLC.

BET = Brunauer-Emmett-Teller.

From Jantzen et al. 2011. *Waste Form Qualification of Hanford Waste FBSR Mineral Product – Initial Results*. Project Briefing February 8, 2011, Savannah River National Laboratory, Aiken, SC.

5.0 FBSR Waste Form Characterization Methods

The materials and methods section describes the preparation techniques, approaches, solids characterization, and experimental test methods used to evaluate the release of contaminants of concern (COC) from encapsulated FBSR samples during the screening test.

5.1 Material Preparation Techniques

Two of the encapsulated FBSR monoliths supplied to PNNL were crushed to provide enough powdered sample material to determine the moisture content and specific surface area and for use in U.S. Environmental Protection Agency (EPA) draft Methods 1313 and 1316, which are discussed in more detail later in this section. The powder samples were prepared by breaking each of the two monoliths into large chunks with a hammer and placing the chunks into a ball mill for further processing. The crushed material was then sieved to a <0.3-mm-diameter size fraction (U.S. sieve 50 mesh). The material of both monoliths was combined to prepare the tests indicated below.

To determine the moisture content of the powdered monolith material, a 10-gram aliquot of powder, of <0.3-mm in diameter, was placed into a tared container and dried in an oven at 105°C until constant weight was achieved (ASTM 1998). With the onset of a constant weight, each container was removed from the oven, sealed, cooled, and reweighed. The moisture content in the powdered monolith material was calculated as the percentage weight change of the powder sample before and after oven drying (i.e., $[(\text{wet weight} - \text{dry weight}) / \text{dry weight}] \times 100$). The powdered material used to determine the moisture content was also used to analyze the surface area before it was discarded. All gravimetric measurements were performed with a calibrated balance.

The specific surface area (SSA) of the powdered monolith material was measured with a Micromeritics ASAP 2020 gas sorption, surface-area analyzer using the N₂-Brunauer-Emmett-Teller (BET) method (Brunauer et al. 1938). Each of the previously dried samples was reheated at 110°C under vacuum for a minimum of 5 hours to remove any water that may have been reintroduced between tests. The surface area was measured at liquid nitrogen temperature (~ 77 K) to allow any N₂ molecules to adsorb at the solid surface. The <0.3-mm-size fractions of powdered FBSR monolithed material resulted in a N₂-BET surface area measurement of $4.8 \pm 0.03 \text{ m}^2/\text{g}$.

5.2 Leachate Solution Characterization

All leachate solutions were monitored for pH, electrical conductivity (EC), alkalinity, major anions, major cations, and trace metals. The pH of the solution samples was measured with a solid-state pH electrode and a pH meter (Hanna, model HI 4521). Before the measurement, the pH probe was calibrated with National Institute of Standards and Technology (NIST) buffers (pH = 4.00, 7.00, 10.00, 12.00 and/or 13.00 at 25°C). The precision of the pH measurement was ± 0.1 pH units. An oxidation-reduction potential (Eh) probe (Hanna, 3131B) was used to measure the Eh of leachate solutions. A platinum 4-ring conductivity probe (Hanna, model HI 76312) with a temperature sensor was used to measure the EC of the leachate solutions. The sensor was calibrated with a range of purchased National Bureau of Standards (NBS) potassium chloride standard solutions, ranging from 0.001 M to 1.0 M. Approximately 20 mL of filtered leachate was used to measure the electrical conductivity. The alkalinity (mg/L as CaCO₃) was measured using a standard acid titration method (total alkalinity at pH = 4.5). The alkalinity procedure is equivalent to the U.S. Geological Survey (USGS) method in the National Field Manual for the Collection of Water-Quality Data (USGS 2004).

The concentrations of nitrate (NO_3^-), phosphate (PO_4^{3-}), and sulfate (SO_4^{2-}) in leachate solutions were determined using ion chromatography (IC) with a Dionex AS17C column. This methodology is based on EPA Method 300.0A (EPA 1984), with the exception of using the gradient elution of sodium hydroxide. The concentration of major cations was measured with inductively coupled plasma optical emission spectroscopy (ICP-OES) (Perkin Elmer OPTIMA 3300 DV [Waltham, MA] with a Perkin Elmer AS93+ autosampler) using high-purity calibration standards to generate calibration curves and verify continuing calibration during the analysis run. Because of the differences in the leachate cation concentration, a number of dilutions, ranging from 100 to 1.01 times, were used to obtain measurable concentrations of the cations of interest. Details of this method are found in EPA Method 6010B (EPA 2000a). Inductively coupled plasma mass spectrometry (ICP-MS) (Perkin Elmer ELAN DRC II with a Perkin Elmer AS93+ autosampler) was used to measure trace metals concentrations, including iodine, mercury, and rhenium. These measurements were performed following the PNNL-AGG-415 method (PNNL 1998), which is similar to EPA Method 6020 (EPA 2000b).

5.3 Solid Characterization

5.3.1 Chemical Composition

The crushed encapsulated FBSR product was milled again to <0.075 mm before chemical digestion to determine the elemental composition. Microwave-assisted strong acid digestions were conducted using 16 M HNO_3 , 12 M HCl , and 29 M hydrofluoric acid (HF). The powdered samples were prepared following EPA Method 3052 (EPA 1996). The solid-acid mixture (0.25 g/14 mL) was typically reacted for 1 hour at $90 \pm 5^\circ\text{C}$. A slight deviation was made because of the presence of undissolved solids using the typical approach. The reaction time was extended to between 2 and 3 hours, and the solid-to-acid ratio was reduced (0.1 g/30 mL). Upon complete dissolution of the sample, 3 mL of a 4.4 M of H_3BO_3 solution was added to the acid solution to neutralize the fluoride. The resulting solution was filtered through a 0.45- μm membrane and analyzed for rhenium and trace metals with ICP-MS and major cations and a limited number of nonmetals (e.g., phosphorus and sulfur) with ICP-OES. This method is not appropriate for anion concentrations (e.g., NO_3^- , chlorine, fluorine, and BO_3^-) due to the acids used in the dissolution procedure.

A separate chemical digestion is necessary to determine the iodide concentration in these samples because iodide can oxidize and volatilize at low pH. Therefore, to minimize volatilization, an alkaline fusion was used to determine total iodide concentration in the powder samples. The sample was mixed with 1.5 g of sodium peroxide and 1 g of sodium hydroxide in a crucible and heated at about 600°C for 15 minutes. The final fusion melt was cooled, and DIW was added. The final solution was filtered and submitted for iodide analysis using ICP-MS.

The carbon content of sediment/solid samples is determined with PNNL Technical Procedure: AGG-TOC-001 Operating of Carbon Analyzer (TOC-V + SSM-5000A + ASI (Shimadzu), which is similar to ASTM Method E 1915-01, Standard Test Methods for Analysis of Metal Bearing Ores and Related Materials by Combustion Infrared Absorption Spectrometry. The carbon content in all samples is determined using a Shimadzu Carbon analyzer Model TOC-V CSN with a SSM-5000A.

Sediment/solid samples are first analyzed for total carbon (TC) content by placing a sample aliquot into a ceramic combustion boat. The combustion boat is placed into the TC furnace introduction tube where it is sparged with ultra-pure oxygen for 2 minutes to remove atmospheric carbon dioxide (CO_2). The sample is then moved into the combustion furnace with an oxidation catalyst and heated to 900°C . The released carbon from the combustion is converted to CO_2 , which is swept from the combustion chamber by ultra-pure oxygen, dehumidified, and scrubbed to remove halogens. The carrier gas then

delivers the sample combustion products to the cell of a non-dispersive infrared (NDIR) gas analyzer where the carbon dioxide is detected and measured. The amount of CO₂ measured is proportional to the total carbon content of the sample.

Sediment/solid samples are then analyzed for inorganic carbon content by placing a sample aliquot into a ceramic combustion boat. The combustion boat is placed into an inorganic carbon introduction tube where it is sparged with ultra pure oxygen for 2 minutes to remove atmospheric carbon dioxide. A small amount (usually 0.6 mL) of 3 M phosphoric acid is then added to the sample, and the combustion boat is moved into the inorganic carbon combustion furnace where it is heated to 200°C. Ultra pure oxygen sweeps the resulting carbon dioxide through a dehumidifier and scrubber into the cell of an NDIR gas analyzer where the carbon dioxide is detected and measured. The amount of CO₂ measured is proportional to the inorganic carbon content of the sample.

The TOC for a solid sample is calculated from the difference of the total carbon analysis and the inorganic carbon analysis.

To measure loss on ignition, approximately 1 gram of oven-dried sample is weighed out in a pre-fired crucible. The crucible is placed in the center of a furnace at 550°C for 4 hrs. The crucible is placed in a desiccator and allowed to cool to ambient temperature. The crucible is weighed. This weight should represent the loss of organic carbon. After weighing, the crucible is placed in the center of a furnace at 950°C for 2 hrs. The crucible is placed in a desiccator and allowed to cool to ambient temperature. The crucible is weighed. This weight should represent the total loss on ignition.

5.3.2 X-Ray Diffraction

In addition to determining the chemical composition of the solid waste forms, X-ray diffraction (XRD) and scanning electron microscopy (SEM) with energy dispersive spectrometry (EDS) were used to characterize cured FBSR monolithed samples.

Ground samples of FBSR product, intact and ground monolith, and intact leached monolith samples were analyzed with XRD analysis to identify the crystalline phases that were present. The intact monolith samples were obtained by dry cutting (with a diamond impregnated blade) monoliths radially that resulted in circular ~5- to 8-mm-thick specimens. Also, the outer surface of an intact monolith was analyzed by using X-ray micro-diffraction analysis to identify any crystalline phases on the monolith surface.

Powder diffraction data were collected with a Panalytical X'Pert Bragg-Brentano diffractometer using Cu K α radiation ($\lambda = 1.5418 \text{ \AA}$), a graphite post-diffraction monochromator, and variable divergence and anti-scatter slits (illuminated length: 10 mm). Powdered specimens were loaded into traditional well-type aluminum holders with a cavity measuring $20 \times 15 \times 2 \text{ mm}$. Intact block specimens were supported on modeling clay in a custom holder positioned so that a flat surface was close to the plane of traditional sample holders.

The material on the outside curved surface of one of the samples was analyzed with a Rigaku D/Max Rapid II microdiffraction system. X-rays were generated (MicroMax 007HF) from a rotating Cr target ($\lambda = 2.2910 \text{ \AA}$) and focused through a 300- μm -diameter collimator onto a region of interest identified using the integral video microscope. Diffraction data recorded on a 2D image plate were integrated to give powder traces using the manufacturer's software.

The phases present were identified with the search/match capabilities of the JADE software (v9.3, Materials Data Inc., California). Reference patterns from the International Committee for Diffraction

Data (ICDD) database were visually compared to the experimental traces after background subtraction in JADE.

The surface morphology and composition of solid phases present in the encapsulated FBSR samples were analyzed with JSM-5900 SEM combined with EDS. For these analyses, an aliquot of sample was mounted with double-sided carbon tape attached to an aluminum stub. After being mounted, each sample was coated with palladium using an argon plasma sputter-coater. The FBSR monolith cylindrical sections, “pucks,” were baked out at ~60°C overnight to remove moisture, vacuum impregnated with epoxy, polished, and then coated with palladium. The SEM used to capture micrographs of these samples was a JSM-5900 (JEOL, Ltd. Tokyo, Japan) with a tungsten filament. An EDAX silicon-drifted 30-mm² detector (AMETEK, Berwyn, PA) was used to collect EDS spectra for qualitative and quantitative elemental analysis of scanned particles.

5.4 FBSR Waste Form Leaching Tests

The specific test methods used to screen the candidate waste forms need to provide a framework to 1) rapidly assess material performance, 2) provide some indication of the dominant release mechanism for each COC, 3) evaluate the strengths and weaknesses of a variety of materials (placing each material on a level playing field), and 4) gain regulatory acceptance by being a standard set of test methods approved by the regulatory community. Although these aforementioned criteria focus on the use of standard methods, these analyses need to be augmented with the specialized characterization techniques previously discussed to examine key processes affecting the release of COC from the waste form that correlates with changes in the measured leachate solution chemistry (increase in concentration of key COC). This type of integrated approach is expected to provide the defense-in-depth needed to evaluate each of the candidate liquid stabilization options effectively to support the decision for further testing.

To address the stated criteria, three draft test methods being developed for the EPA and the American National Standards Institute/American Nuclear Society (ANSI/ANS)-16.1 method were used to screen the supplied FBSR encapsulated waste form. Each of the EPA draft methods examines different aspects of material performance. These methods are currently undergoing EPA approval and are expected to be used to complement the TCLP method for disposal of specific materials, such as waste forms. The test methods used—draft EPA Methods 1313, 1315, 1316 and ANSI/ANS-16.1—are briefly discussed below.

5.4.1 EPA Draft Method 1313—pH Effects

The EPA draft Method 1313 (Liquid-Solid Partitioning as a Function of Extract pH) is a static test method where a set of parallel extraction experiments are conducted in dilute acid or base-laden deionized water (DIW) at a fixed pH (pH range from 4 to 12) and fixed liquid-to-solid ratio (10 mL/g) (EPA 2009a). Before starting the static test, a series of pre-titrations were conducted at a fixed liquid-to-solid ratio (10 mL/g) using <0.3-mm sized material. After a 24-hour period of mixing in the absence of acid or base additions, the sample slurry was centrifuged, the supernatant was removed, and it was used to determine the equilibrated pH. Since the measured pH of the leachate solutions for encapsulated FBSR product was high (pH ~12 to 13), a pre-titration was developed based upon dilute HNO₃ additions to decrease the pH from 12 to lower targeted values after 24 hours of equilibration. Analytical grade HNO₃ (Optima) was used to prepare a solution of 2 N HNO₃ for these experiments. Based upon the pre-titration results, test samples were prepared by mixing 10 g of <0.3-mm-sized material with DIW and a predetermined amount of 2 N HNO₃ and bringing the samples to volume with DIW, Figure 5.1. All samples were placed on a platform shaker and allowed to mix at room temperature (23 ±2°C) for 24 hours. After mixing, the extractant vessels were centrifuged (minimum at 4000±100 RPM) for 10±2 minutes, and the decanted

clear supernatant was filtered using a 0.45- μm polypropylene membrane syringe filter and collected in a vial with minimal head space and submitted for chemical analysis.

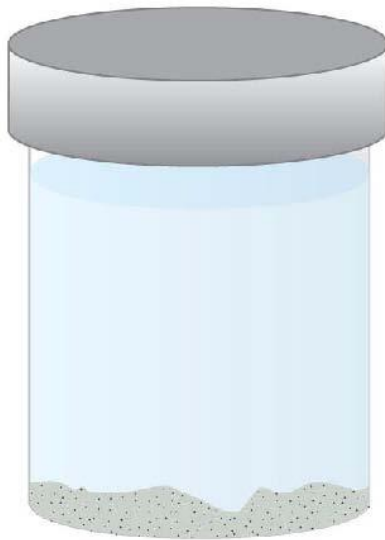


Figure 5.1. An Example of the Type of Static Container Used to Conduct the EPA 1313 and 1316 Draft Test Methods

5.4.2 EPA Draft Method 1316—Liquid-to-Solid Ratio Effects

Similar to 1313, EPA Method 1316 (Liquid-Solid Partitioning as a Function of Liquid to Solid Ratio) also is a static test method that uses DIW as the leachant instead of a dilute acid or base at a variety of liquid-to-solid ratios (EPA 2009c). The purpose of this test method is to evaluate the effect of differing liquid-to-solid ratios on the release of contaminants. These experiments were conducted by adding DIW to the test vessel containing a predetermined amount of powdered material (<0.3 mm). These experiments were conducted at three different liquid-to-solid ratios (10, 5, and 2 mL/g). After preparation, all the samples were placed on a platform shaker and allowed to mix for 24 hours. After the 24-hour contact time was complete, the slurry samples were centrifuged and clear supernatants were filtered with a syringe filter (0.45- μm size polypropylene membrane), and the filtrate was collected in vials with minimal head space and submitted for chemical analyses.

5.4.3 EPA Draft Method 1315 – Mass Transfer Rates

The EPA draft Method 1315 (Mass Transfer Rates of Constituents in Monolith or Compacted Granular Materials) is a 63-day, semi-dynamic, leach experiment that consists of submerging a monolithic sample (with a fixed geometry) in DIW at a fixed liquid volume-to-solid surface area ratio and sampling at fixed periods of time (EPA 2009b). A schematic of this process is shown in Figure 5.2.

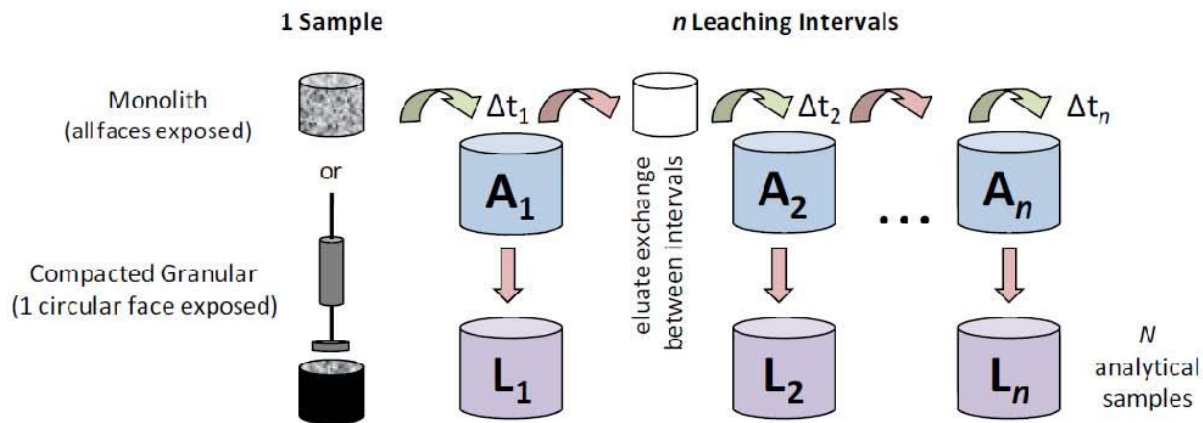


Figure 5.2. A Schematic of the 1315 Test Method^(a)

The geometric surface area is used in this test method and calculated based on the cylindrical dimensions of the sample. The average calculated geometric surface area was $201.13 \pm 0.77 \text{ cm}^2$. At each of the nine pre-determined leaching intervals, the sample mass is recorded, and the leaching solution is changed. This method is similar to ANSI/ANS 16.1 (ANSI 2003), but the leaching intervals are modified.

The cylindrical monolith sample (2-inch diameter by 4-inch height) was placed into the center of a leaching vessel and mixed with DIW to maintain a solid-to-solution ratio of $9 \pm 1 \text{ mL}$ of eluant per cm^2 of sample. The sample stand and holder were used to maximize the contact area of the sample with the leaching solution. In between the sampling/replacement intervals, the experimental vessels were covered with a lid. An example of the experimental setup and sample specimens in the leaching vessels are shown in Figure 5.3. The leaching times at which solution exchanges were made for these experiments were 2 hours and 1, 2, 7, 14, 28, 42, 49, and 63 days. Leachate samples collected during these intervals were stored in screw-top containers with minimal head space under refrigeration until the entire batch of collected samples was submitted for chemical analysis. The leachates were returned to room temperature for several days before analysis.

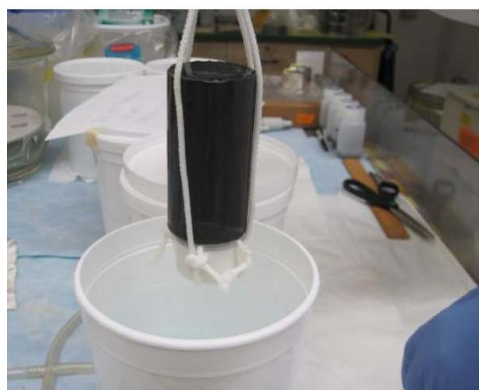


Figure 5.3. Monoliths Submerged into DIW in the Leaching Vessels^(b)

(a) Figure 5. EPA (2009b)

(b) Figure 4.3 (right), Pierce EM, W Um, KJ Cantrell, MM Valenta, JH Westsik, Jr., RJ Serne, KE Parker. 2010. *Secondary Waste Form Screening Test Results – Cast Stone and Alkali Alumino-Silicate Geopolymer.*

5.4.4 ANSI/ANS 16.1

The ANSI/ANS-16.1 (Measurement of the Leachability of Solidified Low-Level Radioactive Wastes by a Short-Term Test Procedure) is a 90-day, semi-dynamic, leach experiment that consists of submerging a monolithic sample (with a fixed geometry) in DIW at a fixed liquid volume-to-solid surface area ratio and sampling at fixed periods of time (ANSI/ANS 16.1 2003).

The geometric surface area is used in this test method and calculated based on the cylindrical dimensions of the sample. The average calculated geometric surface area was $201.5 \pm 0.5 \text{ cm}^2$. At each of the 10 pre-determined leaching intervals, the leaching solution is exchanged with fresh leachant (unused DIW). A schematic of the experimental setup and sample specimens in the leaching vessels is shown in Figure 5.4.

The cylindrical monolith sample (2-in. diameter by 4-in. height) was placed into the center of a leaching vessel and mixed with DIW to maintain a leachant volume-to-sample surface area of $10 \pm 0.2 \text{ cm}$. The sample stand and holder were used to maximize the contact area of the sample with the leaching solution. In between the sampling/replacement intervals, the experimental vessels were covered with a lid. The leaching times at which solution exchanges were made for these experiments were: 2, 7, and 24 hours and 2, 3, 4, 5, 19, 47, and 90 days. Leachate samples collected during these intervals were stored in screw-top containers with minimal head space under refrigeration until the entire batch of collected samples was submitted for chemical analysis. Refrigerated archive samples were allowed to come to room temperature before test aliquots were collected and analyzed.

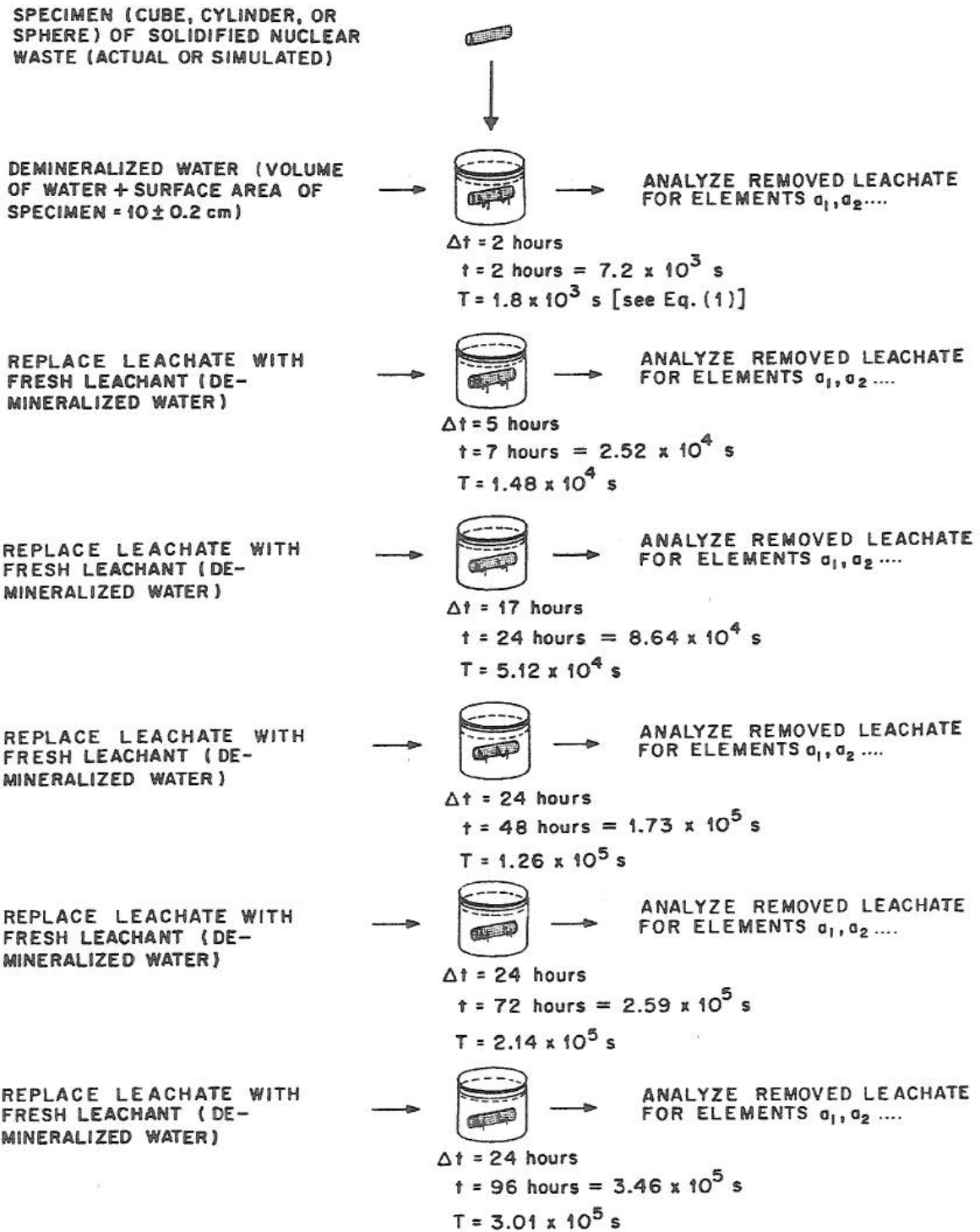


Figure 5.4. A Schematic of the ANSI/ANS 16.1 Test Method^(a)

(a) Figure 2, ANSI/ANS. 2003. Measurement of the Leachability of Solidified Low-Level Radioactive Waste by a Short-Term Test Procedure. ANSI/ANS-16.1, American Nuclear Society, La Grange Park, Illinois.

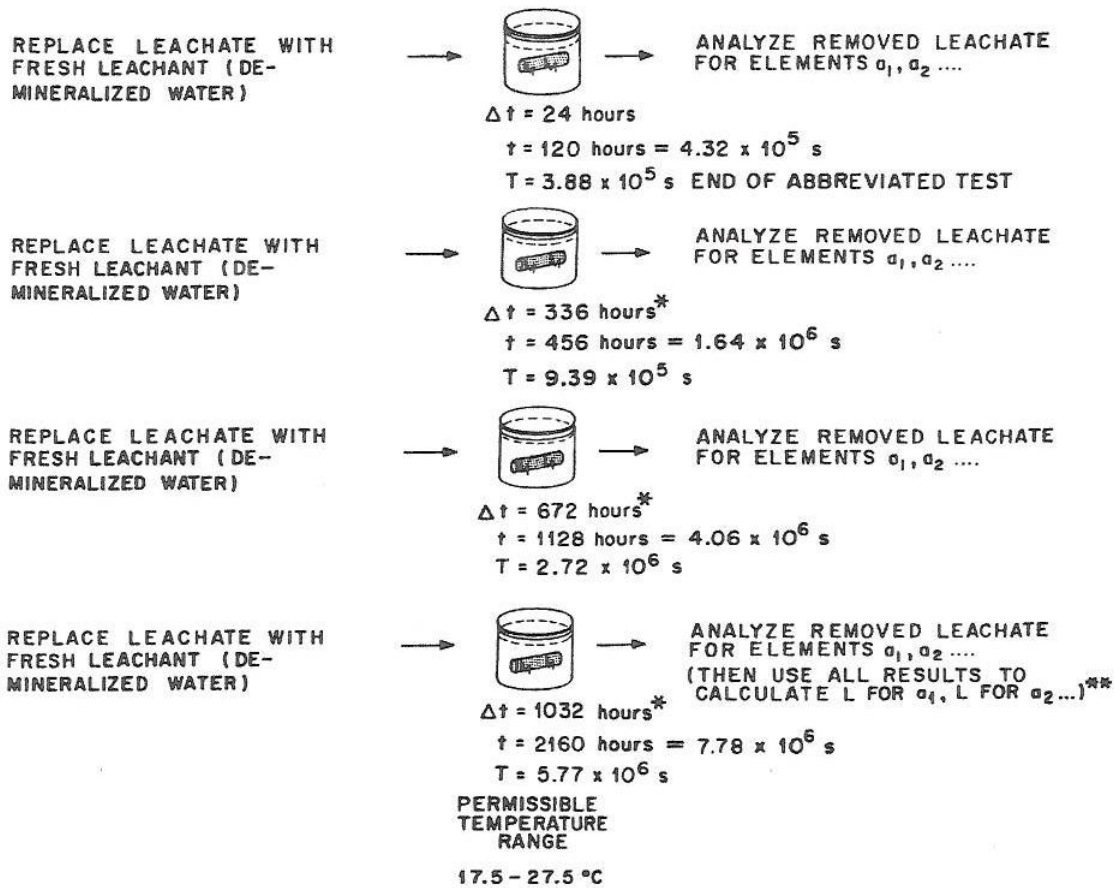


Figure 5.4 (contd)

5.4.5 Diffusivity Calculation

In the EPA draft 1315 Method, the observed diffusivity for each constituent was calculated with the analytical solution, Equation 5.1, for simple radial diffusion from a cylinder into an infinite bath as presented by Crank (1986).

$$D_i = \pi \left[\frac{M_{t_i}}{2\rho C_o (\sqrt{t_i} - \sqrt{t_{i-1}})} \right]^2 \quad (5.1)$$

- where
- D_i = observed diffusivity of a specific constituent for leaching interval [m^2/s]
 - i = leaching interval
 - M_{t_i} = mass released during leaching interval i [mg/m^2]
 - t_i = cumulative contact time after leaching interval i [s]
 - t_{i-1} = cumulative contact time after leaching interval $i-1$ [s]
 - C_o = initial leachable content [mg/Kg -dry]
 - ρ = sample density [Kg -dry/ m^3].

The mass released during the leaching interval i , given by M_{ti} above, is calculated by Equation 5.2.

$$M_{ti} = \frac{C_i V_i}{A} \quad (5.2)$$

where C_i = the constituent concentration in the eluate for interval i [mg/L]
 i = leaching interval
 V_i = the eluate volume in the interval [L]
 A = the specimen external geometric surface area exposed to the eluate [m²].

The mean observed diffusivity for each constituent can be determined by taking the average of the interval observed diffusivity with the standard deviation. The EPA draft Method 1315 diffusivities reported in Sections 6 and 7 of this report are observed diffusivities as calculated by Equation 5.1.

The test sample (monolith) dry-basis density used in the denominator of the observed diffusivity calculation for the EPA draft Method 1315 was calculated by the dry-basis conversion; (wet weight - dry weight)/dry weight and the initial leachable concentrations were converted to the dry-basis using the same conversion.

The ANSI/ANS 16.1 effective diffusivity for each constituent was calculated with the analytical solution, Equation 5.3. The leaching behavior is assumed to be diffusion controlled and of a semi-infinite medium. The ANSI/ANS 16.1 diffusivity values reported in Section 7 of this report are the effective diffusivity results as determined by Equation 5.3.

$$D_n = \pi \left[\frac{a_n}{A_0} \right]^2 \left[\frac{V}{S} \right]^2 \left[\frac{(\sqrt{t_n} + \sqrt{t_{n-1}})}{2} \right]^2 \quad (5.3)$$

where D_n = effective diffusivity of a specific constituent for leaching interval n [cm²/s]
 n = leaching interval
 a_n = quantity of constituent released during leach interval [μg]
 A_0 = the difference between the quantity of constituent in the prepared specimen minus the quantity of constituent in the initial rinse [μg]
 V = volume of the specimen [cm³]
 S = geometric surface area of the specimen [cm²]
 t_n = leach interval [s].

The Leachability Index (LI), the parameter derived directly from immersion test results, evaluates diffusion-controlled contaminant release with respect to time. The LI is used as a performance criterion to assess whether a stabilizing waste form is likely to be acceptable for the subsurface and for disposal in the target waste repository. For Hanford secondary wastes, a target LI of 9 or greater for Tc has been established. The goal is to achieve long-term release performance from solidified secondary wastes that meets or exceeds regulatory requirements based on site-specific risk assessment calculations. The LI is calculated by Equation 5.4.

$$LI_n = -\text{Log}\left(\frac{D_n}{\text{cm}^2 \text{s}}\right) \quad (5.4)$$

where LI is the leach index, and D_n is the effective diffusivity for components of interest (cm^2/s) during the leach interval n . Note the change in units for the effective diffusivity from m^2/s in Equation (5.1) to cm^2/s in Equation (5.3).

6.0 Results

This section presents the data from the analysis, characterization, and testing of the encapsulated FBSR waste form samples. Results from chemical and crystalline characterization are included. In addition to the characterization results, data from the EPA 1313, 1315, and 1316 draft leach methods are also presented.

6.1 FBSR Waste Form Solids Characterization

The supplied FBSR granular product encapsulated in a geopolymer matrix was characterized with respect to crystalline and chemical composition with a variety of techniques, including SEM with EDS, XRD, and chemical digestion followed by ICP-MS and ICP-OES. The results from these analyses are discussed in this section.

Monolithed waste forms were cross-sectioned perpendicular to the axis of symmetry to form round disks about 5 mm thick and slices of the outer surface, and sections of the inner core were collected for characterization, as discussed below.

6.1.1 Chemical Composition

The crushed monolithed waste form material from two supplied cylinders was blended and chemically digested to determine the chemical composition of the FBSR granular material encapsulated in the GEO-7 binder. Microwave-assisted acid digestion was performed on single milled and twice milled material on December 6, 2010, and May 13, 2011, respectively. The digestion cycle was repeated to promote full digestion, and the solution was visually inspected for the dissolution of all components. The solutions were then analyzed by IC, ICP-MS, and ICP-OES for RCRA metals and select constituents. An iodine-specific fusion was performed in December, 2010, and the other select anions on May 13, 2011.

The chemical composition indicated in Table 6.1 contains the average concentrations and less-than detection limits of the select constituents. All analysis results are averaged for the eight constituents (Al, Cd, Cr, Fe, Re, Si, Na and Ti) resulting in detection in all analysis replicates. The average of the detection replicates was used for constituents with detectable concentrations in one digestion revolution (duplicate digestion on the same day), but with the digestion on a different day resulting in “no detection.” For the remaining constituents, with “no detection” in both digestion revolutions, the lower detection limit was used.

Moisture content was determined to be 8.2 weight percent.

Table 6.1. Chemical Composition (moisture free) of FBSR Granular Material Encapsulated in GEO-7 Binder

Constituent	Concentration	
	$\mu\text{g/g-dry}$	wt %
Aluminum ^(a)	3.53E+04	3.53
Antimony ^(b)	2.10E+02	0.02
Arsenic ^(b)	<3.96E+01	0.004
Barium	1.29E+02	0.01
Cadmium ^(a)	1.15E+02	0.012
Calcium	<1.38E+03	0.14
Cesium ^(b)	1.64E+03	0.16
Chloride	3.61E+03	0.36
Chromium ^(a)	4.63E+02	0.05
Fluoride	<2.90E+01	0.003
Iodine	ND	ND
Iron ^(a)	2.43E+04	2.43
Lead	<5.93E+02	0.06
Magnesium	<3.77E+02	0.04
Manganese	1.30E+02	0.013
Nickel	3.67E+02	0.04
Phosphorus	<1.75E+03	0.18
Potassium	<5.08E+03	0.51
Rhenium ^(a)	2.58E+02	0.03
Selenium ^(b)	1.28E+02	0.013
Silicon ^(a)	3.25E+05	32.50
Silver ^(b)	9.46E+01	0.009
Sodium ^(a)	1.27E+05	12.65
Sulfur	<6.32E+03	0.63
Thallium	<1.90E+03	0.19
Titanium ^(a)	5.45E+03	0.54
Zinc	6.27E+02	0.06
Total carbon ^(b)		7.03
Oxygen (calculated)		30.59

(a) Average concentration of four replicate digestions performed December 6, 2010, and May 13, 2011.

(b) Average detected or less than detection limit concentrations from two replicates of the May 13, 2011, digestion.

6.1.2 SEM with EDS

The surface morphology and composition of select solid phases present in the FBSR encapsulated in GEO-7 binder sample were analyzed with JSM-5900 SEM combined with EDS. One of the supplied 2-inch-diameter by 4-inch-long FBSR monoliths was cross-sectioned and a 4- to 5-mm-thick “puck” collected from the center of the cylinder was embedded in epoxy, and allowed cure under vacuum. The epoxy “puck” was polished and allowed to dry in a vacuum desiccator. The specimen was sputter coated with palladium, and SEM was performed with a JEOL 5900 scope with a Robinson backscatter electron detector, and EDS was performed with an EDAX silicon drifted detector.

We investigated several regions within the sample and found many segregated areas throughout the specimen as seen in Figure 6.1A. Figure 6.1A is a typical region showing a few of the different features on a macro scale. Figure 6.1B is a close-up view of a selected area with target features for closer inspection and/or EDS scanning. Figure 6.1C through Figure 6.1E are close-up views of select features in different regions. EDS analysis revealed the chemical makeup of the following selected features.

Large concentric circular regions (i.e., Figure 6.1B, Reg. 1-d; Figure 6.1D, Reg. 3-b), approximately 200 to 400 μm in diameter were determined to be composed of a Na-Al-Si-O mixture, most likely the target $\text{Na}_2\text{O-Al}_2\text{O}_3\text{-SiO}_2$ (NAS) mineral product, nepheline. The concentric circular NAS mineral in Figure 6.1B, Reg. 1-d appears to have grown onto a NAS feed seed while the mineral formed in Figure 6.1D, Reg. 3-b appears to be formed around an iron oxide particle. Figure 6.1A (macro view) illustrates the relative distribution of NAS mineral particles within the encapsulated test monolith.

Various regions rich in iron, calcium silicate, and Na-Ca-Si-O were observed throughout all the regions investigated and are thought to represent the broad range of possible fly ash compositions. Additionally, Fe-rich circular regions (i.e., Figure 6.1B, Reg. 1-a; Figure 6.1C, Reg. 2-a, e, g; Figure 6.1E, Reg. 4-b), approximately 10 to 150 μm in diameter, were composed of various mixtures of alkali-Al-Si-Fe-O where the potassium levels were higher, on average, compared to the other regions analyzed.

A Ca-Si-O region (i.e., Figure 6.1C, Reg. 2-c), which was an irregularly shaped agglomerate with an approximate size of 50 to 76 μm with inclusions, was composed mostly of Ca-Si-O with small-to-moderate quantities of F and Na at 7.07 and 2.29 mass%, respectively. Figure 6.1C, Reg. 2-d, an inclusion in Figure 6.1C, Reg. 2-c approximately 12 μm in size, was composed of mostly Na-Ca-O.

High Fe concentration regions (i.e., Figure 6.1B, Reg. 1-c; Figure 6.1C, Reg. 2-f; Figure 6.1D, Reg. 3-a), varying 10 to 120 μm in diameter, were composed of high mass fractions of Fe (≥ 58 mass%) and small fractions of Na, Al, and Si.

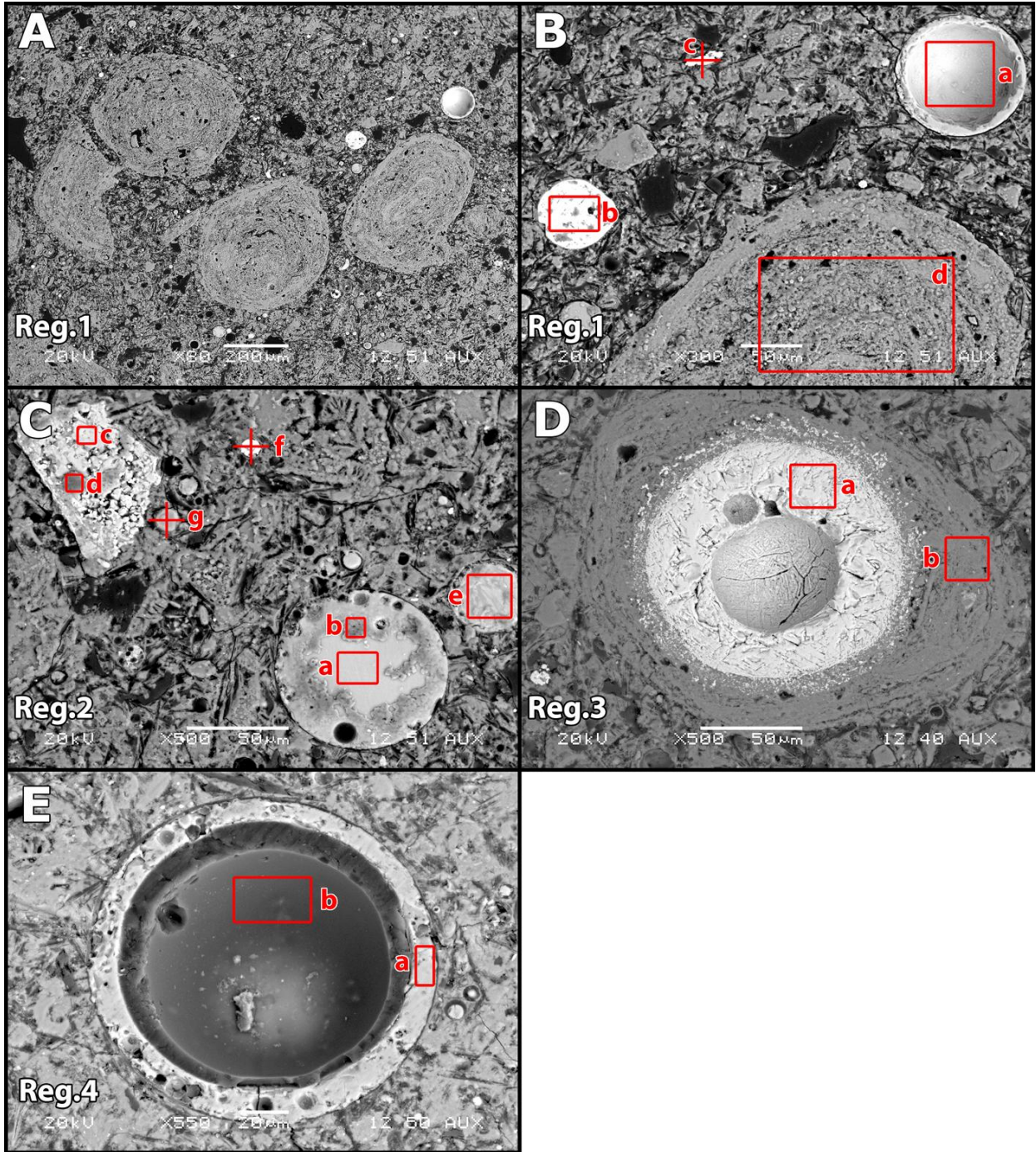


Figure 6.1. SEM Collage Showing Different Regions Analyzed by EDS (called out in red boxes and cross-hairs)

A dark region approximately 120 μm in diameter, in the interior of Figure 6.1, Reg. 4b was composed of carbon and oxygen (78 mass%) with small fractions of Si, Fe, Cl, K, and Al at 6.80, 3.95, 3.31, 3.24, and 2.61 mass%, respectively. These dark spots were observed throughout the specimen and could either be epoxy or perhaps carbon-rich regions segregated out from the sample during curing. The only way to verify the source of these regions would be to cross-section a region of the specimen without first imbedding it in epoxy.

An intact FBSR monolith sample was dry cut radially with a circular saw equipped with a diamond impregnated blade to obtain a circular specimen ~ 5 mm in thickness. A section of the cut surface was coated with a thin layer of carbon to reduce the charging effects and analyzed by using an FEI Quanta 3D FEG scanning electron microscope equipped with an Oxford 80 mm^2 Silicon Drift Detector (SDD) and INCA software. The surface was examined and images were collected in both secondary electron (SE) and backscatter electron (BSE) modes.

A low magnification (250 X) BSE image (Figure 6.2) of the surface indicates the differences in atomic weights (Z contrast) of the dominant elements constituting various phases. The SEM BSE image revealed that the region extending ~ 0.8 mm from the edge of the sample included what appeared to be a dense aggregation of long prismatic mineral phase (Figure 6.1) consisting of lower Z elements. Bright spots of material (higher Z) were randomly embedded in the matrix.

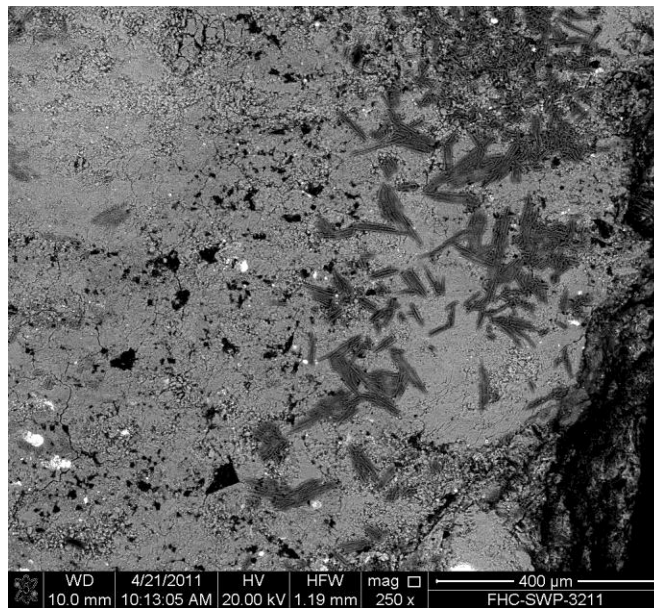


Figure 6.2. Low Magnification SEM BSE Image of the Dry-Cut Surface of a FBSR Monolith

To further characterize these observed features, BSE images at higher magnifications were obtained, and the elemental composition of the features were determined with an energy dispersive spectroscopic system coupled to INCA software (see Figure 6.3).

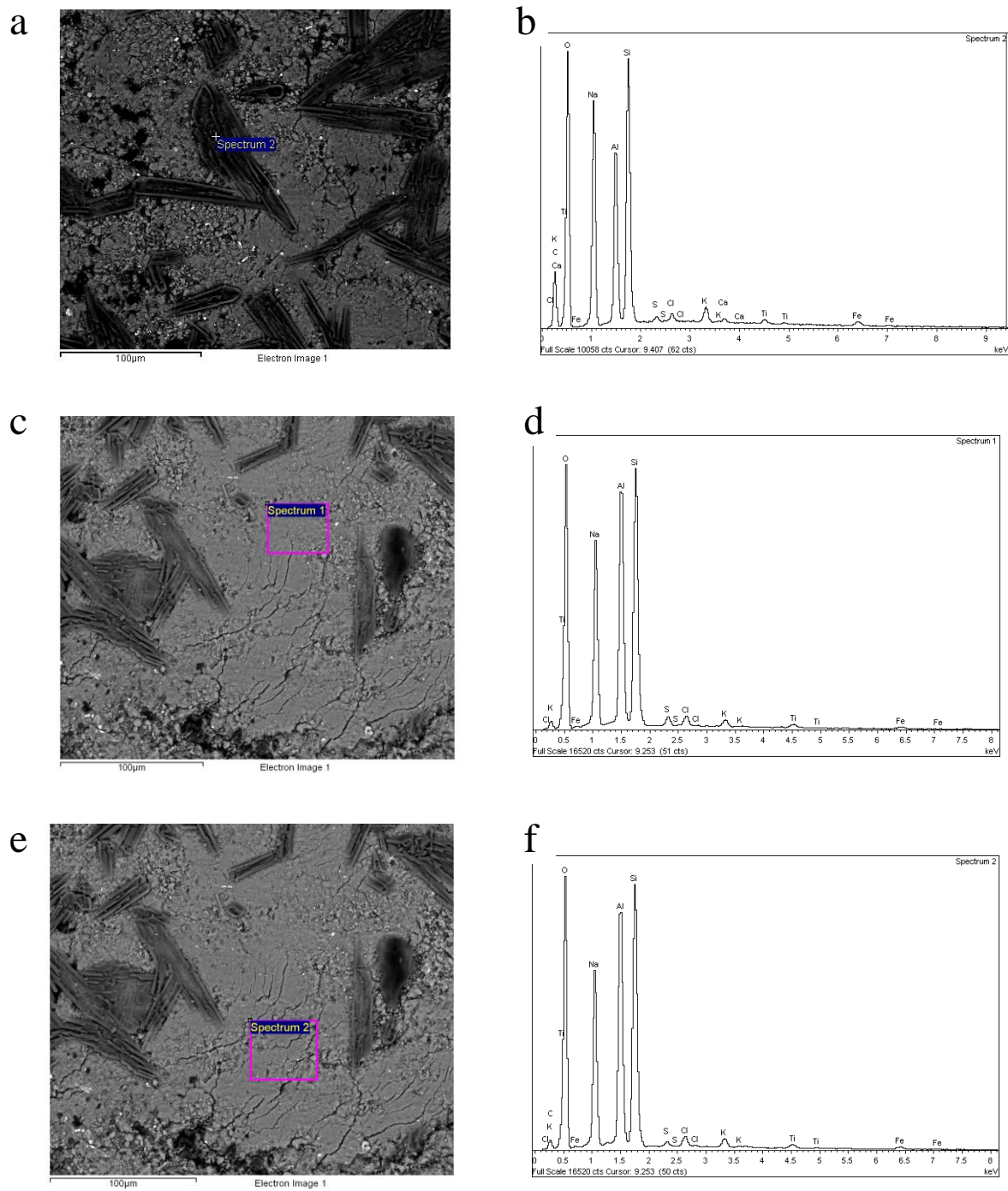


Figure 6.3. SEM BSE Images and Corresponding EDS: a and b: Long Prismatic Mineral Phase; b–f: the Monolith Matrix; g and h: Zr and Si Rich Phase; i–l: Fe-Rich Spherical Particles

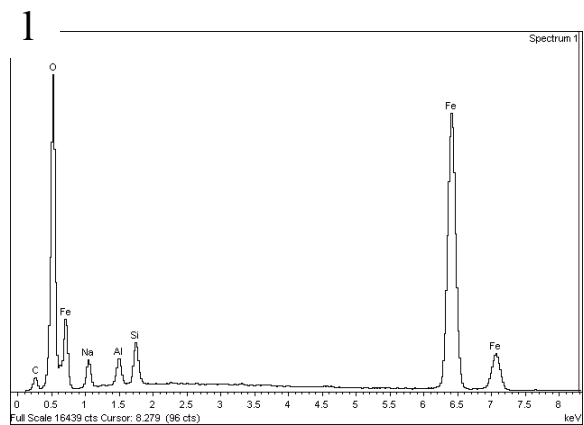
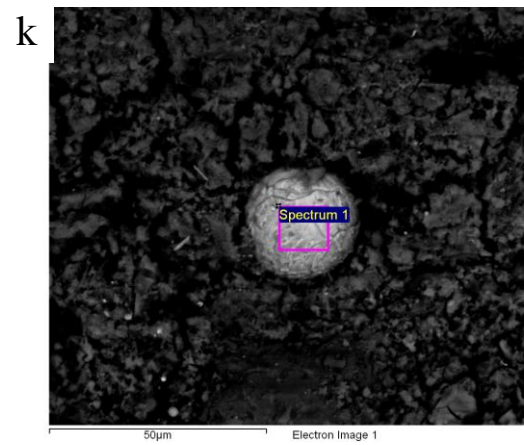
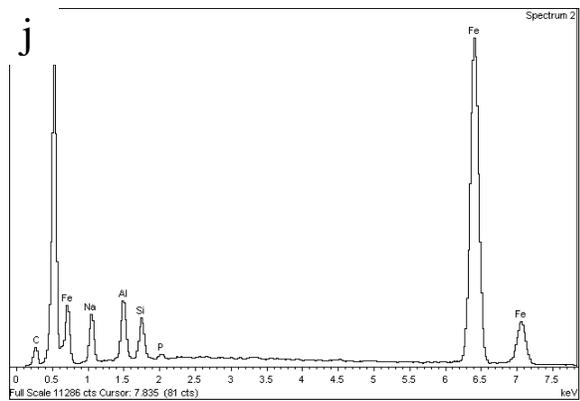
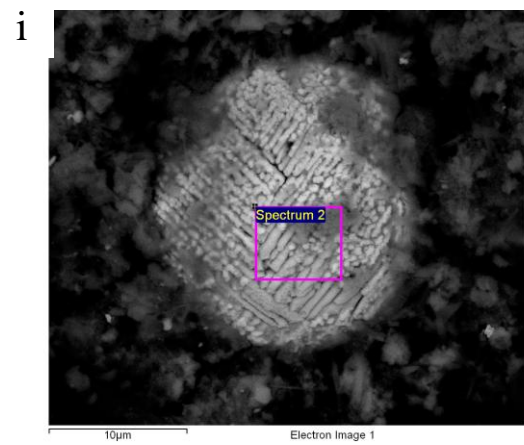
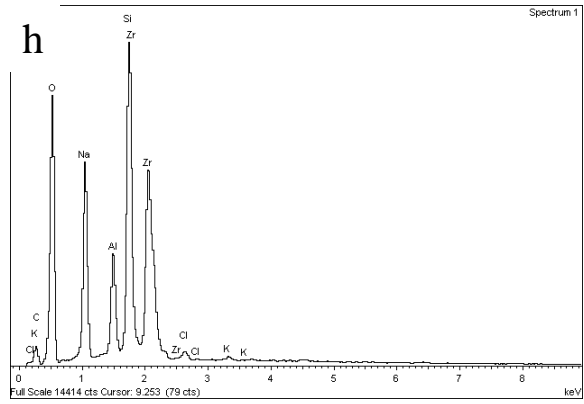
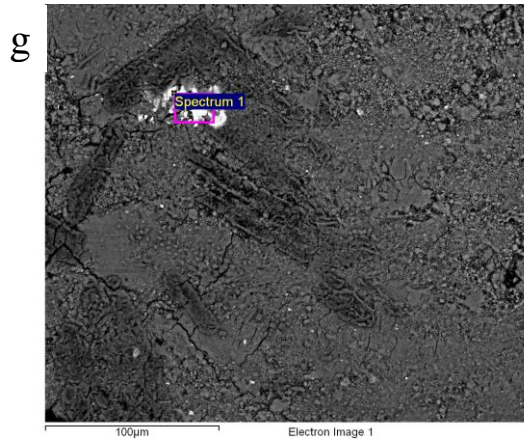


Figure 6.3 (contd)

The EDS of prismatic crystals indicated that these are mainly sodium aluminosilicates with trace amounts of K, Ti, Fe, S and Cl (Figure 6.2a, b). The matrix material of the monolith (Figure 6.2c – f) also consists of sodium aluminosilicates with relatively more aluminum as compared to the prismatic crystal composition. Traces of K, Ti, Fe, S and Cl were also found in the matrix material. Embedded in the sodium aluminosilicate matrix were less common particle aggregates enriched in Zr and Si with trace amounts of K, Ti, Fe, S and Cl (Figure 6.2g, h). Spherical particles (~20 to 25 μm diameter) with regular textured surface features (Figure 6.2i, k) were also found to be dispersed in the matrix. These textured spheres were found to be composed of mainly Fe with trace amounts of Na, Al and Si. (Figure 6.2j, l). Such Fe-rich spheres known as ferrospheres with similar surface features have been observed in magnetic fractions of fly ashes (Small 1976, Mattigod 1982, Vassilev et al. 2004). The presence of these ferrospheres in the FBSR monolith is likely attributable to the use of fly ash as the binder material.

6.1.3 X-Ray Diffraction

Ground samples of FBSR product, intact and ground monolith, and intact leached monolith samples were analyzed with XRD analysis to identify the crystalline phases that were present. The intact monolith samples were obtained by dry cutting (with a diamond-impregnated blade) monoliths radially that resulted in circular ~5- to 8-mm-thick specimens. Also, the outer surface of an intact monolith was analyzed with X-Ray micro-diffraction analysis to identify any crystalline phases on the monolith surface.

Powder diffraction data were collected with a Panalytical X'Pert Bragg-Brentano diffractometer using Cu K α radiation ($\lambda = 1.5418 \text{ \AA}$), a graphite post-diffraction monochromator, and variable divergence and anti-scatter slits (illuminated length: 10 mm). Powdered specimens were loaded into traditional well-type aluminum holders with a cavity measuring $20 \times 15 \times 2 \text{ mm}$. Intact block specimens were supported on modeling clay in a custom holder positioned so that a flat surface was close to the plane of traditional sample holders.

The material on the outside curved surface of one of the samples was analyzed with a Rigaku D/Max Rapid II micro-diffraction system. X-rays were generated (MicroMax 007HF) from a rotating Cr target ($\lambda = 2.2910 \text{ \AA}$) and focused through a 300- μm -diameter collimator onto a region of interest identified with the integral video microscope. Diffraction data recorded on a 2D image plate were integrated to give powder traces using the manufacturer's software.

Analysis of the FBSR product sample indicated that the XRD pattern (Figure 6.4) could be matched with four crystalline phases, namely, a sodium aluminosilicate (NaAlSiO_4) phase (ICDD-PDF# 00-052-1342, thought to be a form of low-carnegeite by Nayak et al. 1998), nepheline (ICDD-PDF# 00-019-1176), sodalite (ICDD-PDF# 00-037-0476), and nosean (ICDD-PDF# 01-072-1614). The phases identified are also listed in Table 6.2.

The XRD patterns for the intact monolith and powdered specimen are virtually identical (Figure 6.5, Table 6.2), except that thermonatrite was not present (peaks around 32° in the blue scan) in the intact monolith. The phases identified are quartz (ICDD-PDF# 00-46-1045), nepheline (ICDD-PDF# 00-019-1176), sodalite (ICDD-PDF# 00-037-0476), nosean (ICDD-PDF# 01-072-1614), thermonatrite (ICDD-PDF# 01-070-2148), zeolite rho (ICDD-PDF# 00-027-0015), and Na-faujasite (ICDD-PDF# 00-012-0228). Several of the crystalline phases (e.g., zeolite-rho, sodalite, and Na-Faujasite) can adopt a variety of chemical compositions with similar XRD patterns; the patterns chosen are close to the observed diffraction peaks; however, these may not represent the chemistry of the samples accurately.

A comparison of leached (blue) and unleached (black) intact FBSR monolith samples is shown in Figure 6.6, and the phases identified (Table 6.2) are quartz (ICDD-PDF# 00-46-1045), nepheline (ICDD-PDF# 00-019-1176), sodalite (ICDD-PDF# 00-037-0476), nosean (ICDD-PDF# 01-072-1614), thermonatrite (ICDD-PDF# 01-070-2148), zeolite rho (ICDD-PDF# 00-027-0015), and Na-faujasite (ICDD-PDF# 00-012-0228). The phases identified in both unleached and leached samples were identical, except the leached sample displayed additional peaks corresponding to calcite (major peak just below 30° is particularly evident) and possibly more Na-faujasite (low angle peak around 6°).

The XRD pattern obtained using micro diffraction of surface coating of an intact monolith is presented in Figure 6.7. The prominent peaks can all be attributed to the mineral trona (ICDD-PDF# 00-29-1447). Additional weaker peaks correspond to the underlying phases of the monolith. Relative intensities can differ from the database in micro XRD scans because the small analysis area may not represent a random orientation of crystallites. This is not unusual in such a scan because the surface could promote preferred orientation, and there are probably a relatively small number of crystallites in the micro-XRD beam.

6.1.4 Additional Observations

The FBSR monolithed waste forms were sliced into sections for the characterization described above. During this “dry-cut” sectioning, a discoloration of the cured waste form was noted. The cylinders demonstrated a “rind” of lighter colored material at the surface about 0.5 cm wide, extending from the outer surface into the core of the cylinder. The cross-sections illustrated in Figure 6.8 and Figure 6.9 demonstrate the lighter colored material at the surface of the supplied monolithed waste forms.

The test monoliths used for the leach testing were received in a cardboard box with the monoliths separated by cardboard dividers. The plastic molds had already been removed. The second shipment of test forms was received with the monoliths still in the plastic molds with open tops and the molds pre-split down the length of the cylindrical axis. The leach test waste forms (without the plastic molds) demonstrated the more pronounced light-colored rind on the surface (Figure 6.8 and 6.9) when dry-cut for sectioning and the forms with the split molds showed only a very slight discoloring on top and along the split seam. The discolored rind of the split mold forms did not appear to penetrate as deeply as the uncovered forms.

The monoliths from the first shipment that were used for the EPA draft Method 1315 and ANSI/ANS 16.1 leach tests (at PNNL) had a wet-basis density of 1.57 to 1.58 g/cc. The second shipment of the same test batch with the specimens still in the plastic molds had a wet-basis density of 1.67 g/cc. Both shipments to PNNL appear to have lower wet-basis densities than the initial density of 1.83 g/cc for the 3-inch × 6-inch cylinders reported by TTT (2009).

Table 6.2. Phases Identified in FBSR Product and Monolith Samples^(a)

Mineral name	Chemical Composition	ICDD PDF #	Reference
FBSR Product Sample			
Low-Carnegieite (?)	NaAlSiO ₄	00-052-1342	Nayak, M., Kuty, T., Mater. Chem. Phys., v57 p138 (1998)
Nepheline	NaAlSiO ₄	00-019-1176	Hughes. Trans. Br. Ceram. Soc., v65 p661 (1966)
Sodalite	Na ₄ Al ₃ Si ₃ O ₁₂ Cl	00-037-0476	Keller, L., Rask, J., Buseck, P., Arizona State University, Tempe, Arizona, USA. ICDD Grant-in-Aid (1986)
Nosean	Na ₈ Al ₆ Si ₆ O ₂₄ SO ₄	01-072-1614	Schulz, H. Z., Kristallogr., Kristallgeom., Kristallphys., Kristallchem., v131 p114 (1970)
FBSR Intact and Ground Monolith Samples			
Quartz	SiO ₂	00-46-1045	Kern, A., Eysel, W., Mineralogisch-Petrograph. Inst., Univ. Heidelberg, Germany. ICDD Grant-in-Aid (1993)
Nepheline	NaAlSiO ₄	00-019-1176	Hughes. Trans. Br. Ceram. Soc., v65 p661 (1966)
Sodalite	Na ₄ Al ₃ Si ₃ O ₁₂ Cl	00-037-0476	Keller, L., Rask, J., Buseck, P., Arizona State University, Tempe, Arizona, USA. ICDD Grant-in-Aid (1986)
Nosean	Na ₈ Al ₆ Si ₆ O ₂₄ SO ₄	01-072-1614	Schulz, H. Z., Kristallogr., Kristallgeom., Kristallphys., Kristallchem., v131 p114 (1970)
Thermonatrite	Na ₂ CO ₃ ·H ₂ O	01-070-2148	Dickens, B., Mauer, F.A., Brown, W.E., J. Res. Natl. Bur. Stand., Sect. A, v74 p319 (1970)
Zeolite rho	Al ₁₂ H ₁₂ Si ₃₆ O ₉₆	00-027-0015	Robson, H. et al., Adv. Chem. Ser., v121 p106 (1973)
Na-Faujasite	Na ₂ Al ₂ Si _{3.3} O _{10.6} ·7H ₂ O	00-012-0228	Barrer et al., J. Chem. Soc. p195 (1959)
FBSR Leached and Unleached Intact Monolith Samples			
Quartz	SiO ₂	00-46-1045	Kern, A., Eysel, W., Mineralogisch-Petrograph. Inst., Univ. Heidelberg, Germany. ICDD Grant-in-Aid (1993)
Nepheline	NaAlSiO ₄	00-019-1176	Hughes. Trans. Br. Ceram. Soc., v65 p661 (1966)
Sodalite	Na ₄ Al ₃ Si ₃ O ₁₂ Cl	00-037-0476	Keller, L., Rask, J., Buseck, P., Arizona State University, Tempe, Arizona, USA. ICDD Grant-in-Aid (1986)
Nosean	Na ₈ Al ₆ Si ₆ O ₂₄ SO ₄	01-072-1614	Schulz, H. Z., Kristallogr., Kristallgeom., Kristallphys., Kristallchem., v131 p114 (1970)
Thermonatrite	Na ₂ CO ₃ ·H ₂ O	01-070-2148	Dickens, B., Mauer, F.A., Brown, W.E., J. Res. Natl. Bur. Stand., Sect. A, v74 p319 (1970)
Zeolite rho	Al ₁₂ H ₁₂ Si ₃₆ O ₉₆	00-027-0015	Robson, H. et al., Adv. Chem. Ser., v121 p106 (1973)
Na-Faujasite	Na ₂ Al ₂ Si _{3.3} O _{10.6} ·7H ₂ O	00-012-0228	Barrer et al., J. Chem. Soc. p195 (1959)
Calcite	CaCO ₃	00-047-1743	Bernstein, L., Menlo Park, CA, USA. Private Comm. (1994)
FBSR Intact Monolith Sample – Surface Coating			
Trona	Na ₃ H(CO ₃) ₂ ·2H ₂ O	00-29-1447	Natl. Bur. Stand. (U.S.) Monogr. 25, v15 p71 (1978)

(a) There is potential for chemical substitution in many of these compounds, and so the compositions given are meant to give an indication of the composition for each of these phases. The actual compositions of phases in the FBSR samples may differ. There are further ICDD patterns for these phases; the ones chosen match the observed peaks relatively closely and have compositions consistent with the expected sample chemistry.

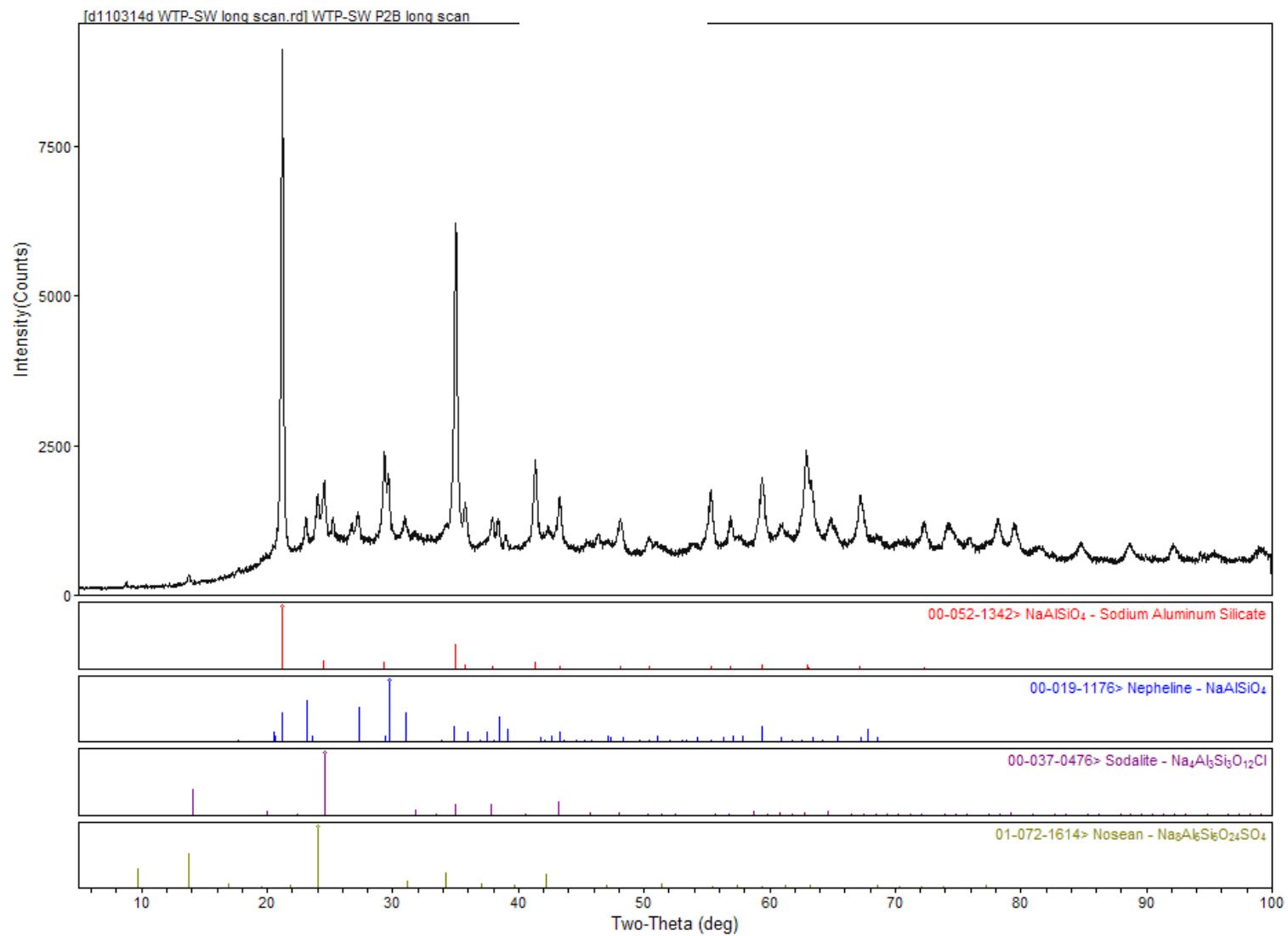


Figure 6.4. XRD Pattern for FBSR Product Sample

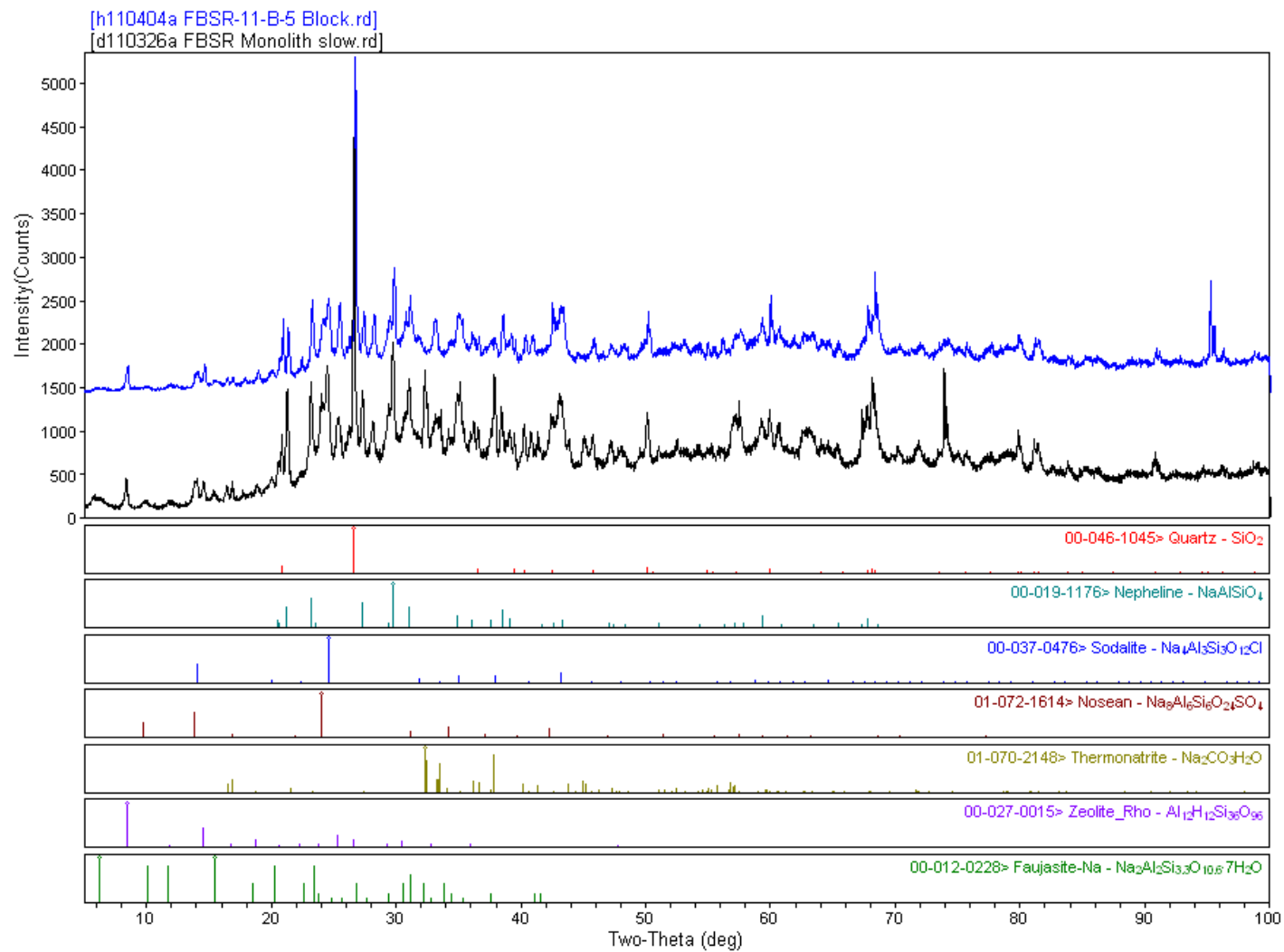


Figure 6.5. XRD Patterns for FBSR Intact and Ground Monolith Samples

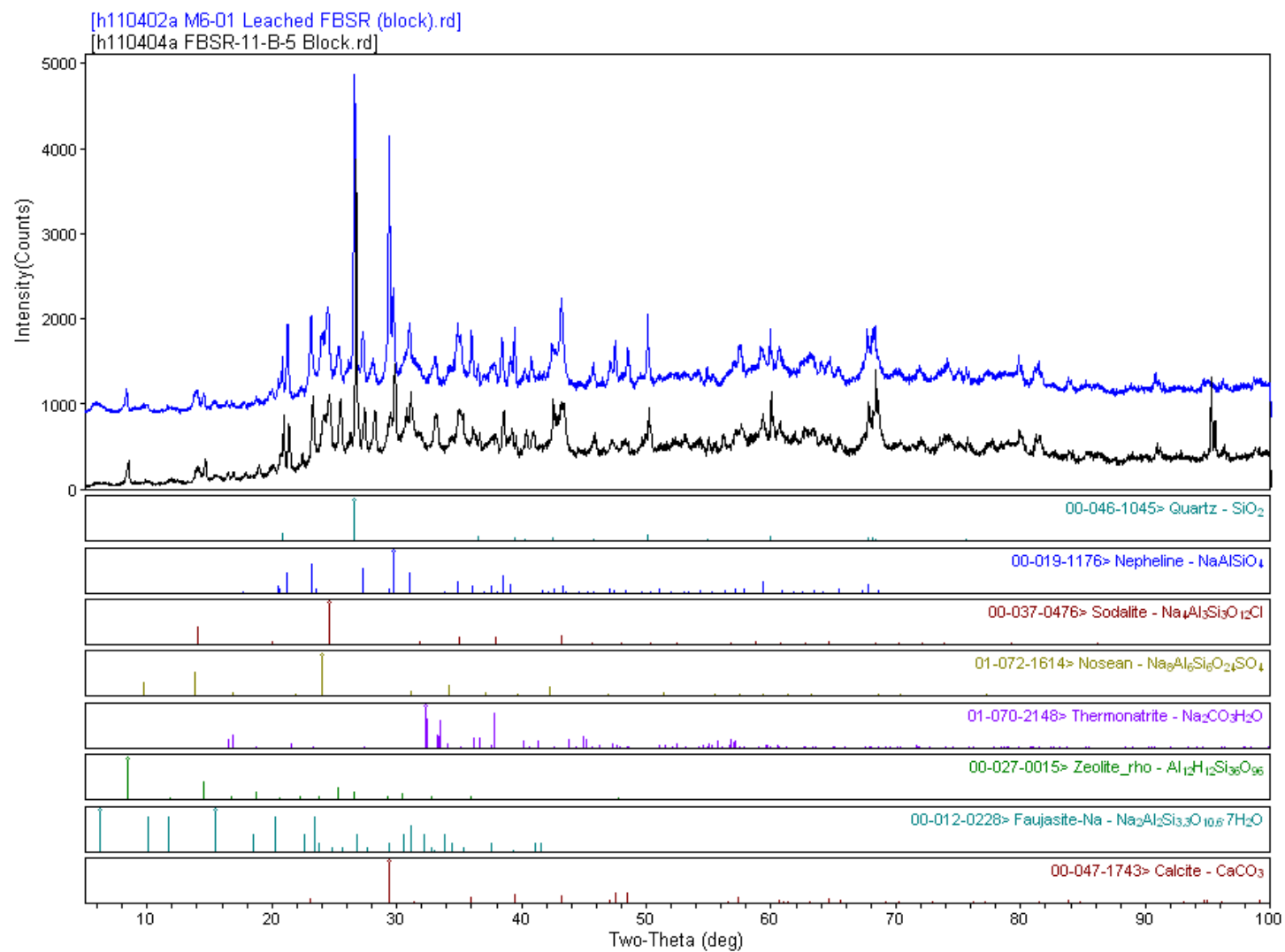


Figure 6.6. Patterns for FBSR Leached and Unleached Intact Monolith Samples

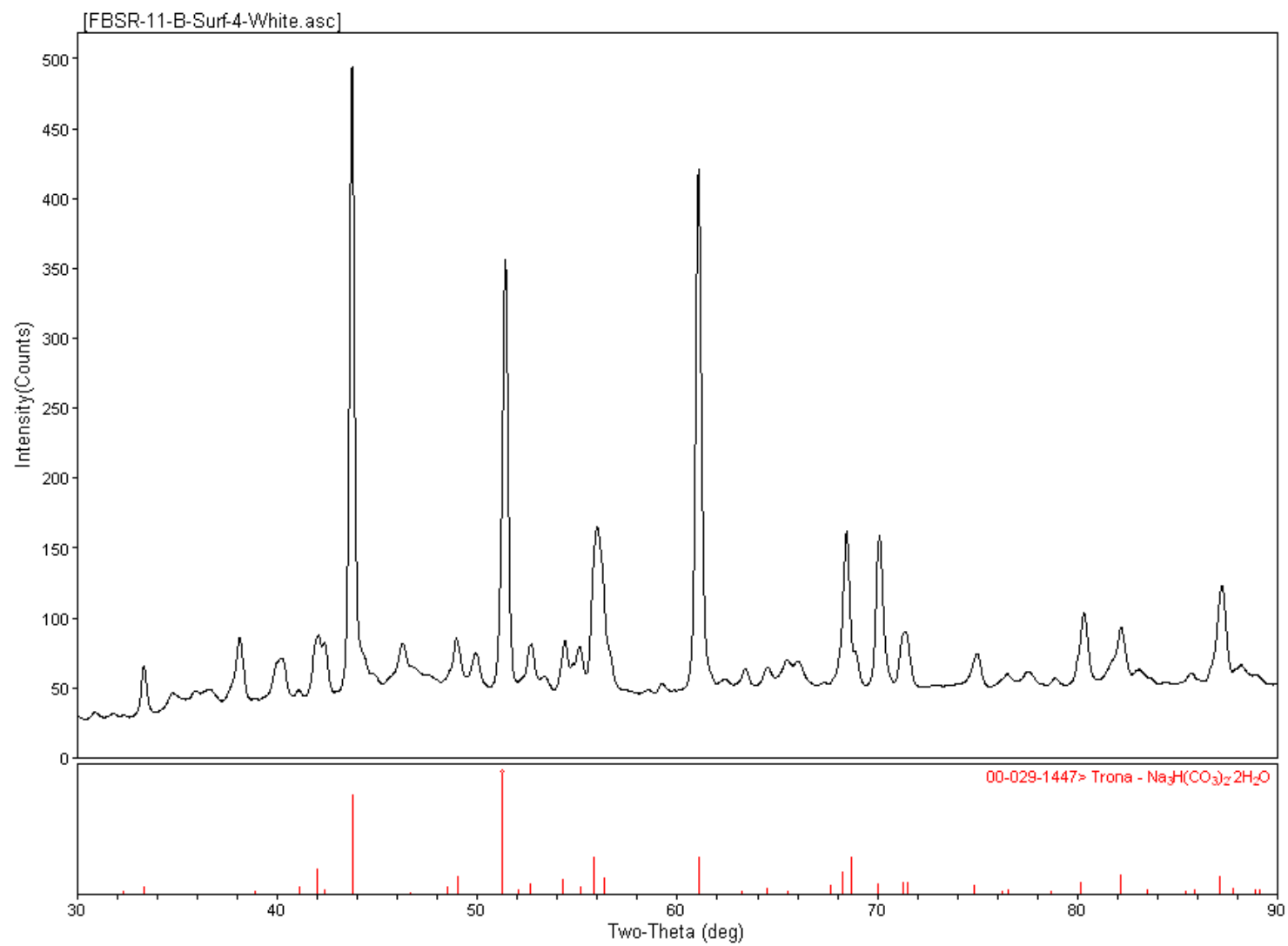


Figure 6.7. Micro-XRD Pattern of Surface Coating of FBSR Intact Monolith



Figure 6.8. FBSR Monolith Cross Sectioned for XRD Sample Collection. Top 8 mm and bottom 1 inch of cylindrical ends and part of a cylindrical edge were removed for SEM analysis.



Figure 6.9. Partial FBSR Monolith Cross Section. Top, bottom, and one edge of cylinder removed.

6.2 Effect of Leachant pH—EPA Draft Method 1313

The results of the pre-titration pH data for the supplied FBSR encapsulated samples with EPA draft Method 1313 are shown in Figure 6.10. The powdered FBSR monolith material forms a high-alkaline solution after equilibrating in DIW for 24 hours, and therefore all pre-titrations and EPA draft Method 1313 leach tests were performed with only acid added to achieve the desired pH. The pre-titrations were used to quantify the amount of acid required to maintain the equilibrating solution at a fixed target pH, which ranged between 4 and 12. Test samples were prepared by mixing 10 g of the powdered FBSR

material (<0.3 mm) with DIW and a predetermined amount of 2 N HNO₃, based upon the pre-titration results, and by adding a sufficient volume of DIW to bring the sample total volume to a liquid-to-solid ratio of 10 mL/g. These samples were reacted for 24 hours, and the resulting solutions were measured for pH, EC, and alkalinity (Table 6.3).

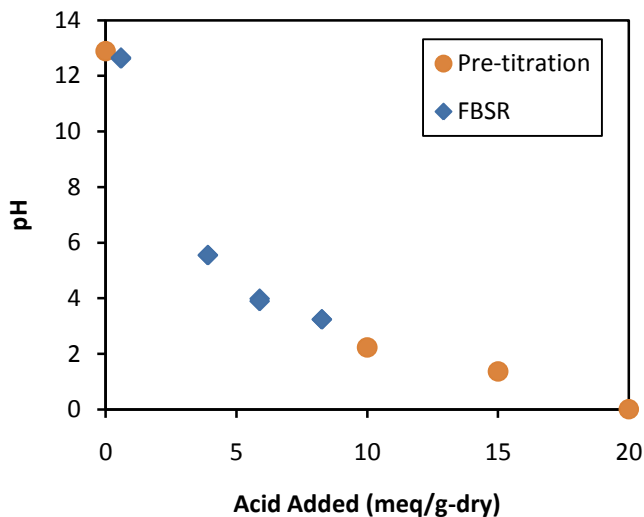


Figure 6.10. Titration Curves with Leaching Data for FBSR Encapsulating Waste Form

Duplicate samples of the FBSR material at targeted equilibrium pHs showed consistent titration results. As expected, the alkalinity of the eluate solution for each waste form decreased with decreasing pH. For example, the alkalinity at a pH of ~ 6 increased from ~ 275 mg/L to ~ 12800 mg/L at a pH of greater than 12 (Table 6.3). Conversely, the EC measurements showed lower dissolved salt content at high pH. The measured EC values represented the concentration of the dissolved ions in solution, and thus the higher concentration values observed at low pHs are indicative of more dissolved ions present in solution.

Table 6.3. The Values of pH, EC, and Alkalinity of FBSR Waste Form Measured from EPA Draft Method 1313

pH	EC mS/cm	Alkalinity mg/L as CaCO ₃
12.2	19.2	12700
12.2	19	12900
5.89	34.5	299
5.99	33.7	252
4.08	47.6	ND
3.97	49.2	ND
3.33	61.7	ND
3.33	59.4	ND

ND indicates “not detected” below quantification level for CaCO₃<23.5 mg/L.

The measured concentrations of rhenium (Tc surrogate) in the leached solution as a function of pH are shown in Figure 6.11. This trend suggests a pH correlation to the release of Re, with the concentration in solution increasing with the decrease in leaching pH. For example, the measured concentration of Re at a pH of ~3.3 was twice that of the leach at ~6 pH. It is important to note that these experiments were conducted using crushed samples of the supplied FBSR monoliths at a fixed solids-to-solution ratio. By using <0.3-mm size material, the percent leached is expected to be high in comparison to the monolith samples of the same material.

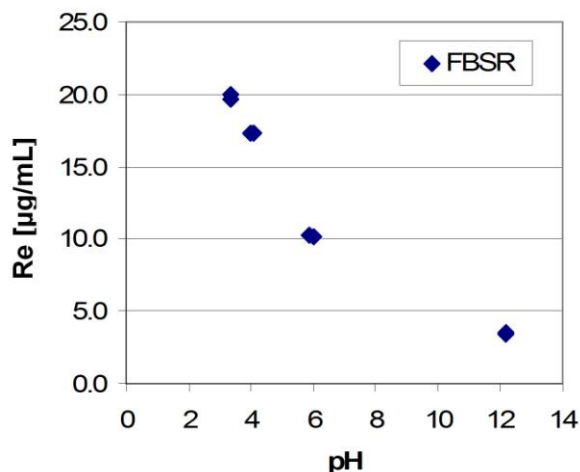


Figure 6.11. Leached Re (Tc surrogate) of the FBSR Encapsulated Waste Form in EPA Draft Method 1313

The measured concentration and calculated fraction of constituent released (in parentheses) of major cations, RCRA metals, and anions are shown in Table 6.4 through Table 6.6. The concentrations of the major cations and anions in solution increased with decreasing pH, consistent with EC measurements. For example, the potassium concentration measured at low pH (pH <4, K ~ 345 mg/L) was significantly higher than the value measured at high pH (pH ~ 6, K ~ 124 mg/L). The dominant cations in solution were sodium, potassium, aluminum, and silicon.

Table 6.4. The Concentrations of Major Cations in Eluate for the FBSR Waste Form from EPA Draft Method 1313

pH	Na (mg/L)	K (mg/L)	Al (mg/L)	Si (mg/L)	S (mg/L)	Fe (mg/L)
12.2	4820 (0.38)	62.4 (0.12)	ND	95.5 (0.003)	70.7 (0.11)	1.34 (0.001)
12.2	5130 (0.41)	66.4 (0.13)	ND	114 (0.004)	73.4 (0.12)	1.52 (0.001)
5.89	8170 (0.65)	123 (0.24)	10.4 (0.003)	60.2 (0.002)	119 (0.19)	ND
5.99	8150 (0.64)	124 (0.24)	9.86 (0.003)	57.9 (0.002)	118 (0.19)	ND
4.08	11200 (0.89)	276 (0.54)	240 (0.068)	138 (0.004)	93.5 (0.15)	2.1 (0.001)
3.97	11000 (0.87)	273 (0.54)	297 (0.084)	149 (0.005)	98.3 (0.16)	4.94 (0.002)
3.33	12100 (0.96)	343 (0.68)	2130 (0.60)	246 (0.008)	116 (0.18)	34.1 (0.014)
3.33	12200 (0.96)	348 (0.68)	2130 (0.60)	227 (0.007)	111 (0.18)	36.6 (0.015)

ND indicates “not detected” below quantification level for Al<0.329 mg/L; Fe<0.2 mg/L
Value in parentheses is the fraction of constituent released during the test.

Table 6.5 shows the concentrations of the RCRA metals, iodine, and rhenium in the EPA 1313 leachates. The RCRA metals detectable in the leach solution were cadmium, chromium, lead, and mercury. Detectable concentrations of arsenic were not observed in EPA draft Method 1313 leachate, which is consistent with the use of ppm concentration of arsenic in the simulated feed stream fed into the FBSR. Silver was not detected. The Re release was greatest at pH~3.3 and the lowest at pH>12.

The major anion concentrations for EPA draft Method 1313 are presented in Table 6.6. The total concentration of sulfur and phosphorus as measured by ICP-OES were converted to SO_4^{2-} and PO_4^{3-} , respectively, and are also listed in Table 6.6. The calculated concentrations of SO_4^{2-} from ICP-OES measurements are presented alongside measured IC concentrations of SO_4^{2-} . Measured concentrations of SO_4^{2-} and PO_4^{3-} were not detected. The apparent increase in concentration of the calculated SO_4^{2-} may be associated with the presence of other sulfur species in the solution, such as S^{2-} and HS^- .

Table 6.5. The Concentrations of Select RCRA Metals, Iodine and Rhenium in Eluate for the FBSR Waste Form from EPA Draft Method 1313

pH	Cd (µg/L)	Cr (µg/L)	Pb (µg/L)	Hg (µg/L)	I µg/L	Re µg/L
12.2	35.2 (0.003)	55.7 (0.001)	21.5 (0.0004)	43.2	1.29E+03	3.41E+03 (0.13)
12.2	36.2 (0.003)	56.3 (0.001)	22.4 (0.0004)	43.7	1.30E+03	3.50E+03 (0.14)
5.89	50.3 (0.004)	238 (0.005)	ND	6.15	2.27E+03	1.03E+04 (0.40)
5.99	46.5 (0.004)	ND	ND	6.07	2.10E+03	1.01E+04 (0.39)
4.08	3720 (0.32)	ND	107 (0.0018)	ND	9.93E+02	1.73E+04 (0.67)
3.97	3620 (0.31)	ND	115 (0.0019)	ND	1.33E+03	1.73E+04 (0.67)
3.33	7110 (0.61)	ND	778 (0.013)	ND	3.65E+02	1.97E+04 (0.76)
3.33	6980 (0.61)	ND	775 (0.013)	ND	3.53E+02	2.00E+04 (0.76)

ND indicates “not detected” below quantification level for Cr<9.58 µg/L;
Pb<4.66 µg/L; Hg<1.81 µg/L.
Value in parentheses is the fraction of constituent released during the test

Table 6.6. The Concentrations of Major Anions in Eluate for the FBSR Waste Form from EPA Draft Method 1313

pH	PO ₄ ³⁻ (mg/L)	PO ₄ ³⁻ (mg/L) ^(a)	SO ₄ ²⁻ (mg/L)	SO ₄ ²⁻ (mg/L) ^(a)
12.2	ND	1.42E+02	ND	2.12E+02
12.2	ND	1.47E+02	ND	2.20E+02
5.89	ND	ND	ND	3.57E+02
5.99	ND	ND	ND	3.54E+02
4.08	ND	ND	ND	2.80E+02
3.97	ND	ND	ND	2.94E+02
3.33	ND	5.73E+00	ND	3.48E+02
3.33	ND	6.90E+00	ND	3.33E+02

(a) PO₄³⁻ and SO₄²⁻ were also calculated based on phosphorus and sulfur concentrations analyzed by ICP-OES. ND indicates “not detected” below quantification level for PO₄³⁻<1500 mg/L; P<1.43 mg/L; SO₄²⁻<1500 mg/L; S<6.65 mg/L

6.3 Effect of Liquid-to-Solid Ratio—EPA Draft Method 1316

The results of pH, EC, and alkalinity for the leached FBSR monolithed material are shown in Table 6.7. In EPA draft Method 1316, the liquid-to-solid ratio is varied (10, 5, and 2 mL/g) to evaluate how these changes will impact the leaching characteristics of the constituents of interest. Unlike the investigation in EPA draft Method 1313, the leached solution pH is not modified, and the powdered test material is leached and allowed to come to equilibrium in DIW. This results in the majority of the measured pH being greater than pH 12, irrespective of the liquid-to-solid ratio. The alkalinity is consistent with the substantial sodium released which may be due, in part, to residual unreacted NaOH from the geopolymer binder preparation. The measured EC and alkalinity values decreased with an increase in liquid-to-solid ratio. The observed decrease in EC and alkalinity values are probably the result of a dilution effect, as the measured values at 10 mL/g were slightly higher than calculated EC and alkalinity values for 10 mL/g using those measured at 5 and 2 mL/g ratios divided by 2 and 5 dilution factors, respectively. Proportionately more dissolution occurred as the volume of test solution used in EPA draft Method 1316 was increased.

Table 6.7. The Values of pH, EC, and Alkalinity of FBSR Waste Form Measured from EPA Draft Method 1316

pH	LS ratio mL/g	EC mS/cm	Alkalinity mg/L as CaCO ₃
12.5	10	21.4	1.29E+04
12.6	10	21.1	1.51E+04
12.6	5	34.6	2.12E+04
12.7	5	33.9	2.25E+04
12.8	2	62.6	4.05E+04
12.8	2	65.4	4.64E+04

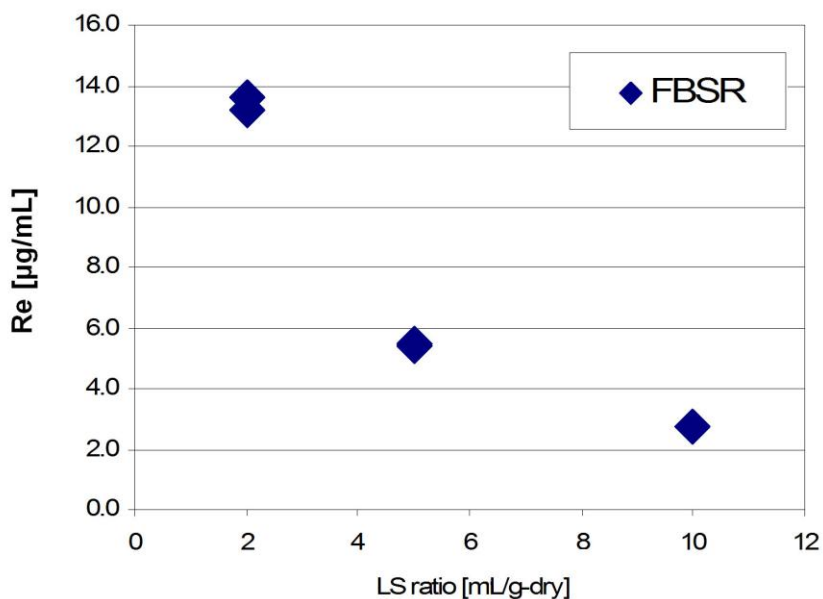


Figure 6.12. Leached Re (Tc surrogate) of the FBSR Encapsulated Waste Form in EPA Draft Method 1316

The measured concentration of rhenium (Tc surrogate) released from the powdered FBSR monolith material into the leachate is shown as a function of the liquid-to-solid ratio in Figure 6.12. The concentration of rhenium in the leachate decreases with an increase in the liquid-to-solid ratio. This suggests that at the increased volumes associated with the higher liquid-to-solid ratio, the tests are effectively diluting the rhenium concentration in the leachate. It is important to note that these experiments were conducted with a powdered sample of the supplied FBSR monolithed material at multiple solution volume-to-solids mass ratios and that by using <0.3-mm-size material, the percent leached is expected to be high in comparison to the monolith samples of the same material.

The measured concentrations and calculated fraction of constituent released (in parentheses) of major cations, RCRA metals, and anions are shown in Table 6.8 through Table 6.10. In general, the major cations and anions showed increased dissolved concentrations in samples with lower liquid-to-solid ratios. The predominant cations are sodium and potassium.

Table 6.8. The Concentrations of Major Elements in Eluate for the FBSR Waste Form from EPA Draft Method 1316

LS Ratio mL/g	Na mg/L	K mg/L	Al mg/L	Si mg/L	S mg/L	Fe mg/L
10	4.65E+03 (0.37)	66.9 (0.132)	5.61 (0.002)	320 (0.01)	69.7 (0.11)	6.50 (0.003)
10	4.73E+03 (0.37)	67.7 (0.133)	2.85 (0.001)	144 (0.004)	68 (0.11)	4.92 (0.002)
5	8.80E+03 (0.35)	129 (0.127)	7.51 (0.001)	1.92E+03 (0.03)	138 (0.11)	7.17 (0.001)
5	8.84E+03 (0.35)	128 (0.126)	8.72 (0.001)	1.99E+03 (0.03)	140 (0.11)	2.62 (0.001)
2	2.23E+4 (0.35)	326 (0.128)	54.0 (0.003)	8.39E+03 (0.05)	344 (0.11)	23.2 (0.002)
2	2.24E+4 (0.35)	334 (0.131)	68.4 (0.004)	8.43E+03 (0.05)	360 (0.11)	21.3 (0.002)

Value in paratheses is the fraction of constituent released during the test

The measured RCRA metal concentrations are shown in Table 6.9 and also indicate higher concentrations at lower liquid-to-solid ratios. The RCRA metals detectable in the leach solution were cadmium, chromium, lead, silver, and mercury. Detectable concentrations of arsenic were not present in EPA draft Method 1313, which is consistent with the use of ppm concentration of arsenic in the simulated feed stream fed into the FBSR.

Table 6.9. The Concentrations of Select RCRA Metals, Iodine and Rhenium in Eluate for the FBSR Waste Form from EPA Draft Method 1316

LS ratio mL/g	Cd µg/L	Cr µg/L	Pb µg/L	Ag µg/L	Hg µg/L	I µg/L	Re µg/L
10	97 (0.008)	101 (0.002)	94.2 (0.002)	52 (.0055)	47.3	1.39E+03	2.73E+03 (0.11)
10	89.1 (0.008)	93.5 (0.002)	84.2 (0.001)	11.6 (0.0012)	48.6	1.28E+03	2.71E+03 (0.11)
5	103 (0.004)	114 (0.001)	164 (0.001)	3.23 (.0002)	100	1.94E+03	5.43E+03 (0.11)
5	106 (0.005)	117 (0.001)	177 (0.001)	ND	98.6	1.94E+03	5.44E+03 (0.11)
2	271 (0.005)	248 (0.001)	1120 (0.004)	ND	233	3.98E+03	1.36E+04 (0.11)
2	258 (0.004)	246 (0.001)	1090 (0.004)	ND	235	4.06E+03	1.32E+04 (0.10)

ND indicates “not detected” below quantification level for Ag < 3 µg/L.
Value in paratheses is the fraction of constituent released during the test

The major anion concentrations for EPA draft Method 1316 are presented in Table 6.10. The total concentration of sulfur and phosphorus as measured by ICP-OES were converted to SO_4^{2-} and PO_4^{3-} , respectively, and are also listed in Table 6.10. The calculated concentration of SO_4^{2-} from ICP-OES measurements are presented alongside measured IC concentrations of SO_4^{2-} and were slightly higher than the IC measured concentration. The higher calculated concentration of SO_4^{2-} is thought to be associated with the presence of other sulfur species in the solution. Anions NO_3^- and NO_2^- were not detected and would not be expected to be detected because the FBSR process destroys the NO_x species.

Table 6.10. The Concentrations of Major Anions in Eluate for the FBSR Waste Form from EPA Draft Method 1316

LS ratio mL/g	NO_3^- mg/L	NO_2^- mg/L	PO_4^{3-} mg/L	PO_4^{3-} (mg/L) ^(a)	SO_4^{2-} mg/L	SO_4^{2-} (mg/L) ^(a)
10	ND	ND	1.53E+02	1.47E+02	1.86E+02	2.09E+02
10	ND	ND	ND	1.46E+02	1.84E+02	2.04E+02
5	ND	ND	2.93E+02	2.99E+02	3.73E+02	4.13E+02
5	ND	ND	2.94E+02	3.03E+02	3.72E+02	4.19E+02
2	ND	ND	7.36E+02	7.54E+02	9.44E+02	1.03E+03
2	ND	ND	7.52E+02	7.67E+02	9.52E+02	1.08E+03

(a) PO_4^{3-} and SO_4^{2-} were also calculated based on phosphorus and sulfur concentrations analyzed by ICP-OES. ND indicates “not detected” below quantification level for $\text{NO}_3^- < 100$ mg/L; $\text{NO}_2^- < 100$ mg/L; $\text{PO}_4^{3-} < 150$ mg/L; $\text{SO}_4^{2-} < 150$ mg/L.

6.4 Leachability—EPA Draft Method 1315

Per EPA draft Method 1315, the supplied 2-in. diameter × 4-in cylindrical FBSR encapsulating monolith waste forms were suspended in DIW with a liquid volume-to-specimen surface area ratio of 9 ± 1 mL/cm². The leachate solutions were collected and renewed at the specified time interval, and the results for the pH, EC, and alkalinity measurements for each of the monoliths with respect to time interval

are presented in Table 6.11. The final leachate pH levels ranged from > pH 10 to > pH 12, and they correlated with the time interval. Initially, the shorter leaching periods tended to have the lower pHs, and the longer intervals the higher, with a 14-day leaching interval resulting in pH levels > pH 12. The lower pHs at cumulative leach times of 14 days or less were lower than the final pH levels measured for the EPA draft Method 1316 liquid-to-solids ratio 24-hour tests, suggesting that the lower EPA draft Method 1315 pH values resulted from the larger volume-to-specimen surface areas. For the time intervals beyond the recommended total 63 day leach duration, the pH values trend back down suggesting that the amount of available hydroxide, presumably unreacted excess from the binder formulation, is depleted.

The measured EC values ranged from ~1.14 mS/cm to ~7.44 mS/cm and the alkalinity values from < 800 mg/L as CaCO₃ to <8000 mg/L as CaCO₃. The FBSR test monoliths indicated no measurable change in size or shape after 63 days of cumulative exposure to DIW and no visible formation of precipitate on the monolith surface, in the leach vessel, or in the collected leachate.

The leach test was continued with one test specimen for a total of 306 days, and the leachate was collected and analyzed for pH, EC, and constituent concentrations at total durations of 149, 189, 222, and 306 days. The test monoliths demonstrated no measurable change in size or shape and no precipitate formation on the surface or in the test container. The extended leach period data are included for information only.

The diffusivity values of Re (Tc surrogate) were calculated for the measured concentrations collected during EPA draft Method 1315 and are displayed in Figure 6.13. Rhenium diffusivity values for the FBSR monolith samples range from $\sim 5.5 \times 10^{-9}$ cm²/s at a cumulative leaching time of 7 days to $\sim 2.7 \times 10^{-10}$ cm²/s at a cumulative leaching time of 63 days. The FBSR monolithed waste form showed a slightly decreasing trend in calculated Re diffusivity as the contact time increased.

The measured cation values are presented in Table 6.12.

Table 6.11. The Values of pH, EC, and Alkalinity of FBSR Waste Form Measured from EPA Draft Method 1315

Cumulative Leach Time days	pH	EC mS/cm	Alkalinity mg/L as CaCO ₃
0.08	10.3	1.14	756
0.08	10.4	1.49	985
1	10.5	4.59	6890
1	10.6	4.16	5730
2	10.7	1.33	3410
2	10.7	1.38	871
7	10.3	5.41	5510
7	11.8	6.98	5350
14	11.5	5.16	5510
14	12.1	7.13	5350
28	12.1	6.93	6560
28	12.2	7.44	6980
42	12.1	4.04	5850
42	12	4.12	5570
49	11.7	1.55	4250
49	11.8	1.53	3920
63	11.4	1.39	2540
63	11.5	1.4	3010
149	10.2	0.875	
189	9.49	0.357	
222	8.9	0.209	
306	8.9	0.341	

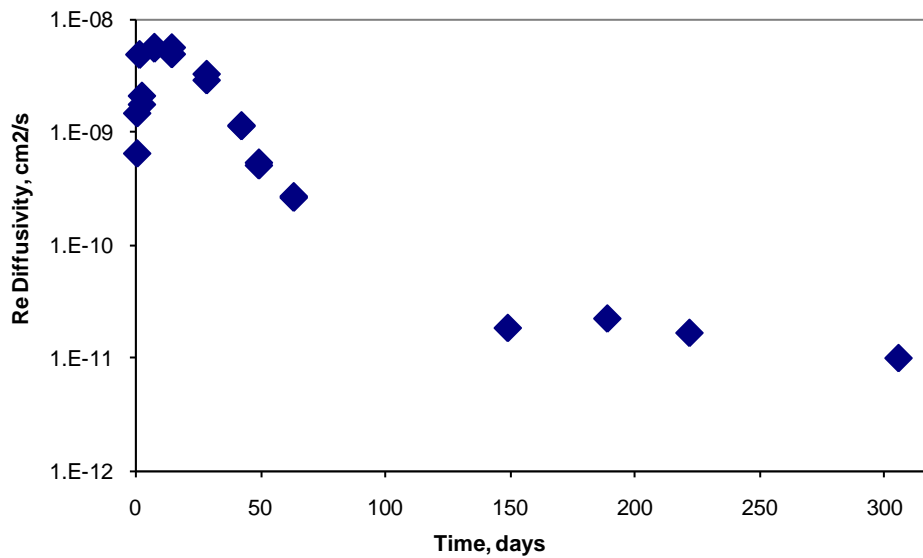


Table 6.12. The Concentrations of Major Cations in Eluate for the FBSR Waste Form from EPA Draft Method 1315

Cumul. Leach								
Time days	Na mg/L	Ca mg/L	K mg/L	Al mg/L	Si mg/L	Mg mg/L	S mg/L	Fe mg/L
0.08	2.52E+02	ND	4.14E+00	ND	4.50E+00	ND	ND	ND
0.08	3.33E+02	ND	5.78E+00	ND	7.32E+00	ND	4.53E+00	ND
1	1.21E+03	ND	1.79E+01	ND	4.46E+01	ND	1.97E+01	ND
1	1.06E+03	ND	1.69E+01	ND	7.84E+01	ND	1.87E+01	ND
2	2.93E+02	ND	4.73E+00	ND	2.48E+01	ND	4.49E+00	ND
2	3.01E+02	ND	4.78E+00	ND	6.51E+01	ND	4.51E+00	ND
7	1.49E+03	ND	2.21E+01	ND	2.18E+02	ND	2.35E+01	1.42E-01
7	1.70E+03	ND	2.97E+01	6.45E-01	7.52E+02	4.58E-01	2.37E+01	2.33E+00
14	1.37E+03	ND	2.36E+01	8.41E-01	8.49E+02	3.68E-01	1.71E+01	1.89E+00
14	1.48E+03	7.39E-01	2.60E+01	1.15E+00	7.25E+02	9.55E-01	1.73E+01	4.46E+00
28	1.57E+03	6.33E-01	2.87E+01	1.74E+00	9.74E+02	1.02E+00	1.85E+01	4.49E+00
28	1.53E+03	7.81E-01	2.64E+01	1.35E+00	8.47E+02	1.35E+00	1.73E+01	5.68E+00
42	7.96E+02	ND	1.40E+01	1.33E+00	4.49E+02	7.80E-01	7.02E+00	3.13E+00
42	7.52E+02	ND	1.28E+01	1.21E+00	4.04E+02	9.01E-01	6.81E+00	3.53E+00
49	2.47E+02	ND	4.65E+00	1.23E+00	1.36E+02	3.57E-01	ND	1.36E+00
49	2.46E+02	ND	4.25E+00	1.09E+00	1.25E+02	4.24E-01	ND	1.66E+00
63	2.29E+02	ND	3.97E+00	1.19E+00	1.30E+02	5.55E-01	ND	2.09E+00
63	2.28E+02	ND	3.86E+00	1.30E+00	1.25E+02	6.78E-01	ND	2.61E+00
149	2.01E+02	ND	ND	7.71E-01	5.79E+01	5.57E-01	ND	2.47E+00
189	8.26E+01	ND	ND	4.66E-01	2.52E+01	1.34E-01	ND	7.44E-01
222	4.78E+01	ND	ND	1.73E+00	2.95E+01	5.91E-02	ND	3.91E-01
306	6.97E+01	2.62E+00	ND	4.00E+00	1.97E+01	3.34E-01	ND	7.00E-01

ND indicates “not detected” below quantification level for Ca<0.981 mg/L; K<5.92 mg/L; Al<0.33 mg/L; Si<2.62 mg/L; Mg<0.069 mg/L; S<6.65 mg/L; Fe<0.2 mg/L.

The RCRA metal leachate concentration results for the FBSR monolithed waste form are shown in Table 6.13. The detectable RCRA metals were cadmium, chromium, lead, and mercury. Copper, arsenic, and silver were not detected in EPA draft Method 1315. This is due to the absence of copper and a very low concentration (ppm) of arsenic in the simulated feed stream fed into the FBSR. The dominant anions present in the FBSR monolithed waste form leachate solutions are presented in Table 6.14. The total concentration of sulfur and phosphorus as measured by ICP-OES were converted to SO_4^{2-} and PO_4^{3-} , respectively, and are also listed in Table 6.14. The calculated concentrations of SO_4^{2-} from ICP-OES measurements are presented alongside measured IC concentrations of SO_4^{2-} . The FBSR leachate concentrations of NO_3^- and SO_4^{2-} were below detection limits. The iodine concentration was high enough to be measured at all cumulative time intervals for the FBSR monolithed waste form leachate.

Table 6.13. The Concentrations of Select Elements in Eluate for the FBSR Waste Form from Draft Method 1315

Cumulative Leach Time days	Cd $\mu\text{g/L}$	Cr $\mu\text{g/L}$	Pb $\mu\text{g/L}$	Hg $\mu\text{g/L}$	Cs $\mu\text{g/L}$	I $\mu\text{g/L}$	Re $\mu\text{g/L}$
0.08	ND	ND	ND	ND	2.84E+02	1.70E+01	9.04E+01
0.08	ND	ND	ND	ND	3.41E+02	2.77E+01	1.37E+02
1	ND	ND	ND	ND	1.13E+03	1.75E+02	6.27E+02
1	ND	ND	ND	ND	9.58E+02	2.31E+02	6.33E+02
2	ND	ND	ND	ND	3.08E+02	6.39E+01	2.03E+02
2	ND	ND	ND	ND	3.02E+02	9.72E+01	2.23E+02
7	ND	ND	2.09E+01	ND	1.25E+03	4.62E+02	1.14E+03
7	2.94E+01	1.79E+01	2.31E+01	ND	1.40E+03	4.78E+02	1.13E+03
14	2.13E+01	2.27E+01	2.68E+01	ND	1.25E+03	4.50E+02	1.01E+03
14	5.23E+01	2.37E+01	4.61E+01	ND	1.24E+03	4.67E+02	9.50E+02
28	4.62E+01	3.90E+01	5.34E+01	ND	1.50E+03	5.45E+02	1.09E+03
28	6.79E+01	2.79E+01	5.53E+01	ND	1.25E+03	5.48E+02	1.03E+03
42	3.19E+01	2.20E+01	3.56E+01	ND	8.07E+02	2.60E+02	4.96E+02
42	4.22E+01	1.54E+01	3.84E+01	ND	6.48E+02	2.62E+02	4.95E+02
49	1.32E+01	ND	1.66E+01	ND	2.92E+02	8.48E+01	1.44E+02
49	1.77E+01	ND	2.04E+01	ND	2.38E+02	8.55E+01	1.49E+02
63	1.90E+01	1.34E+01	2.74E+01	ND	2.91E+02	1.06E+02	1.87E+02
63	2.50E+01	1.07E+01	3.42E+01	ND	2.43E+02	1.02E+02	1.91E+02
149	1.41E+01	1.95E+01	3.90E+01	ND	2.02E+02	1.36E+02	2.26E+02
189	3.60E+00	ND	1.43E+01	ND	8.21E+01	5.37E+01	8.98E+01
222	ND	ND	8.08E+00	ND	4.88E+01	3.19E+01	5.80E+01
306	ND	1.17E+01	1.56E+01	ND	7.71E+01	5.76E+01	1.01E+02

ND indicates "not detected" below quantification level for Cd<3.4 $\mu\text{g/L}$; Cr<9.58 $\mu\text{g/L}$; Pb<4.66 $\mu\text{g/L}$; Hg<7.5 $\mu\text{g/L}$.

Table 6.14. The Concentrations of Major Anions in Eluate for the FBSR Waste Form from Draft Method 1315

Cumul. Leach Time days	NO ₃ ⁻ mg/L	NO ₂ ⁻ mg/L	PO ₄ ³⁻ mg/L	PO ₄ ³⁻ (mg/L) ^(a)	SO ₄ ²⁻ mg/L	SO ₄ ²⁻ (mg/L) ^(a)
0.08	ND	ND	4.72E+00	5.34E+00	7.99E+00	ND
0.08	ND	ND	ND	7.33E+00	1.25E+01	1.36E+01
1	ND	ND	2.76E+01	2.75E+01	5.35E+01	5.90E+01
1	ND	ND	2.68E+01	2.73E+01	5.08E+01	5.60E+01
2	ND	ND	7.94E+00	8.37E+00	1.43E+01	1.35E+01
2	ND	ND	8.31E+00	8.22E+00	1.36E+01	1.35E+01
7	ND	ND	3.66E+01	3.86E+01	6.18E+01	7.04E+01
7	ND	ND	3.74E+01	3.96E+01	6.27E+01	7.10E+01
14	ND	ND	3.08E+01	3.28E+01	4.59E+01	5.12E+01
14	ND	ND	3.78E+01	3.99E+01	4.72E+01	5.18E+01
28	ND	ND	5.18E+01	4.94E+01	5.01E+01	5.54E+01
28	ND	ND	4.98E+01	5.03E+01	4.68E+01	5.18E+01
42	ND	ND	3.08E+01	3.10E+01	1.92E+01	2.10E+01
42	ND	ND	2.93E+01	2.87E+01	1.87E+01	2.04E+01
49	ND	ND	9.82E+00	9.41E+00	ND	ND
49	ND	ND	9.58E+00	9.72E+00	ND	ND
63	ND	ND	7.70E+00	7.27E+00	ND	ND
63	ND	ND	7.92E+00	8.19E+00	ND	ND
149	ND	ND	2.52E+00	2.92E+00	9.47E-01	ND
189	ND	ND	1.51E+00	ND	ND	ND
222	ND	ND	1.03E+00	ND	ND	ND
306	ND	ND	1.57E+00	ND	1.00E+00	ND

(a) PO₄³⁻ and SO₄²⁻ were also calculated based on phosphorus and sulfur concentrations analyzed by ICP-OES. ND indicates “not detected” below quantification level for NO₃⁻<0.5 mg/L; NO₂⁻<0.5 mg/L; P<0.715 mg/L; SO₄²⁻<0.75 mg/L; S<3.32 mg/L.

6.5 Leachability—ANSI/ANS 16.1

The ANSI/ANS 16.1-2003 test method was performed in parallel with the EPA draft Method 1315. For the ANSI/ANS 16.1-2003 leach tests, 2-in. diameter × 4-in. cylindrical FBSR monoliths were suspended in DIW at a liquid volume-to-specimen surface area ratio of 10 ± 0.2 mL/cm². Leach solutions were collected and exchanged with DIW at prescribed time intervals for a total of 90 days, extending the leach test an additional 27 days beyond EPA Method 1315. The measured results of the pH, EC, and alkalinity for each of the FBSR leachates are displayed in Table 6.15. The final leachate pH levels ranged from > pH 10 to > pH 12 and correlated with the time interval. Initially, the shorter leaching periods tended to have the lower pHs and the longer intervals higher, with leaching intervals of 14 and 28 days resulting in pH levels > pH 12. ANSI/ANS 16.1 pH measurements are consistent with values of the EPA draft Method 1315 tests. The pH values for the cumulative leach durations at 90 days and beyond also trend lower with increased total leach time, and as with the EPA draft Method 1315, are thought to be the result of the reduction in available hydroxide present as a result of the binder formulation.

The measured EC values ranged from 1.1 mS/cm at 0.08 days to 12.1 mS/cm at 19 days and the alkalinity values from 1660 mg/L as CaCO₃ at 0.08 days to 9880 mg/L as CaCO₃ at 19 days. The EC and alkalinity values are consistent with the values measured for the EPA draft Method 1315 tests. The longer cumulative 90 day exposure to DIW of the ANSI/ANS 16.1 test indicated no measurable change in size or shape of the test monoliths and no visible formation of precipitates on the test form surface, in the test vessel or in the leachate.

The leach test was continued with one test specimen for a total of 306 days, and the leachate was collected and analyzed for pH, EC, and constituent concentrations at total durations of 149, 189, 222, and 306 days. The extended leaches did not indicate measurable changes in shape or size and no precipitate formation was observed on the monolith or test vessel. Extended period data are included for information only.

Table 6.15. The Values of pH, EC, and Alkalinity of FBSR Waste Form Leachates from ANSI/ANS 16.1

Cumulative Leach Time days	pH	EC mS/cm	Alkalinity mg/L as CaCO ₃
0.08	10.3	1.66	2320
0.08	10.4	1.17	1660
0.29	10.5	1.79	3160
0.29	10.6	1.76	4060
1	10.7	2.72	4200
1	10.9	2.8	5070
2	10.8	2.06	3460
2	11.3	2.21	3670
3	11	1.93	2890
3	11.6	2.59	3900
4	11.2	1.73	2440
4	11.7	2.34	2650
5	11.3	1.62	2540
5	11.6	2.11	ND
19	12.3	11.8	9880
19	12.3	12.7	9610
47	12.2	8.54	8550
47	12.2	8.42	7750
90	11.7	2.91	3890
90	11.7	3.04	3890
149	10.4	1.21	
189	9.47	0.467	
222	8.93	0.249	
306	8.76	0.299	

ND indicates “not detected” below quantification level for CaCO₃<23.5 mg/L.

The diffusivity values of Re (Tc surrogate) were calculated for the measured concentrations collected during ANSI/ANS/ANS 16.1 and are displayed in Figure 6.14. Diffusivity values for the FBSR monolith samples range from $\sim 5 \times 10^{-9}$ cm²/s at a cumulative leaching time of 3 days to $\sim 1.8 \times 10^{-10}$ cm²/s at a cumulative leaching time of 90 days. The FBSR monolithed waste form showed a decreasing trend in calculated diffusivity as the contact time increased. The decreasing Re concentration trend and the range of Re diffusivities are consistent with those observed for the EPA draft Method 1315 tests. The measured cation values are presented in Table 6.16 and are consistent with the concentration values recorded for the EPA draft Method 1315. The predominant components were Na, Si, and K and show a slight increase in concentration at the longest leach intervals.

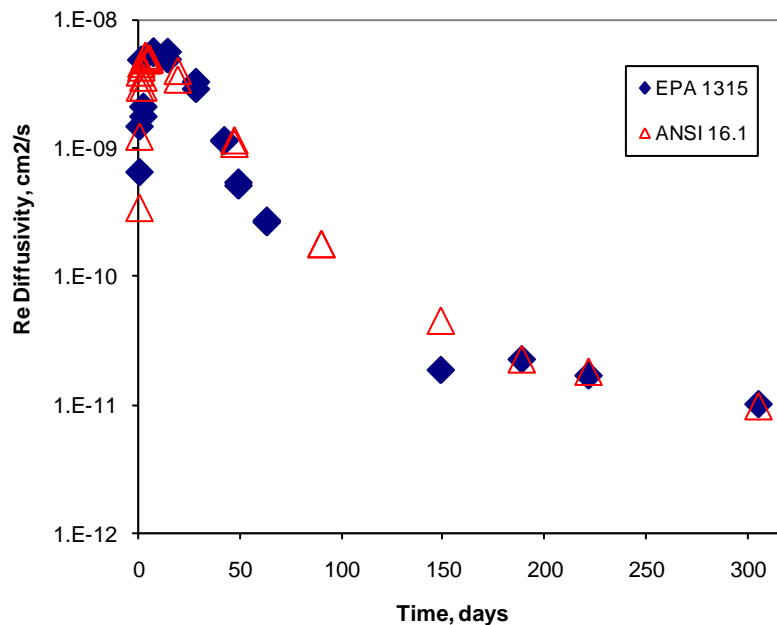


Figure 6.14. Diffusivity of Re in FBSR Monolith Waste Form for EPA Draft Method 1315 and ANSI/ANS 16.1

The RCRA metal leachate concentration results for the ANSI/ANS 16.1 test on the FBSR monolithed waste form are shown in Table 6.17. Low concentration levels were measured for cadmium, chromium, lead, and mercury, and there was no detection for copper, arsenic, and silver. The general magnitude of the concentrations measured is consistent with observations of the EPA draft Method 1315 tests.

Table 6.16. The Concentrations of Major Cations in Eluate for the FBSR Waste Form from ANSI/ANS 16.1

Cumul. Leach Time days	Na mg/L	Ca mg/L	K mg/L	Al mg/L	Si mg/L	Mg mg/L	S mg/L	Fe mg/L
0.08	3.36E+02	ND	5.82E+00	ND	7.25E+00	ND	4.56E+00	ND
0.08	2.33E+02	ND	4.34E+00	ND	5.02E+00	ND	ND	ND
0.29	3.58E+02	ND	5.85E+00	ND	1.89E+01	ND	7.19E+00	ND
0.29	3.61E+02	ND	6.03E+00	ND	2.24E+01	ND	7.23E+00	ND
1	6.03E+02	ND	9.36E+00	ND	6.07E+01	ND	1.03E+01	ND
1	6.08E+02	ND	9.95E+00	1.79E-01	1.54E+02	ND	1.17E+01	1.87E-01
2	4.32E+02	ND	7.08E+00	ND	9.75E+01	ND	7.55E+00	ND
2	4.52E+02	ND	8.05E+00	2.18E-01	1.59E+02	7.70E-02	7.26E+00	4.30E-01
3	4.14E+02	ND	6.43E+00	1.78E-01	1.58E+02	4.10E-02	6.26E+00	2.61E-01
3	4.69E+02	ND	8.75E+00	2.94E-01	1.65E+02	1.59E-01	6.90E+00	8.93E-01
4	3.65E+02	ND	6.02E+00	2.17E-01	1.60E+02	6.58E-02	5.43E+00	4.01E-01
4	3.95E+02	ND	7.26E+00	2.93E-01	1.63E+02	1.72E-01	5.38E+00	9.20E-01
5	3.24E+02	ND	5.68E+00	2.15E-01	1.61E+02	8.69E-02	4.65E+00	5.06E-01
5	3.09E+02	ND	5.86E+00	3.19E-01	1.47E+02	1.66E-01	4.61E+00	9.02E-01
19	2.50E+03	1.72E+00	4.70E+01	1.85E+00	7.51E+02	1.78E+00	3.24E+01	8.27E+00
19	2.27E+03	1.48E+00	4.02E+01	1.89E+00	1.09E+03	1.80E+00	2.99E+01	7.89E+00
47	1.68E+03	8.54E-01	2.80E+01	1.64E+00	8.72E+02	1.75E+00	1.69E+01	6.60E+00
47	1.63E+03	7.39E-01	2.66E+01	1.71E+00	7.98E+02	1.68E+00	1.66E+01	6.19E+00
90	6.16E+02	ND	9.68E+00	1.72E+00	3.02E+02	1.57E+00	ND	5.47E+00
90	5.88E+02	ND	8.92E+00	1.72E+00	2.78E+02	1.53E+00	ND	5.42E+00
149	2.80E+02	ND	3.92E+00	9.66E-01	8.55E+01	8.24E-01	ND	3.39E+00
189	1.07E+02	ND	ND	5.42E-01	2.97E+01	2.58E-01	ND	1.26E+00
222	5.82E+01	ND	ND	1.22E+00	2.82E+01	1.22E-01	ND	6.86E-01
306	7.89E+01	ND	ND	3.37E+00	2.06E+01	1.76E-01	ND	1.20E+00

ND indicates "not detected" below quantification level for Ca<0.490 mg/L; K<2.96 mg/L; Al<0.165 mg/L; Mg<0.034 mg/L; S<3.32 mg/L; Fe<0.1 mg/L.

The dominant anions present in the FBSR, monolithed, waste form leachate solutions are presented in Table 6.18. The total concentration of sulfur and phosphorus as measured by ICP-OES were converted to SO_4^{2-} and PO_4^{3-} , respectively, and are also listed in Table 6.18. The calculated concentrations of SO_4^{2-} from ICP-OES measurements are presented alongside measured IC concentrations of SO_4^{2-} . The FBSR leachate concentration values for NO_3^- and NO_2^- were not detected. The FBSR leachate IC measured concentrations of SO_4^{2-} and the calculated "equivalents based on the concentration of sulfur and phosphorous were comparable to those measured and calculated in EPA draft Method 1315. Iodine-127 and Re concentration values were consistent with the general magnitudes measured during the EPA draft Method 1315 testing of the FBSR monolithed waste form.

Table 6.17. Concentrations of Select RCRA Metals, Iodine and Rhenium in Leachate for the FBSR Waste Form from ANSI/ANS 16.1

Cumul. Leach Time days	Cd µg/L	Cr µg/L	Pb µg/L	Hg µg/L	Cs µg/L	I µg/L	Re µg/L
0.08	ND	ND	ND	ND	3.38E+02	2.69E+01	1.35E+02
0.08	ND	ND	ND	ND	2.27E+02	1.93E+01	7.22E+01
0.29	ND	ND	ND	ND	3.66E+02	5.96E+01	2.09E+02
0.29	ND	ND	ND	ND	3.43E+02	6.23E+01	1.85E+02
1	ND	ND	ND	ND	5.53E+02	1.56E+02	4.00E+02
1	ND	ND	ND	ND	5.46E+02	1.63E+02	4.19E+02
2	ND	ND	ND	ND	3.94E+02	1.41E+02	3.29E+02
2	5.91E+00	ND	4.78E+00	ND	4.04E+02	1.17E+02	3.05E+02
3	4.59E+00	ND	ND	ND	3.69E+02	1.33E+02	3.03E+02
3	1.08E+01	ND	8.94E+00	ND	4.20E+02	1.21E+02	3.12E+02
4	5.04E+00	ND	5.13E+00	ND	3.10E+02	1.05E+02	2.49E+02
4	1.03E+01	ND	8.76E+00	ND	3.40E+02	1.00E+02	2.52E+02
5	6.60E+00	ND	5.96E+00	ND	2.91E+02	9.10E+01	2.23E+02
5	1.02E+01	ND	8.90E+00	ND	3.07E+02	8.82E+01	2.23E+02
19	8.68E+01	3.99E+01	7.73E+01	7.96E+00	1.97E+03	8.61E+02	1.79E+03
19	8.17E+01	3.95E+01	7.26E+01	1.07E+01	1.78E+03	8.40E+02	1.68E+03
47	7.88E+01	2.97E+01	6.89E+01	ND	1.27E+03	6.03E+02	1.13E+03
47	6.86E+01	2.81E+01	6.34E+01	ND	1.16E+03	5.62E+02	1.11E+03
90	5.48E+01	2.29E+01	7.70E+01	ND	5.12E+02	2.80E+02	4.70E+02
90	4.95E+01	2.20E+01	7.93E+01	ND	4.77E+02	2.71E+02	4.75E+02
149	2.33E+01	1.89E+01	5.81E+01	ND	2.16E+02	1.36E+02	2.44E+02
189	7.50E+00	ND	2.46E+01	ND	8.75E+01	5.30E+01	9.77E+01
222	4.81E+00	ND	1.59E+01	ND	4.90E+01	3.16E+01	6.54E+01
306	6.65E+00	1.07E+01	2.87E+01	ND	7.85E+01	5.44E+01	1.08E+02

ND indicates "not detected" below quantification level for Cd<3.4 µg/L; Cr<9.58 µg/L; Pb<4.66 µg/L; Hg<7.5 µg/L.

Table 6.18. The Concentrations of Major Anions in Leachate for the FBSR Waste Form from ANSI/ANS -16.1

Cumul. Leach Time days	NO ₃ ⁻ µg/mL	NO ₂ ⁻ µg/mL	PO ₄ ³⁻ µg/mL	PO ₄ ³⁻ (µg/mL) ^(a)	SO ₄ ²⁻ µg/mL	SO ₄ ²⁻ (µg/mL) ^(a)
0.08	ND	ND	ND	6.68E+00	1.21E+01	1.37E+01
0.08	ND	ND	4.30E+00	4.78E+00	7.99E+00	ND
0.29	ND	ND	9.51E+00	9.72E+00	2.06E+01	2.15E+01
0.29	ND	ND	9.51E+00	9.23E+00	1.92E+01	2.17E+01
1	ND	ND	1.68E+01	1.62E+01	3.04E+01	3.09E+01
1	ND	ND	1.63E+01	1.66E+01	3.01E+01	3.51E+01
2	ND	ND	1.26E+01	1.23E+01	2.09E+01	2.26E+01
2	ND	ND	1.10E+01	1.10E+01	2.02E+01	2.17E+01
3	ND	ND	1.07E+01	1.08E+01	1.76E+01	1.88E+01
3	ND	ND	1.22E+01	1.15E+01	1.96E+01	2.07E+01
4	ND	ND	8.76E+00	8.89E+00	1.42E+01	1.63E+01
4	ND	ND	1.05E+01	1.02E+01	1.51E+01	1.61E+01
5	ND	ND	7.12E+00	7.54E+00	1.22E+01	1.39E+01
5	ND	ND	9.21E+00	9.20E+00	1.23E+01	1.38E+01
19	ND	ND	8.31E+01	7.42E+01	8.30E+01	9.71E+01
19	ND	ND	7.70E+01	7.21E+01	7.86E+01	8.96E+01
47	ND	ND	ND	6.04E+01	ND	5.06E+01
47	ND	ND	ND	5.89E+01	ND	4.97E+01
90	ND	ND	1.82E+01	1.71E+01	ND	ND
90	ND	ND	1.67E+01	1.65E+01	ND	ND
149	ND	ND	5.02E+00	5.03E+00	1.20E+00	ND
189	ND	ND	1.92E+00	2.42E+00	ND	ND
222	ND	ND	1.13E+00	ND	ND	ND
306	ND	ND	1.52E+00	2.24E+00	9.66E-01	ND

(a) PO₄³⁻ and SO₄²⁻ were also calculated based on phosphorus and sulfur concentrations analyzed by ICP-OES. ND indicates “not detected” below quantification level for NO₃⁻<0.5 µg/mL; NO₂⁻<0.5 µg/mL; PO₄³⁻<7.5 µg/mL; P<0.715 µg/mL; SO₄²⁻<0.75 µg/mL S<3.32 µg/mL.

7.0 Discussion

The release of Re (^{99}Tc surrogate), I, and RCRA metals from FBSR granular product encapsulated in the geopolymer matrix may proceed by a series of sequential and/or simultaneously competing chemical and physical reactions that control the mass transfer of these components from the immobilizing waste form to the surrounding test solution.

These reactions and processes include, but are not limited to, the following:

- diffusion/advection
- dissolution/precipitation
- adsorption/absorption/desorption
- oxidation/reduction
- paragenetic sequence of mineral transformation.

The overall impact of individual or coupled reactions and processes on the release of COCs depends on a number of variables, such as the waste form composition, material's resistance to physical and chemical degradation, dominant mechanism controlling release, and experimental conditions (Pierce et al. 2010).

For a discussion of release rates bound by the short-term test conditions discussed in this report, it is assumed that diffusion is the primary release mechanism, especially under the conditions evaluated in EPA draft Method 1315 and ANSI/ANS 16.1. All reported diffusivity values are derived from calculations assuming diffusion-controlled release and a constant liquid volume-to-specimen surface area ratio of the test form during the test interval.

The calculated diffusivity values for detectable RCRA metals, Re (^{99}Tc surrogate), and other select elements for the EPA draft Method 1315 tests are presented in Table 7.1, Table 7.2, and Table 7.3, and for the ANSI/ANS 16.1 tests Table 7.4 through Table 7.6. The diffusivity values for Cd, Pb, Al, Ti, and Fe, for both leach test methods, contain a number of calculated diffusivities derived from both detected and non-detected leachate concentrations. The diffusivities calculated using the estimated quantitation limit concentrations represent the maximum diffusivity for that leach interval. These are shown as less than (<) values. The maximum diffusivities for Cd, Pb, Al, Ti, and Fe dominate at low leach intervals and are replaced by measured values as the interval is increased. Longer leach intervals allow for more of the diffusing species to concentrate in the solution, increasing the potential for measurement by the available analytical techniques. Diffusivity and LI calculated results for EPA draft Method 1315 and ANSI/ANS 16.1 tests have similar detection and average value trending. We were not able to measure the iodine inventory in the FBSR waste form and so no diffusivities were calculated.

In parallel with the preparation of this report, SRNL has been characterizing other monoliths from the same batch of FBSR/GEO-7 waste form monoliths from which the PNNL specimens were provided. In comparing unpublished results from SRNL with PNNL results, it was found that SRNL measured higher initial rhenium concentrations, higher wet densities, and lower moisture contents. It is beyond the scope of this report to investigate the source(s) for the differences. It is acknowledged that this could have an impact on the reported diffusivities depending upon the magnitude of the differences.

Table 7.1. The Diffusivity and Leachability Index for Cd and Pb in Eluate for FBSR Waste Form from EPA Method 1315

Cumulative Leach Time days	Cd Diffusivity (cm ² /s)	LI	Pb Diffusivity (cm ² /s)	LI	Cs Diffusivity (cm ² /s)	LI
0.08	<4.55E-12	>11.3	<3.24E-13	>12.5	1.57E-10	9.8
0.08	<4.49E-12	>11.3	<3.20E-13	>12.5	2.24E-10	9.7
1	<7.07E-13	>12.2	<5.04E-14	>13.3	3.87E-10	9.4
1	<6.98E-13	>12.2	<4.97E-14	>13.3	2.74E-10	9.6
2	<2.45E-12	>11.6	<1.74E-13	>12.8	9.93E-11	10.0
2	<2.42E-12	>11.6	<1.72E-13	>12.8	9.43E-11	10.0
7	<2.50E-13	>12.6	3.58E-13	12.4	1.67E-10	9.8
7	1.84E-11	10.7	4.32E-13	12.4	2.07E-10	9.7
14	1.24E-11	10.9	7.43E-13	12.1	2.11E-10	9.7
14	7.37E-11	10.1	2.17E-12	11.7	2.05E-10	9.7
28	2.91E-11	10.5	1.47E-12	11.8	1.52E-10	9.8
28	6.21E-11	10.2	1.56E-12	11.8	1.04E-10	10.0
42	2.36E-11	10.6	1.11E-12	12.0	7.47E-11	10.1
42	4.08E-11	10.4	1.28E-12	11.9	4.76E-11	10.3
49	2.12E-11	10.7	1.27E-12	11.9	5.13E-11	10.3
49	3.76E-11	10.4	1.89E-12	11.7	3.36E-11	10.5
63	1.35E-11	10.9	1.06E-12	12.0	1.56E-11	10.8
63	2.30E-11	10.6	1.63E-12	11.8	1.08E-11	11.0
149	3.58E-13	12.4	1.04E-13	13.0	3.63E-13	12.4
189	1.79E-13	12.7	1.07E-13	13.0	3.24E-14	13.5
222	<2.86E-13	>12.5	6.11E-14	13.2	5.33E-14	13.3
306	<5.63E-14	>13.2	4.50E-14	13.3	6.87E-14	13.2

Table 7.2. The Diffusivity and Leachability Index for Al, Ti and Fe in Eluate for FBSR Waste Form from EPA Method 1315

Cumulative Leach Time days	Al Diffusivity (cm ² /s)	LI	Ti Diffusivity (cm ² /s)	LI	Fe Diffusivity (cm ² /s)	LI
0.08	<1.14E-13	>12.9	<4.46E-12	>11.4	<8.87E-14	>13.1
0.08	<1.13E-13	>12.9	<4.41E-12	>11.4	<8.76E-14	>13.1
1	<1.78E-14	>13.8	<6.94E-13	>12.2	<1.38E-14	>13.9
1	<1.76E-14	>13.8	<6.86E-13	>12.2	<1.36E-14	>13.9
2	<6.15E-14	>13.2	<2.40E-12	>11.6	<4.77E-14	>13.3
2	<6.07E-14	>13.2	<2.37E-12	>11.6	<4.71E-14	>13.3
7	<6.28E-15	>14.2	<2.45E-13	>12.6	9.83E-15	14.0
7	9.47E-14	13.0	1.03E-12	12.0	2.61E-12	11.6
14	2.06E-13	12.7	9.00E-13	12.0	2.20E-12	11.7
14	3.80E-13	12.4	5.48E-12	11.3	1.21E-11	10.9
28	4.41E-13	12.4	2.60E-12	11.6	6.21E-12	11.2
28	2.62E-13	12.6	4.07E-12	11.4	9.81E-12	11.0
42	4.38E-13	12.4	2.28E-12	11.6	5.12E-12	11.3
42	3.58E-13	12.4	3.27E-12	11.5	6.43E-12	11.2
49	1.96E-12	11.7	2.91E-12	11.5	5.07E-12	11.3
49	1.52E-12	11.8	5.21E-12	11.3	7.46E-12	11.1
63	5.64E-13	12.2	2.94E-12	11.5	3.68E-12	11.4
63	6.65E-13	12.2	5.19E-12	11.3	5.66E-12	11.2
149	1.14E-14	13.9	4.87E-13	12.3	2.48E-13	12.6
189	3.20E-14	13.5	6.50E-13	12.2	1.72E-13	12.8
222	7.89E-13	12.1	4.89E-13	12.3	8.52E-14	13.1
306	8.32E-13	12.1	3.38E-13	12.5	5.39E-14	13.3

Table 7.3. The Diffusivity and Leachability Index for Re and Na in Eluate for FBSR Waste Form from EPA Draft Method 1315

Cumulative Leach Time days	Re Diffusivity (cm ² /s)	LI	Na Diffusivity (cm ² /s)	LI
0.08	6.44E-10	9.2	2.08E-08	7.7
0.08	1.46E-09	8.8	3.58E-08	7.4
1	4.82E-09	8.3	7.45E-08	7.1
1	4.85E-09	8.3	5.65E-08	7.2
2	1.75E-09	8.8	1.51E-08	7.8
2	2.08E-09	8.7	1.57E-08	7.8
7	5.63E-09	8.2	3.99E-08	7.4
7	5.46E-09	8.3	5.13E-08	7.3
14	5.58E-09	8.3	4.26E-08	7.4
14	4.87E-09	8.3	4.91E-08	7.3
28	3.25E-09	8.5	2.80E-08	7.6
28	2.86E-09	8.5	2.62E-08	7.6
42	1.14E-09	8.9	1.22E-08	7.9
42	1.12E-09	8.9	1.08E-08	8.0
49	5.05E-10	9.3	6.17E-09	8.2
49	5.34E-10	9.3	6.04E-09	8.2
63	2.61E-10	9.6	1.63E-09	8.8
63	2.69E-10	9.6	1.59E-09	8.8
149	1.84E-11	10.7	6.04E-11	10.2
189	2.23E-11	10.7	7.83E-11	10.1
222	1.67E-11	10.8	4.69E-11	10.3
306	9.96E-12	11.0	1.97E-11	10.7

The FBSR, monolithed, waste form-derived diffusivities for sodium range from 7.4×10^{-8} cm²/s to 1.6×10^{-9} cm²/s at a total of 63 days for EPA draft Method 1315 and from 4.9×10^{-8} cm²/s to 1.3×10^{-9} cm²/s for ANSI/ANS 16.1. These sodium diffusivity values result in LI values of 7.1 to 8.8 for EPA draft Method 1315 up to 63 days and 7.3 to 8.9 for ANSI/ANS 16.1. The sodium diffusivity values decrease slightly with the increase in cumulative leach time. Note that for sodium, the fraction leached after approximately two weeks exceeds 20% of the initial inventory and the assumption of a semi-infinite solid used for Equation 5.3 becomes invalid. More precise estimates of the sodium diffusivity require more complete calculations.

The Re (⁹⁹Tc surrogate) diffusivities for the FBSR monolithed waste form range from $\sim 5.5 \times 10^{-9}$ cm²/s to $\sim 2.7 \times 10^{-10}$ cm²/s at a total of 63 days for EPA draft Method 1315 and from $\sim 5 \times 10^{-9}$ cm²/s to $\sim 1.8 \times 10^{-10}$ cm²/s for ANSI/ANS 16.1 over the same total leach interval, resulting in LI values of 8.2 to 9.8 for both test methods.

Although the Re LI for the FBSR waste form met the Tc target LI of 9 or greater after 42 days of leaching in both the ANS-16.1 and EPA 1315 test methods, the Re release from the waste form was higher than expected. We hypothesize that this is because not all of the Re in the waste may have entered the sodalite cage structure. Mattigod et al. (2006) showed that the Re(VII) in the +7 oxidation state is captured in the sodalite cage as NaReO₄. Rhenium (IV) in the +4 oxidation state is not captured in the cage as ReO₂. Jantzen and Crawford (2010) and TTT (2009) report the reduction/oxidation conditions for the FBSR granular product from the PR and from the HTF based on the Fe⁺²/ΣFe. The HTF product experienced much more reducing conditions with a Fe⁺²/ΣFe ratio in the range of 0.734 to 0.902 for both the LAW and WTP-SW granular product. Based on this ratio, Jantzen and Crawford (2010) estimated that only 2.5% of the rhenium is as Re(VII) in the HTF product. The PR granular product experienced more oxidizing conditions with the Fe⁺²/ΣFe ratio in the range of 0.410 to 0.581. At this ratio, 94 to 95%

of the rhenium remains as Re(VII) in the PR product (Jantzen and Crawford 2010). Thus, the rhenium (VII) in the PR product fraction would be inside the sodalite cage, and the Re(IV) in the HTF product fraction would be outside the sodalite cage in some other form. This appears to be confirmed by the results from the PCT conducted on the HTF and PR materials from the LAW and WTP-SW pilot-scale tests. Average PCT results for the PR materials from both the LAW and WTP-SW tests were in the range of 0.013 to 0.015 g/m² normalized release based on sodium. The average normalized releases based on Re for the PR material were below that of sodium at 0.0068 to 0.007 g/m². For the HTF product, the average normalized releases based on Re were above that of sodium at 0.024 g/m² for the LAW HTF product and 0.019 g/m² for the WTP-SW HTF product (Vora et al. 2009, TTT 2009).

Table 7.4. The Diffusivity and Leachability Index for Cd, Pb and Cs in Eluate for FBSR Waste Form from ANSI/ANS 16.1

Cumulative Leach Time days	Cd Diffusivity (cm ² /s)	LI	Pb Diffusivity (cm ² /s)	LI	Cs Diffusivity (cm ² /s)	LI
0.08	<3.88E-12	>11.4	<2.76E-13	>12.6	1.90E-10	9.7
0.08	<3.77E-12	>11.4	<2.68E-13	>12.6	8.52E-11	10.1
0.29	<5.11E-12	>11.3	<3.64E-13	>12.4	2.93E-10	9.5
0.29	<4.97E-12	>11.3	<3.54E-13	>12.5	2.56E-10	9.6
1	<1.53E-12	>11.8	<1.09E-13	>13.0	2.00E-10	9.7
1	<1.49E-12	>11.8	<1.06E-13	>13.0	1.94E-10	9.7
2	<1.88E-12	>11.7	<1.34E-13	>12.9	1.25E-10	9.9
2	5.53E-12	11.3	1.37E-13	12.9	1.31E-10	9.9
3	5.83E-12	11.2	<2.28E-13	>12.6	1.86E-10	9.7
3	3.14E-11	10.5	8.15E-13	12.1	2.41E-10	9.6
4	9.88E-12	11.0	3.88E-13	12.4	1.85E-10	9.7
4	4.02E-11	10.4	1.10E-12	12.0	2.22E-10	9.7
5	2.18E-11	10.7	6.75E-13	12.2	2.10E-10	9.7
5	5.07E-11	10.3	1.46E-12	11.8	2.33E-10	9.6
19	4.67E-11	10.3	1.40E-12	11.9	1.19E-10	9.9
19	4.03E-11	10.4	1.20E-12	11.9	9.68E-11	10.0
47	2.78E-11	10.6	8.06E-13	12.1	3.58E-11	10.4
47	2.05E-11	10.7	6.64E-13	12.2	2.97E-11	10.5
90	1.21E-11	10.9	9.07E-13	12.0	5.23E-12	11.3
90	9.62E-12	11.0	9.36E-13	12.0	4.53E-12	11.3
149	2.05E-12	11.7	4.83E-13	12.3	8.72E-13	12.1
189	6.62E-13	12.2	2.70E-13	12.6	5.83E-14	13.2
222	4.87E-13	12.3	2.02E-13	12.7	4.58E-14	13.3
306	1.84E-13	12.7	1.30E-13	12.9	6.07E-14	13.2

Table 7.5. The Diffusivity and Leachability Index for Al, Ti and Fe in Eluate for FBSR Waste Form from ANSI/ANS 16.1

Cumulative Leach Time days	Al Diffusivity (cm ² /s)	LI	Ti Diffusivity (cm ² /s)	LI	Fe Diffusivity (cm ² /s)	LI
0.08	<9.74E-14	>13.0	<3.80E-12	>11.4	<7.56E-14	>13.1
0.08	<9.47E-14	>13.0	<3.70E-12	>11.4	<7.36E-14	>13.1
0.29	<1.28E-13	>12.9	<5.02E-12	>11.3	<9.97E-14	>13.0
0.29	<1.25E-13	>12.9	<4.88E-12	>11.3	<9.70E-14	>13.0
1	<3.84E-14	>13.4	<1.50E-12	>11.8	<2.98E-14	>13.5
1	4.39E-14	13.4	<1.46E-12	>11.8	1.01E-13	13.0
2	<4.73E-14	>13.3	<1.85E-12	>11.7	<3.67E-14	>13.4
2	8.03E-14	13.1	<1.80E-12	>11.7	6.61E-13	12.2
3	9.35E-14	13.0	<3.14E-12	>11.5	4.25E-13	12.4
3	2.48E-13	12.6	<3.05E-12	>11.5	4.84E-12	11.3
4	1.95E-13	12.7	<4.42E-12	>11.4	1.41E-12	11.9
4	3.47E-13	12.5	<4.30E-12	>11.4	7.23E-12	11.1
5	2.47E-13	12.6	<5.69E-12	>11.2	2.89E-12	11.5
5	5.30E-13	12.3	<5.53E-12	>11.3	8.95E-12	11.0
19	2.26E-13	12.6	4.28E-12	11.4	9.56E-12	11.0
19	2.30E-13	12.6	3.52E-12	11.5	8.47E-12	11.1
47	1.29E-13	12.9	2.05E-12	11.7	4.40E-12	11.4
47	1.36E-13	12.9	1.71E-12	11.8	3.77E-12	11.4
90	1.27E-13	12.9	2.27E-12	11.6	2.72E-12	11.6
90	1.24E-13	12.9	2.25E-12	11.6	2.60E-12	11.6
149	3.76E-14	13.4	1.55E-12	11.8	9.79E-13	12.0
189	3.69E-14	13.4	1.17E-12	11.9	4.21E-13	12.4
222	3.34E-13	12.5	9.56E-13	12.0	2.23E-13	12.7
306	5.03E-13	12.3	7.08E-13	12.2	1.35E-13	12.9

Table 7.6. The Diffusivity and Leachability Index for Re and Na in Eluate for FBSR Waste Form from ANSI/ANS 16.1

Cumulative Leach Time days	Re Diffusivity cm ² /s	LI	Na Diffusivity cm ² /s	LI
0.08	1.23E-09	8.9	3.16E-08	7.5
0.08	3.41E-10	9.5	1.48E-08	7.8
0.29	3.87E-09	8.4	4.72E-08	7.3
0.29	2.95E-09	8.5	4.67E-08	7.3
1	4.24E-09	8.4	4.00E-08	7.4
1	4.52E-09	8.3	3.96E-08	7.4
2	3.53E-09	8.5	2.53E-08	7.6
2	2.95E-09	8.5	2.70E-08	7.6
3	5.09E-09	8.3	3.95E-08	7.4
3	5.25E-09	8.3	4.93E-08	7.3
4	4.84E-09	8.3	4.32E-08	7.4
4	4.82E-09	8.3	4.92E-08	7.3
5	5.00E-09	8.3	4.39E-08	7.4
5	4.86E-09	8.3	3.88E-08	7.4
19	3.98E-09	8.4	3.23E-08	7.5
19	3.41E-09	8.5	2.59E-08	7.6
47	1.15E-09	8.9	1.05E-08	8.0
47	1.08E-09	9.0	9.66E-09	8.0
90	1.79E-10	9.7	1.28E-09	8.9
90	1.78E-10	9.8	1.13E-09	8.9
149	4.51E-11	10.3	2.47E-10	9.6
189	2.25E-11	10.6	1.12E-10	9.9
222	1.81E-11	10.7	5.95E-11	10.2
306	9.72E-12	11.0	2.16E-11	10.7

8.0 Conclusions and Recommendations

Screening tests are being conducted to evaluate waste forms for immobilizing secondary liquid wastes from the WTP. Adding a stabilization treatment unit to the Effluent Treatment Facility is planned to provide the needed capacity for treating these wastes from WTP. The current baseline is to use a Cast Stone cementitious waste form to solidify the wastes. Through a literature survey, DuraLith alkali-aluminosilicate geopolymer, FBSR granular product encapsulated in a geopolymer matrix, and a Ceramicrete phosphate-bonded ceramic were identified both as candidate waste forms and alternatives to the baseline. These waste forms have been shown to meet waste disposal acceptance criteria, including compressive strength and universal treatment standards for RCRA metals (as measured by TCLP). Thus, these non-cementitious waste forms should also be acceptable for land disposal. Information is needed on all four waste forms with respect to their capability to minimize the release of technetium. Technetium is a radionuclide predicted to be in the secondary liquid wastes in small quantities, but the IDF risk assessment analyses show that technetium, even at low mass, produces the largest contribution to the estimated IDF disposal impacts to groundwater.

To support a final waste form down-selection, PNNL is conducting screening tests on the candidate waste forms to provide a basis for comparison. This report documents the screening test results on the FBSR granular product encapsulated in a geopolymer (GEO-7) matrix. Ultimately, either one or a few waste forms will be chosen in a down-selection process. The down-selected waste form(s) will be compliant to regulations and performance criteria and will lead to cost-effective disposal of the WTP secondary wastes. Later, more comprehensive and longer-term performance testing will be conducted, following the guidance provided by the secondary waste form selection, development, and performance evaluation roadmap.

Three draft test protocols (e.g., 1313, 1315, and 1316) being developed for EPA were used to screen the encapsulated FBSR stabilization technologies.

- EPA draft Method 1313—Leaching Test (Liquid-Solid Partitioning as a Function of Extract pH) of Constituents in Solid Materials Using a Parallel Batch Extraction Test (EPA 2009a)
- EPA draft Method 1315—Mass Transfer Rates of Constituents in Monolith or Compacted Granular Materials Using a Semi-Dynamic Tank Leaching Test (EPA 2009b)
- EPA draft Method 1316—Leaching Test (Liquid-Solid Partitioning as a Function of Liquid-to-Solid Ratio) of Constituents in Solid Materials Using a Parallel Batch Extraction Test (EPA 2009c).

These EPA draft methods are a combination of static and semi-dynamic leach experiments that can be used to provide more detailed mechanistic information on material performance in comparison to the current standard leach methods, such as ANSI/ANS 16.1 and TCLP. The EPA draft Method 1313 is a static-leach test method where extraction experiments are conducted in dilute acid or base with DIW over a range of pHs at a fixed liquid-to-solid ratio. Instead of a dilute acid or base at a fixed liquid-to-solid ratio, draft Method 1316 uses DIW as the leachant for a range of liquid-to-solid ratios. The EPA draft Method 1315 is a 63-day, semi-dynamic, leach experiment that consists of submerging a monolithic sample (with a fixed geometry) in water at a fixed liquid-to-solid ratio for a fixed period of time. At each of the nine pre-determined leaching intervals, the sample mass is recorded, and the leachant is changed. This method is similar to ANSI/ANS 16.1, but the leaching intervals are different.

As part of the ART Project, a simulated WTP secondary waste stream based on the effluent generated during LAW vitrification and the off-gas treatment, and more specifically, the SBS and the WESP condensate was processed through the THOR[®] FBSR ESTD located at the Hazen Research facility in

Golden, Colorado. SRNL evaluated a number of binder technologies for the FBSR LAW granular product and selected a geopolymer material designated GEO-7. This GEO-7 geopolymer was then used for the WTP-SW waste simulant. The FBSR/geopolymer cylinders were provided to PNNL by SRNL.

For the screening tests, 4-in. by 2-in.-diameter cylinders of FBSR product encapsulated in geopolymer (GEO-7) were used as the source material for the EPA draft leach test methods. The supplied FBSR monoliths were prepared by encapsulating the solids discharge product from a steam reformer into an alkali-silico-aluminate (Geopolymer). The waste simulant fed into the steam reformer was spiked with rhenium, a surrogate for ^{99}Tc , and formulated to resemble a SW simulant based on an early LAW treatment scenario in which the LAW melter off-gas SBS and WESP condensate are combined with the caustic scrubber solution. The waste loading of the supplied FBSR monolithed waste forms contains 65.2^(a) wt% FBSR granular product encapsulated in the fly ash and NaOH binding material.

The FBSR monolithed waste form was characterized with respect to chemical and crystalline composition. Solids characterization (X-ray diffraction [XRD] analysis) of the supplied waste forms confirmed the presence of target alkali aluminosilicate (NAS) minerals (e.g., nepheline, sodalite, nosean) plus low-carnegeite previously observed in the FBSR granular product. Other phases identified in the geopolymer waste form included quartz, zeolite rho, Na-faujasite, and a sodium carbonate phase. Scanning electron microscopy (SEM) with energy dispersive spectrometry (EDS) analysis confirmed the presence and even distribution of NAS-like minerals, quartz, and iron oxide compounds.

The EPA draft Methods 1313 and 1316 were conducted on the FBSR waste form to get an indication of the impact of pH and the solution-to-solids ratio on the release of contaminant. The natural solution pH, after soaking the FBSR granular product/geopolymer in DIW, is approximately 12.

The diffusivity of Re (^{99}Tc surrogate) in FBSR encapsulated in Geopolymer (GEO-7) was determined by EPA draft Method 1315 and ANSI/ANS 16.1. The diffusivity for the release of rhenium in the FBSR monolith was $\sim 5.5 \times 10^{-9} \text{ cm}^2/\text{s}$ after 7 days and $\sim 2.7 \times 10^{-10} \text{ cm}^2/\text{s}$ after 63 days by EPA draft Method 1315 and $\sim 5 \times 10^{-9} \text{ cm}^2/\text{s}$ after 3 days and $\sim 1.8 \times 10^{-10} \text{ cm}^2/\text{s}$ after 90 days per ANSI/ANS 16.1. The associated leachability index (LI) for rhenium bettered the target LI for Tc (>9) after approximately 42 days of leaching. Supplied FBSR monoliths demonstrated comparable leaching trends between EPA draft Method 1315 and ANSI/ANS 16.1 methods.

Following a final waste form selection, the secondary waste form testing will be directed toward testing to support detailed design of the STU for IDF; data collection to support risk assessments and long-term performance assessments; and, as appropriate, further optimization of the waste form to reduce costs and improve performance (Pierce et al. 2010).

(a) Waste loading published at 68.8% in “Report for Treating Hanford LAW and WTP SW Simulants: Pilot Plant Mineralizing Flowsheet,” RT-21-002 rev. 1, April 2009, THOR Treatment Technologies, LLC. Test Plan (57925-P2-T3-Rev. 1) review comments indicated that this value was corrected in a later revision.

9.0 References

ANSI—American National Standards Institute. 2003. *Measurement of the Leachability of Solidified Low-Level Radioactive Waste by a Short-Term Test Procedure*. ANSI/ANS-16.1, American Nuclear Society, La Grange Park, Illinois.

ASTM—American Society for Testing and Materials. 1998. “D2216-98 Standard Test Method for Laboratory Determination of Water (Moisture) Content of Soil and Rock by Mass.” *American Society for Testing and Materials*. West Conshohocken, Pennsylvania.

Barrer RM, JW Baynham, FW Bultitude and WM Meier. 1959. “Hydrothermal chemistry of the silicates. Part VIII. Low-temperature crystal growth of aluminosilicates, and of some gallium and germanium analogues.” *J. Chem. Soc.* 195–208.

Brunauer S, PH Emmett, and E Teller. 1938. “Adsorption of Gases in Multimolecular Layers.” *Journal of the American Chemical Society* 60:309–319.

Crank J. 1986. *Mathematics of Diffusion*. 2nd ed. pp. 424. Oxford University Press, London, UK.

Dickens B, FA Mauer, and WE Brown. 1970. “A refinement of the crystal structure of Na₂CO₃ · H₂O.” *J. Res. Natl. Bur. Stand. Sect. A* 74:319-325. Ecology, EPA, and DOE—Washington State Department of Ecology, U.S. Environmental Protection Agency and U.S. Department of Energy. 1989. *Hanford Facility Agreement and Consent Order, As Amended*. Olympia, Washington.

EPA—U.S. Environmental Protection Agency. 1984. “Determination of Inorganic Anions.” *EPA Method 300.0A, in Test Method for the Determination of Inorganic Anions in Water by Ion Chromatography*. EPA-600/4-84-0 17, Washington, D.C.

EPA—U.S. Environmental Protection Agency. 1996. “Microwave Assisted Acid Digestion of Siliceous and Organically Based Matrices.” *EPA Method 3052, in Test Method for Evaluating Solid Waste, Physical/Chemical Methods.. SW-846*, Washington, D.C.

EPA—U.S. Environmental Protection Agency. 2000a. “Inductively Coupled Plasma-Atomic Emission Spectrometry.” EPA Method 6010B, in *Test Methods for Evaluating Solid Waste, Physical/Chemical Methods*. SW-846, Washington, D.C. Available at: <http://www.epa.gov/epaoswer/hazwaste/test/sw846.htm>. Accessed September 20, 2008.

EPA—U.S. Environmental Protection Agency. 2000b. “Inductively Coupled Plasma-Mass Spectrometry.” EPA Method 6020, in *Test Methods for Evaluating Solid Waste, Physical/Chemical Methods*. SW-846, Washington, D.C. Available at: <http://www.epa.gov/epaoswer/hazwaste/test/sw846.htm>. Accessed September 20, 2008.

EPA—U.S. Environmental Protection Agency. 2009a. Leaching Test (Liquid-Solid Partitioning as a Function Liquid to Solid Ratio) of Constituents in Solid Materials Using a Parallel Batch Extraction Test. Draft Method 1313, Washington, D.C.

EPA—U.S. Environmental Protection Agency. 2009b. Mass Transfer Rates of Constituents in Monolith or Compacted Granular Materials Using a Semi-Dynamic Tank Leaching Test. Draft Method 1315, Washington, D.C.

EPA—U.S. Environmental Protection Agency. 2009c. Leaching Test (Liquid-Solid Partitioning as a Function of Extract pH) of Constituents in Solid Materials Using a Parallel Batch Extraction Test. Draft Method 1316, Washington, D.C.

Hughes. H. 1966. "Formation of alkali silicates and aluminosilicates and their occurrence in blast furnaces." *Trans. Br. Ceram. Soc.* 65:661-679.

Jantzen CM, TH Lorier, JM Pareizs, and JC Marra. 2007. "Fluidized Bed Steam Reformed (FBSR) Mineral Waste Forms: Characterization and Durability Testing." In: *Scientific Basis for Nuclear Waste Management XXX* 985:379-386. Materials Research Society, Warrendale, Pennsylvania.

Jantzen CM. 2008. Mineralization of Radioactive Wastes by Fluidized Bed Steam Reforming (FBSR): Comparisons to Vitreous Waste Forms, and Pertinent Durability Testing. WSRC-STI-2008-00268, Savannah River National Laboratory, Aiken, South Carolina.

Jantzen CM and CL Crawford. 2010. Mineralization of Radioactive Waste Wastes by Fluidized Bed Steam Reforming (FBSR): Radionuclide Incorporation, Monolith Formation, and Durability Testing. WM2010, WM Symposia, Phoenix, Arizona.

Jantzen CM, CL Crawford, PR Burket, WG Daniel, AD Cozzi, CJ Bannochie. 2011. Radioactive Demonstrations of Fluidized Bed Steam Reforming (FBSR) as a Supplemental Treatment for Hanford's Low-Activity Waste (LAW) and Secondary Wastes (SW). WM2011 Conference, February 27-March 3, 2011, Phoenix, Arizona.

Keller L, J Rask, and P Buseck. 1986. ICDD Grant-in-Aid, Arizona State University, Tempe, Arizona. International Centre for Diffraction Data, Newton Square, Pennsylvania.

Kern A and W Eysel. 1993. Mineralogisch-Petrograph. Inst., ICDD Grant-in-Aid, Univ. Heidelberg, Germany. International Centre for Diffraction Data, Newton Square, Pennsylvania.

Koci GI. 2005. Conceptual Design Report for Effluent Treatment Facility Solidification Treatment Unit. Fluor Hanford, Richland, Washington.

Mann FM. 2002. *Annual Summary of ILAW Performance Assessment for 2002*. CH2M Hill Hanford Group, Inc., Richland, Washington.

Mason JB, J McKibbin, K Ryan, and D Schmoker. 2003. "Steam Reforming Technology for Denitration and Immobilization of DOE Tank Wastes." *Waste Management Conference*, February 23-27, Tucson, Arizona.

Mattigod SV. 1982. Characterization of Fly ash Particles. *Scanning Electron Microscopy*. 2:611-617.

Mattigod SV, B Peter McGrail, DE McCready, L-Q Wang, KE Parker, and JS Young. 2006. "Synthesis and Structure of Perrhenate Sodalite." *Microporous and Mesoporous Materials* 91:139-144.

Nayak M and TRN Kuty. 1998. "Luminescence of Fe³⁺ doped NaAlSiO₄ prepared by gel to crystallite conversion." *Mater. Chem. Phys.* 57:138-146.

Olson AL, NR Soelberg, DW Marshall, and GL Anderson. 2004. *Fluidized Bed Steam Reforming of Hanford LAW Using THOR Mineralizing Technology*. INEEL/EXT-04-02492, Idaho National Engineering and Environmental Laboratory, Idaho Falls, Idaho.

Pierce EM, W Um, KJ Cantrell, MM Valenta, JH Westsik, Jr., RJ Serne, KE Parker. 2010. *Secondary Waste Form Screening Test Results – Cast Stone and Alkali Alumino-Silicate Geopolymer*. PNNL-19505, Pacific Northwest National Laboratory, Richland, Washington.

PNNL—Pacific Northwest National Laboratory. 1998. *Inductively Coupled Plasma Mass Spectrometric (ICP-MS) Analysis*. PNNL-AGG-415, Pacific Northwest National Laboratory, Richland, Washington.

PNNL—Pacific Northwest National Laboratory. 2009. *Hanford Site Secondary Waste Roadmap*. PNNL-18196, Pacific Northwest National Laboratory, Richland, Washington.

Robson HE, DP Shoemaker, RA Ogilvie and PC Manor. 1973. “Method for preparing small pore synthetic zeolite.” In: *Molecular Sieves*. Eds. WM Meier and JB Uytterhoven. *Adv. Chem. Ser.* 121:106-117.

Russell RL, MJ Schweiger, JH Westsik, Jr, PR Hrma, DE Smith, AB Gallegos, MR Telander, and SG Pitman. 2006. *Low Temperature Waste Immobilization Testing*. PNNL-16052 Rev 1, Pacific Northwest National Laboratory, Richland, Washington.

Schulz H. 1970. “Struktur- und Überstrukturuntersuchungen an Nosean-Einkristallen.” *Zeitschrift für Kristallographie* 131:114–138.

Small JA. 1976. An elemental and morphological characterization of the emissions from Dickerson and Chalk Point coal-fired power plants. University of Maryland Ph.D. thesis. University Microfilm International. pp 360.

Sundaram SK, J Chun, W Um, KE Parker, C-W Chung, JH Westsik Jr, ME Valenta, ML Kimura, SG Pitman, and CA Burns. 2011. *Secondary Waste Form Development and Optimization—Cast Stone*. PNNL-20159 Rev 1, Pacific Northwest National Laboratory, Richland, Washington.

TTT. 2009. “Report for Treating Hanford LAW and WTP SW Simulants: Pilot Plant Mineralizing Flowsheet.” RT-21-002 Revision 1, THOR Treatment Technologies, LLC, Denver, Colorado.

USGS—U.S. Geological Survey. 2004. “Alkalinity and Acid Neutralizing Capacity.” In: *National Field Manual for the Collection of Water-Quality Data, Second Edition*. Eds. SA Rounds and FD Wilde. Available at: at <http://water.usgs.gov/owq/FieldManual/Chapter6/section6.6/html/section6.6.htm>. Accessed September 20, 2008.

Vassilev SV, R Menendez, AG Borrego, M Diaz-Somoano, and MR Martinez-Tarazona. 2004. Phase-mineral and chemical composition of coal fly ashes as a basis for their multicomponent utilization. Characterization of magnetic and char concentrates. *Fuel*. 93:1563-1583

Vora V, A Olson, B Mason, B Evans, and K Ryan. 2009. “Steam Reforming Technology Demonstration for Conversion of Hanford LAW Tank Waste and LAW Recycle Waste into a Leach Resistant Alkali Aluminosilicate Waste Form.” Waste Management Conference, Phoenix, Arizona.

Supplemental Information

Pierce EM, SV Mattigod, RJ Serne, JP Icenhower, RD Scheele, W Um, N Qafoku, and JH Westsik, Jr. 2010. *Review of Potential Candidate Stabilization Technologies for Liquid and Solid Secondary Waste Streams*. PNNL-19122, Pacific Northwest National Laboratory, Richland, Washington.

PNNL—Pacific Northwest National Laboratory. 2009. *Operation of the MARS 5 microwave accelerated reaction system*. PNNL-AGG-MARS-001, Pacific Northwest National Laboratory, Richland, Washington.

Appendix A

Scanning Electron Microscopy and Energy Dispersive Spectroscopy on FBSR Waste Form Specimen

Appendix A: Scanning Electron Microscopy and Energy Dispersive Spectroscopy on FBSR Waste Form Specimen

Methods

Scanning electron microscopy (SEM) and energy dispersive spectroscopy (EDS) were performed on a cross-section of the baseline cement monolith. The cross-section was polished and allowed to dry in a vacuum desiccator. The specimen was sputter coated with palladium. SEM was performed with a JEOL 5900 scope with a Robinson backscatter electron detector, and EDS was performed with an EDAX silicon drifted detector.

Results

We investigated several regions within the sample and found many segregated areas throughout the specimen as seen in Figure A.1A, (Reg. 1) of a typical region showing a few of the different features on a macro scale. EDS analysis revealed the chemical make-up of the following features (these are broken up by like composition and presented in Table A.1):

- *Large concentric circular regions* (i.e., Figure A.1B, Reg. 1-d; Figure A.1D, Reg. 3-b), approximately 200 to 400 μm in diameter, were composed of a Na-Al-Si-O mixture, likely $\text{Na}_2\text{O}-\text{Al}_2\text{O}_3-\text{SiO}_2$.
- *Smaller Fe-enriched circular regions* (i.e., Figure A.1B, Reg. 1-a; Figure A.1C, Reg. 2-a,e,g; Figure A.1E, Reg. 4-b), approximately 10 to 150 μm in diameter, were composed of various mixtures of alkali-Al-Si-Fe-O where the potassium levels were higher, on average, compared to other regions analyzed.
- *High-Fe regions* (i.e., Figure A.1B, Reg. 1-c; Figure A.1C, Reg. 2-f; Figure A.1D, Reg. 3a), varying 10 to 120 μm in diameter, were composed of high mass fractions of Fe (≥ 58 mass%) and small fractions of Na, Al, and Si.
- *Ca-Si-O region* (i.e., Figure A.1C, Reg. 2-c), an irregularly-shaped agglomerate with an approximate size of 50 to 76 μm with inclusions, was composed mostly of Ca-Si-O with small-to-moderate quantities of F and Na at 7.07 and 2.29 mass%, respectively.
- *Na-Ca-Si-O region* (i.e., Figure A.1C, Reg. 2-d), an inclusion in Figure A.1C, Reg. 2-c approximately 12 μm in size, was composed of mostly Na-Ca-O.
- *High-Fe region* (i.e., Figure A.1B, Reg. 1b), a bright, somewhat irregularly shaped circular region approximately 60 μm in size, was composed of a very high amount of Fe (61.57 mass%) with moderate quantities of Na and O at 16.98 and 20.12 mass%, respectively.
- *Fe-alkali-Al-Si-O region* (i.e., Figure A.1C, Reg. 2b), a dark inclusion in Figure A.1C, Reg. 2a, approximately 14 to 28 μm in size, was composed of Na-K-Al-Si-O (90.53 mass% total) with a small amount of Fe at 7.54 mass%.

- *Dark region* (i.e., Figure A.1E, Reg. 4b), a dark region approximately 120 μm in diameter, in the interior of Figure A.1E, Reg. 4a, was composed of carbon and oxygen (78 mass%) with small fractions of Si, Fe, Cl, K, and Al at 6.80, 3.95, 3.31, 3.24, and 2.61 mass%, respectively. These dark spots were observed throughout the specimen and could either be epoxy or perhaps carbon-rich regions segregated out from the sample during curing. The only way to verify the source of these regions would be to cross-section a region of the specimen without first imbedding it in epoxy.

Table A.1. EDS Data Summary from Regions Analyzed in Figure A.1

Mass% by element																				
Reg	CK	OK	FK	NaK	MgK	AlK	SiK	YL	PK	SK	ClK	KK	CaK	CsL	TiK	LaL	CrK	MnK	FeK	NiK
1a	0.00	37.95	0.00	4.13	1.26	13.41	23.61	0.00	0.08	0.00	0.00	3.41	0.27	0.07	0.63	0.00	0.00	0.00	14.83	0.34
1b	0.00	20.12	0.00	16.98	0.07	0.16	0.25	0.00	0.07	0.11	0.07	0.00	0.13	0.00	0.00	0.47	0.00	0.00	61.57	0.00
1c	0.00	22.53	0.00	6.43	0.00	1.95	4.30	0.00	0.00	0.12	0.00	0.23	0.44	0.00	0.17	0.39	0.00	0.00	63.44	0.00
1d	0.00	36.82	0.00	18.79	0.15	17.57	21.75	0.00	0.09	0.82	1.80	0.70	0.18	0.00	0.70	0.00	0.00	0.00	0.62	0.00
2a	0.00	34.80	0.00	0.41	1.30	16.13	26.15	0.00	0.00	0.00	0.00	2.85	0.18	0.00	1.91	0.00	0.00	0.00	16.26	0.00
2b	0.00	38.61	0.00	21.57	0.51	8.46	19.70	0.00	0.00	0.20	0.00	2.19	0.18	0.00	1.04	0.00	0.00	0.00	7.54	0.00
2c	0.00	26.39	7.07	2.29	0.77	0.28	17.29	0.67	0.08	0.00	0.00	0.00	42.98	0.00	0.00	0.00	0.33	0.77	0.59	0.49
2d	0.00	45.63	0.00	37.31	0.12	0.61	4.06	0.15	0.11	0.25	0.00	0.23	10.27	0.00	0.00	0.25	0.00	0.25	0.76	0.00
2e	0.00	36.10	0.00	2.77	0.90	17.97	24.32	0.19	0.02	0.08	0.00	3.45	0.29	0.00	1.33	0.00	0.00	0.00	12.59	0.00
2f	0.00	25.52	0.00	2.28	0.72	4.89	5.96	0.07	0.12	0.00	0.00	0.64	0.57	0.00	0.75	0.00	0.00	0.00	58.07	0.41
2g	0.00	37.92	0.00	7.33	0.79	7.97	32.65	0.40	0.00	0.00	0.00	2.12	2.43	0.00	1.01	0.00	0.00	0.00	7.39	0.00
3a	0.00	19.54	0.00	4.46	0.07	0.45	0.58	0.00	0.00	0.00	0.00	0.00	0.00	0.00	0.00	0.30	0.06	0.56	73.77	0.21
3b	0.00	36.12	0.00	16.88	0.17	18.94	22.12	0.25	0.00	1.17	1.72	0.70	0.21	0.00	0.79	0.00	0.00	0.00	0.93	0.00
4a	0.00	39.42	0.00	1.05	1.73	18.18	29.87	0.20	0.00	0.00	0.00	4.66	0.19	0.00	0.90	0.00	0.00	0.00	3.81	0.00
4b	57.22	20.38	0.00	1.34	0.12	2.61	6.80	0.00	0.00	0.00	3.31	3.24	0.00	0.00	1.02	0.00	0.00	0.00	3.95	0.00

Atomic% by Element																				
Reg	CK	OK	FK	NaK	MgK	AlK	SiK	YL	PK	SK	ClK	KK	CaK	CsL	TiK	LaL	CrK	MnK	FeK	NiK
1a	0.00	54.86	0.00	4.16	1.20	11.50	19.45	0.00	0.06	0.00	0.00	2.02	0.16	0.01	0.31	0.00	0.00	0.00	6.14	0.13
1b	0.00	40.17	0.00	23.59	0.09	0.19	0.29	0.00	0.07	0.11	0.06	0.00	0.11	0.00	0.00	0.11	0.00	0.00	35.21	0.00
1c	0.00	45.77	0.00	9.10	0.00	2.35	4.98	0.00	0.00	0.12	0.00	0.19	0.36	0.00	0.11	0.09	0.00	0.00	36.92	0.00
1d	0.00	49.19	0.00	17.47	0.13	13.92	16.56	0.00	0.06	0.55	1.08	0.38	0.10	0.00	0.31	0.00	0.00	0.00	0.24	0.00
2a	0.00	51.99	0.00	0.43	1.27	14.29	22.26	0.00	0.00	0.00	0.00	1.74	0.11	0.00	0.95	0.00	0.00	0.00	6.96	0.00
2b	0.00	52.33	0.00	20.35	0.46	6.80	15.21	0.00	0.00	0.14	0.00	1.22	0.10	0.00	0.47	0.00	0.00	0.00	2.93	0.00
2c	0.00	42.29	9.54	2.55	0.81	0.27	15.78	0.19	0.07	0.00	0.00	0.00	27.50	0.00	0.00	0.00	0.16	0.36	0.27	0.21
2d	0.00	57.72	0.00	32.84	0.10	0.46	2.92	0.03	0.07	0.16	0.00	0.12	5.18	0.00	0.00	0.04	0.00	0.09	0.27	0.00
2e	0.00	52.49	0.00	2.80	0.86	15.49	20.14	0.05	0.01	0.06	0.00	2.05	0.17	0.00	0.64	0.00	0.00	0.00	5.24	0.00
2f	0.00	49.63	0.00	3.08	0.92	5.63	6.60	0.02	0.12	0.00	0.00	0.51	0.44	0.00	0.49	0.00	0.00	0.00	32.35	0.22
2g	0.00	53.25	0.00	7.16	0.73	6.63	26.11	0.10	0.00	0.00	0.00	1.22	1.36	0.00	0.47	0.00	0.00	0.00	2.97	0.00
3a	0.00	43.72	0.00	6.94	0.11	0.60	0.73	0.00	0.00	0.00	0.00	0.00	0.00	0.00	0.00	0.08	0.04	0.36	47.28	0.13
3b	0.00	48.74	0.00	15.85	0.15	15.15	17.00	0.06	0.00	0.79	1.05	0.38	0.11	0.00	0.36	0.00	0.00	0.00	0.36	0.00
4a	0.00	54.39	0.00	1.00	1.57	14.87	23.48	0.05	0.00	0.00	0.00	2.63	0.10	0.00	0.41	0.00	0.00	0.00	1.50	0.00
4b	71.02	18.99	0.00	0.87	0.07	1.44	3.61	0.00	0.00	0.00	1.39	1.24	0.00	0.00	0.32	0.00	0.00	0.00	1.05	0.00

A.

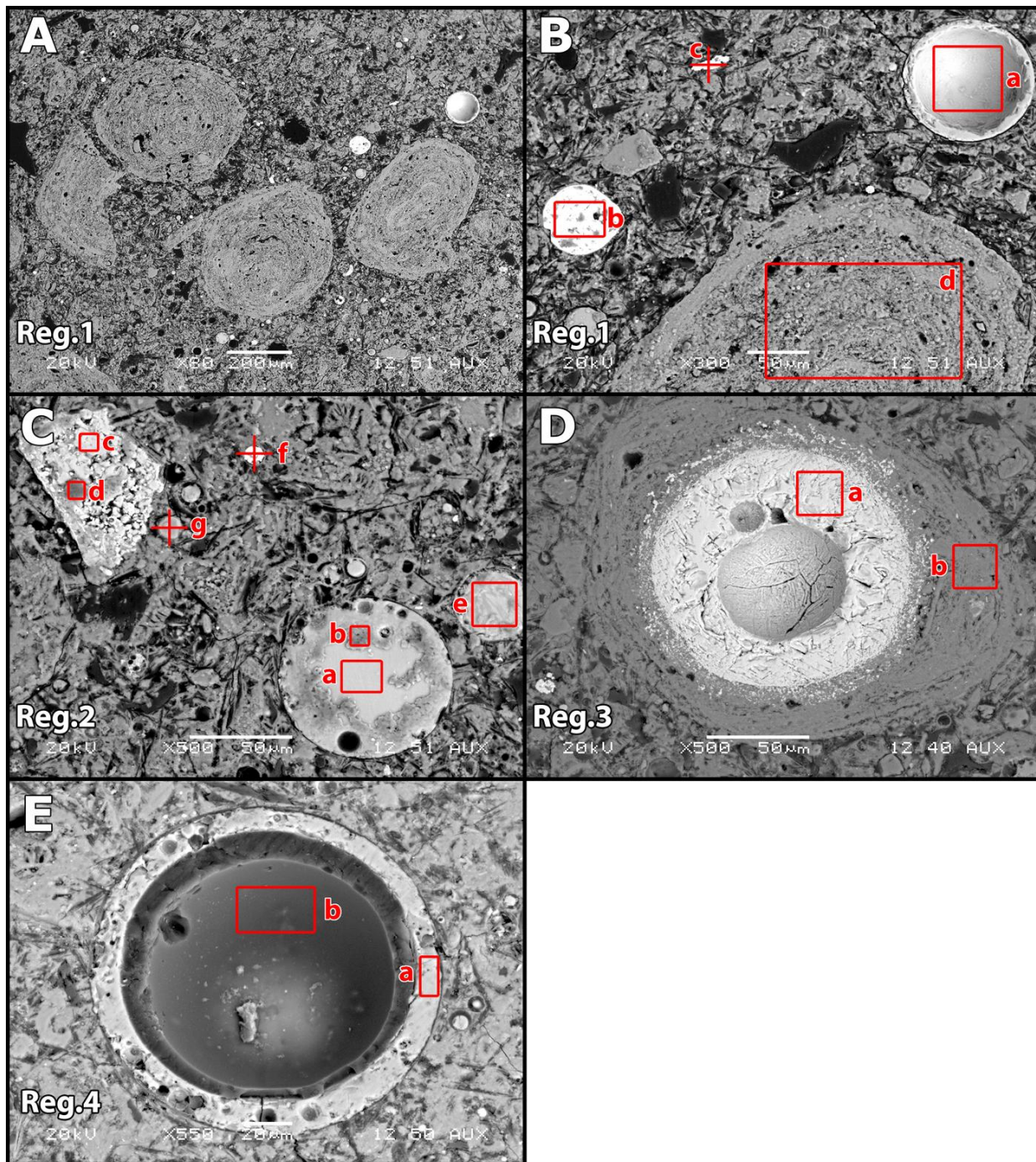


Figure A.1. SEM Collage Showing Different Regions Analyzed by EDS (called out in red boxes and cross-hairs)

Table A.2. EDS Composition Data. Like compositional regions (in mass%) are broken out into sections for comparison purposes. Cells highlighted in red are values ≥ 10 mass%.

Reg	CK	OK	FK	NaK	MgK	AlK	SiK	YL	PK	SK	ClK	KK	CaK	CsL	TiK	LaL	CrK	MnK	FeK	NiK
<i>Large (~200-400 μm diameter) concentric circular regions</i>																				
1d	0.00	36.82	0.00	18.79	0.15	17.57	21.75	0.00	0.09	0.82	1.80	0.70	0.18	0.00	0.70	0.00	0.00	0.00	0.62	0.00
3b	0.00	36.12	0.00	16.88	0.17	18.94	22.12	0.25	0.00	1.17	1.72	0.70	0.21	0.00	0.79	0.00	0.00	0.00	0.93	0.00
<i>Bright circular regions</i>																				
1a	0.00	37.95	0.00	4.13	1.26	13.41	23.61	0.00	0.08	0.00	0.00	3.41	0.27	0.07	0.63	0.00	0.00	0.00	14.83	0.34
2a	0.00	34.80	0.00	0.41	1.30	16.13	26.15	0.00	0.00	0.00	0.00	2.85	0.18	0.00	1.91	0.00	0.00	0.00	16.26	0.00
2e	0.00	36.10	0.00	2.77	0.90	17.97	24.32	0.19	0.02	0.08	0.00	3.45	0.29	0.00	1.33	0.00	0.00	0.00	12.59	0.00
2g	0.00	37.92	0.00	7.33	0.79	7.97	32.65	0.40	0.00	0.00	0.00	2.12	2.43	0.00	1.01	0.00	0.00	0.00	7.39	0.00
4a	0.00	39.42	0.00	1.05	1.73	18.18	29.87	0.20	0.00	0.00	0.00	4.66	0.19	0.00	0.90	0.00	0.00	0.00	3.81	0.00
<i>High Fe regions</i>																				
1c	0.00	22.53	0.00	6.43	0.00	1.95	4.30	0.00	0.00	0.12	0.00	0.23	0.44	0.00	0.17	0.39	0.00	0.00	63.44	0.00
2f	0.00	25.52	0.00	2.28	0.72	4.89	5.96	0.07	0.12	0.00	0.00	0.64	0.57	0.00	0.75	0.00	0.00	0.00	58.07	0.41
3a	0.00	19.54	0.00	4.46	0.07	0.45	0.58	0.00	0.00	0.00	0.00	0.00	0.00	0.00	0.00	0.30	0.06	0.56	73.77	0.21
<i>Ca-Si-O rich region</i>																				
2c	0.00	26.39	7.07	2.29	0.77	0.28	17.29	0.67	0.08	0.00	0.00	0.00	42.98	0.00	0.00	0.00	0.33	0.77	0.59	0.49
<i>Na-Ca-Si region</i>																				
2d	0.00	45.63	0.00	37.31	0.12	0.61	4.06	0.15	0.11	0.25	0.00	0.23	10.27	0.00	0.00	0.25	0.00	0.25	0.76	0.00
<i>High Fe region with Na-O</i>																				
1b	0.00	20.12	0.00	16.98	0.07	0.16	0.25	0.00	0.07	0.11	0.07	0.00	0.13	0.00	0.00	0.47	0.00	0.00	61.57	0.00
<i>Fe-Al-Si-O region</i>																				
2b	0.00	38.61	0.00	21.57	0.51	8.46	19.70	0.00	0.00	0.20	0.00	2.19	0.18	0.00	1.04	0.00	0.00	0.00	7.54	0.00
<i>Dark region (epoxy or carbon inclusions?)</i>																				
4b	57.22	20.38	0.00	1.34	0.12	2.61	6.80	0.00	0.00	0.00	3.31	3.24	0.00	0.00	1.02	0.00	0.00	0.00	3.95	0.00

A.

Appendix B

Dimensions of Supplied FBSR Test Monoliths Used in EPA Draft Method 1315 and ANSI/ANS 16.1 Leach Tests

Appendix B: Dimensions of Supplied FBSR Test Monoliths Used in EPA Draft Method 1315 and ANSI/ANS 16.1 Leach Tests

Table B.1. FBSR Monolith Dimensions of Cylinders Used in the EPA Draft Method 1315 Leach Test

Monolith ID	Average Diameter (inches)	Average Height (inches)	As Received Weight (g)	Area (cm²)	Volume (cm³)
M-14	2.00	3.97	322.14	201.7	204.6
M-21	2.00	3.94	322.45	200.6	203.4

Table B.2. FBSR Monolith Dimensions of Cylinders Used in the ANSI/ANS 16.1 Leach Test

Monolith ID	Average Diameter (inches)	Average Height (inches)	As Received Weight (g)	Area (cm²)	Volume (cm³)
M-10	2.00	3.96	320.23	201.1	203.9
M-6	2.01	3.95	324.07	201.9	205.3

Distribution

No. of Copies		No. of Copies
OFFSITE		ONSITE
1	C Jantzen Savannah River National Laboratory P.O. Box 616 Aiken, SC 29802	4 Washington River Protection Solutions MA Melvin E6-30 DJ Swanberg B1-55 KE Smith E6-30 LE Thompson E6-20
1	EM Pierce Building 1505, MS 6038 Oak Ridge National Laboratory P.O. Box 2008 Oak Ridge, TN 37831-6038	15 Pacific Northwest National Laboratory PR Bredt K9-09 CF Brown K6-81 EC Golovich K5-25 SV Mattigod K3-62 KE Parker K3-62 LM Peurrung K9-09 RP Pires (5) K6-28 N Qafoku P7-54 RJ Serne K6-81 MM Valenta P7-54 JH Westsik, Jr K7-15



Pacific Northwest
NATIONAL LABORATORY

902 Battelle Boulevard
P.O. Box 999
Richland, WA 99352
1-888-375-PNNL (7665)
www.pnl.gov



U.S. DEPARTMENT OF
ENERGY